



UNIVERSITY OF RIJEKA  
DEPARTMENT OF BIOTECHNOLOGY

Tamara Martinović

**Proteomic and glycomic analyses of the  
potential protective role of zeolite on an  
osteoporotic rat model**

DOCTORAL THESIS

Mentor: prof. dr. sc. Đuro Josić

Rijeka, 2018

Mentor: prof. dr. sc. Đuro Josić

Doktorski rad obranjen je dana 20.03.2018. u Rijeci, pred povjerenstvom u sastavu:

1. Prof. dr. sc. Krešimir Pavelić, Odjel za biotehnologiju, Sveučilište u Rijeci
2. Izv. prof. dr. sc. Sandra Kraljević Pavelić, Odjel za biotehnologiju, Sveučilište u Rijeci
3. Prof. dr. sc. Dražen Vikić Topić, Institut Ruđer Bošković
4. Prof. dr.sc. Đuro Josić, Odjel za biotehnologiju, Sveučilište u Rijeci

Ova doktorska disertacija sadrži 77 stranica, 13 tablica, 43 slike i 88 bibliografskih podataka.

## Zahvale

Ponajprije hvala mom mentoru prof. dr. sc. Đuri Josiću koji mi je omogućio da dođem do cilja; naučio me kako biti samostalna, kritički razmišljati i uspješno izraditi znanstveni rad. Pored neizmjenno važnog znanstvenog usmjerenja koje mi je moj mentor pružio, moram mu posebno zahvaliti za mnoge sate ugodnih i obrazovnih razgovora iz kojih sam puno naučila o povijesti, ljudima i životu općenito. Profesore, hvala Vam na svemu. Posebno hvala izv. prof. dr. sc. Sandri Kraljević Pavelić koja me cijelim putem pratila u izradi ovog doktorskog rada i pružala mi podršku kada mi je bila najpotrebnija. Hvala i prof. Paveliću na čitanju ovog manuskripta i na svim savjetima i konstruktivnim diskusijama. Uroše, u vokativu, hvala ti na svakom savjetu i pomoći te na nadasve ugodnoj radnoj atmosferi u našem laboratoriju, hvala na prijateljstvu, kao i na nebrojenim psihoterapeutskim razgovorima. Ivane, hvala na silnom smijehu i pjevanju uz Daleku obalu, veselim se ponovnoj suradnji. Marko, hvala ti na pomoći oko analize glikana na MS-u i na svoj dobroj volji. Daira i Karlo, hvala vam na nebrojenim ručkovima prepunim smijeha i izlascima, kupanjima ili sađenjima trešnje; nadam se da će ih biti još i više. Veliko hvala i svim ostalim djelatnicima Odjela za biotehnologiju koji su na bilo koji način pomogli u realizaciji ovog doktorata, bilo kroz naručivanje i posuđivanje kemikalija, kroz savjete i diskusije, ili kroz tračeve u odjelskim kuloarima. Najdraži moj Luka, hvala ti na moralnoj potpori koju si mi cijelo vrijeme pružao; bez tvoje ljubavi, razumijevanja i pauza za slatko, pisanje ovog rada bilo bi puno teže. Draga Borja, hvala ti na svim večerama, izlascima, odlascima u shopping i putovanjima, hvala na tome što si vjerovala u mene. Bila si mi primjer snage duha i uspjeha, kao prava starija sestra, i ponosna sam što sam baš tebe pratila u koracima. Najdraži mama i tata, hvala vam na ljubavi, sigurnosti i slobodi koju ste mi uvijek pružali; najbolji ste roditelji na svijetu. Hvala vam što ste mi omogućili da ostvarim svoje želje i bili mi bezrezervna podrška, bez vas ovo ne bi bilo moguće.

Ova doktorska disertacija napravljena je dijelom u sklopu projekta "Methods for High-throughput glycoproteomics analysis" (HTP-GlycoMet, voditelj: dr. sc. Đuro Josić), koji se financira sredstvima FP7 Marie Curie Actions-Industry-Academia Partnerships and Pathways (IAPP). Pristup dijelu opreme korištene za izradnju ovog rada omogućio je projekt Sveučilišta u Rijeci „Razvoj istraživačke infrastrukture na Kampusu Sveučilišta u Rijeci“ financiran je iz Europskog fonda za regionalni razvoj (EFRR).

## Summary

Bone homeostasis is secured by a combined action of bone forming osteoblasts and bone resorbing osteoclasts. When this balance is impaired, osteopenia is induced, which in time develops into osteoporosis. Antibody glycosylation influences osteoclast differentiation. It is known that immunoglobulin G (IgG) immune complexes positively stimulate osteoclast differentiation, resulting in subsequent inflammatory bone loss. In order to further investigate this process, a method was developed to isolate IgG from serum and to investigate the changes in IgG glycosylation patterns in osteoporotic rats treated with clinoptilolite, a natural zeolite with great detoxification and ion exchange properties. An experimental rat model was set up, and following groups of animals were analysed: healthy control, sham control, ovariectomized control (OVX), OVX supplemented with synthetic zeolite, OVX supplemented with natural clinoptilolite and OVX supplemented with micro activate clinoptilolite. Using affinity chromatography by use of monolithic supports with immobilized immunoglobulin binding ligands as a robust tool for isolation of immunoglobulins, IgG can be purified from rat sera. Compared to proteins A and G, recombinant protein L binds by far the largest number of isoforms of all immunoglobulins. For this reason, this ligand immobilized on a monolithic column has been used in this work. To procure a highly enriched IgG preparation, the fraction with proteins eluted from the column was analysed on a 1D polyacrylamide gel, after which in-gel tryptic digestion of this protein was performed. The resulting peptides were successfully identified by MALDI-TOF/TOF mass spectrometry as parts of IgG heavy and light chains. In the next step, the IgG glycan structure was analysed by use of the same technique, after the glycans have been removed from the protein using deglycosylation enzyme PNGase F. Next to the IgG analysis, liver proteomes of healthy, sham operated and ovariectomized (OVX) rats treated with zeolites were fractionated according to hydrophobicity and each fraction was separately analysed by SDS PAGE. Finally, liver cryo slices were examined by Synchrotron radiation. Present results give us the evidence that the developed high throughput protocols for analysis of glycosylation of rat immunoglobulins, namely IgG, IgA and IgM, as well as the protocol for quantitative proteomic investigations of rat liver proteome, give us the fundament for further investigations by use of a larger number of experimental animals. We suggest that clinoptilolite positively affects bone status in osteoporotic rats as a consequence of signalling changes in the body, particularly those initiated by the liver and the systemic spread of IgG molecules.

**Key Words**

Immunoglobulin G, osteoporosis, glycosylation, liver proteome, monolith, affinity chromatography, mass spectrometry

## **Prošireni sažetak**

### Ciljevi

Homeostaza kosti je posljedica kombiniranog djelovanja osteoblasta, stanica koje sudjeluju u biosintezi kosti, i stanica koje je razgrađuju, osteoklasta. Kada je ova ravnoteža narušena, dolazi do osteopenije, koja se s vremenom razvije u osteoporozu. Poznato je da glikozilacija antitijela utječe na diferencijaciju osteoklasta. Imunološki kompleksi imunoglobulina G (IgG) stimuliraju diferencijaciju osteoklasta, rezultirajući upalnim gubitkom koštane mase. Cilj ovog doktorskog rada je istražiti potencijalni terapijski učinak prirodnog zeolita klinoptilolita, koji zbog svog ionsko izmjenjivačkog svojstva ima mnoge terapijske aplikacije. Pokusi su provedeni na osteoporotičnom modelu štakora. Slijedeći postavljeni zadatak, imunoglobulin G je izoliran iz seruma zdravih štakora, osteoporotičnih štakora, i osteoporotičnih štakora tretiranih klinoptilolitom, te deglikozilacija izoliranih protutijela i analiza i usporedba njihovih IgG glikozilacijskih profila. Usporedno, kvantitativno je analiziran proteom jetre istih štakora kako bi se uvidjele moguće razlike u ekspresiji pojedinih proteina ili grupe proteina.

### Postupci

Imunoglobulin G je izoliran iz uzoraka seruma sljedećih grupa pokusnih životinja: zdrava kontrola, sham kontrola, ovariektomizirana (OVX) kontrola, OVX + tretirani sintetskim zeolitom, OVX + tretirani jednostruko aktiviranim klinoptilolitom i OVX + tretirani PMA dvostruko aktiviranim klinoptilolitom. Nadalje, analizirana je i glikanska struktura IgG na MALDI-TOF/TOF masenom spektrometru, nakon što su glikani odvojeni od proteina koristeći enzim PNGaza F koji specifično cijepa glikanske lance. Pored analize imunoglobulina G, istražen je i proteom jetre istih štakora. Jetra je homogenizirana, a proteini su frakcionirani po hidrofobnosti koristeći odgovarajući komercijalni kit za ekstrakciju. Svaka je frakcija posebno analizirana na SDS PAGE gelu.

### Rezultati

Prvo je razvijena metoda za izolaciju i separaciju IgA, IgM i IgG iz humanog seruma koristeći afinitetnu kromatografiju. Imunoglobulin G je izoliran iz uzoraka seruma štakora koristeći protein L imobiliziran na monolitni disk, a eluat je nanešen na poliakrilamidni gel. Nakon enzimske digestije proteina separiranih na SDS PAGE, MALDI-TOF/TOF masenom spektrometrijom uspješno je identificiran štakorski IgG. Glikanska struktura IgG analizirana je masenom spektrometrijom, s posebnim naglaskom na detekciju sjalinske kiseline. Proteom

jetre također je analiziran, moguće promjene u ekspresiji proteina na 1D poliakrilamidnom gelu su analizirane koristeći raspoloživu metodu.

### Zaključci

Uspješno razvijeni visokoprotlačni protokoli za analizu glikozilacije štakorskih imunoglobulina, posebice imunoglobulina G, kao i protokoli za kvantitativna proteomska istraživanja štakorske jetre, služe kao podloga za daljnja istraživanja koristeći veći broj eksperimentalnih životinja. Predlažemo da klinoptilolit pozitivno utječe na gustoću kosti osteoporotičnih štakora kao posljedica promjena u staničnoj signalizaciji, posebice onih započetih u jetri, te posljedičnog sistemskog širenja IgG molekula.

### **Ključne riječi**

Imunoglobulin G, osteoporoza, glikozilacija, proteom jetre, monolit, afinitetna kromatografija, masena spektrometrija



## Table of Contents

1. INTRODUCTION.....	1
1.1 Osteoporosis .....	1
1.2 IgG glycosylation.....	3
1.3 Zeolites .....	5
1.4 Affinity monolith chromatography.....	7
2. RESEARCH GOALS AND HYPOTHESIS.....	12
3. MATERIALS AND METHODS.....	13
3.1 Experimental animals.....	13
3.2 Tested substances.....	14
3.3 Tissue sampling .....	14
3.4 Materials and chemicals.....	14
3.5 Instrumentation.....	14
3.6 Affinity monolith chromatography.....	15
3.7 Protein fractionation.....	15
3.8 Sodium dodecyl sulfate-polyacrylamide gel electrophoresis (SDS-PAGE) .....	15
3.9 In-gel PNGase F digest, glycan derivatization and glycan enrichment .....	16
3.10 In-gel digest and ZipTip purification.....	17
3.11 MALDI plate sample spotting .....	17
3.12 Synchrotron measurements.....	18
4. RESULTS.....	19
4.1. Immunoglobulin isolation from human serum .....	19
4.1.1 Identification of isolated immunoglobulins .....	22
4.1.2 High-throughput automation of immunoglobulin isolation.....	25
4.2 IgG isolation from rat serum.....	26
4.2.1 Validation of rat IgG isolation .....	32
4.3 Rat serum IgG glycosylation.....	34
4.4 Rat liver fractionation .....	50
4.5 Presence of aluminium and silicone in rat liver .....	53
5. DISCUSSION.....	54
6. CONCLUSIONS.....	60
7. LITERATURE.....	61
8. CURRICULUM VITAE.....	69
9. SUPPLEMENT.....	73
9.1 List of tables.....	73

9.2 List of figures.....	74
9.3 List of abbreviations.....	77

# 1. INTRODUCTION

## 1.1 Osteoporosis

Osteoporosis is a metabolic disease characterized by a reduction in bone mass and density. In 2010, 27.5 million people in Europe suffered from osteoporosis [1]. It is manifested through an imbalance between bone adsorption and resorption. Bone is a live tissue that is being regenerated throughout our lives and bone homeostasis is maintained by the right balance between osteoblasts, bone forming cells, and osteoclasts, bone resorbing cells (Figure 1). Activation of these cells and their interconnected interplay is well studied and is regulated by various molecular signals. The three main mechanisms responsible for the development of osteoporosis are inadequate bone mass growth during development, excessive bone resorption and inadequate bone formation. Moreover, hormonal factors strongly influence the speed of bone resorption; lack of oestrogen significantly enhances bone resorption, restricting the formation of new bone tissue at the same time [2].

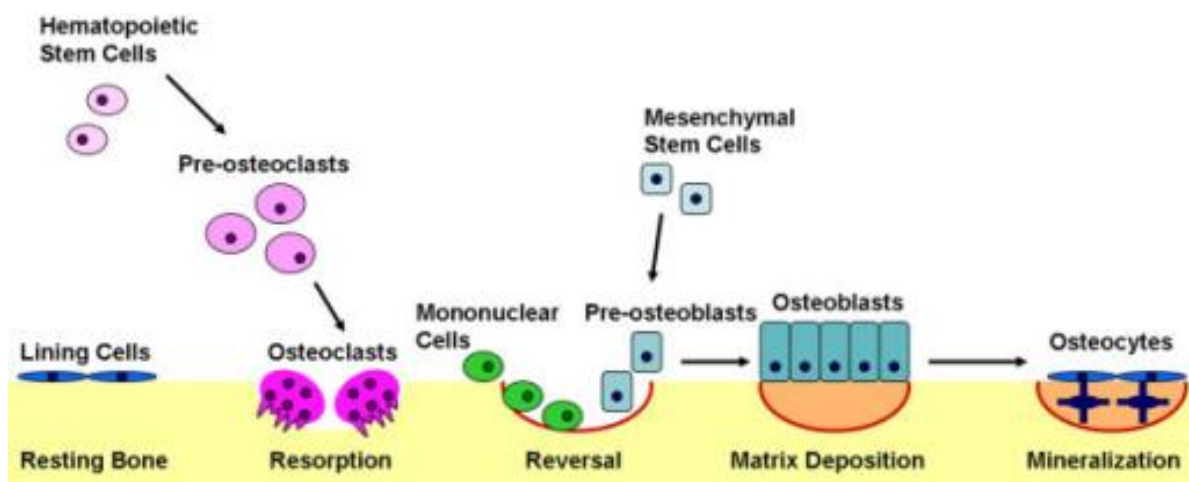


**Figure 1.** Bone remodelling [3].

Osteoclasts, multinucleated giant bone resorbing cells, are derived from a monocyte/macrophage lineage, and they firstly develop into mononucleated osteoclast precursor cells. Fusion of these cells into an immature osteoclast or a polykaryon requires three stimulatory signals coming from a growth factor, a macrophage colony-stimulating factor (M-CSF) and the receptor activator of nuclear factor  $\kappa$ B ligand (RANKL), a tumour necrosis factor

produced by osteoblasts [4]. RANKL induces expression of transcription factor NFAT2 which is required for the development of functional osteoclasts by expressing Siglec15, a lectin which recognizes  $\alpha$  (2,6)-linked sialic acid, contributing to cell fusion and bone resorption in osteoclasts [5]. The dependency of osteoclastogenesis on osteoblasts, cells of the mesenchymal lineage, is evident in the interplay of RANKL and its receptor RANK, both membrane bound proteins, and osteoprotegerin (OPG), a secreted glycoprotein (Figure 2). Osteoblasts secrete both RANKL and OPG, and OPG acts as a decoy receptor for RANKL, thus inhibiting osteoclastogenesis by competitively binding to RANKL and not allowing it to bind to RANK receptors on osteoclasts [6].

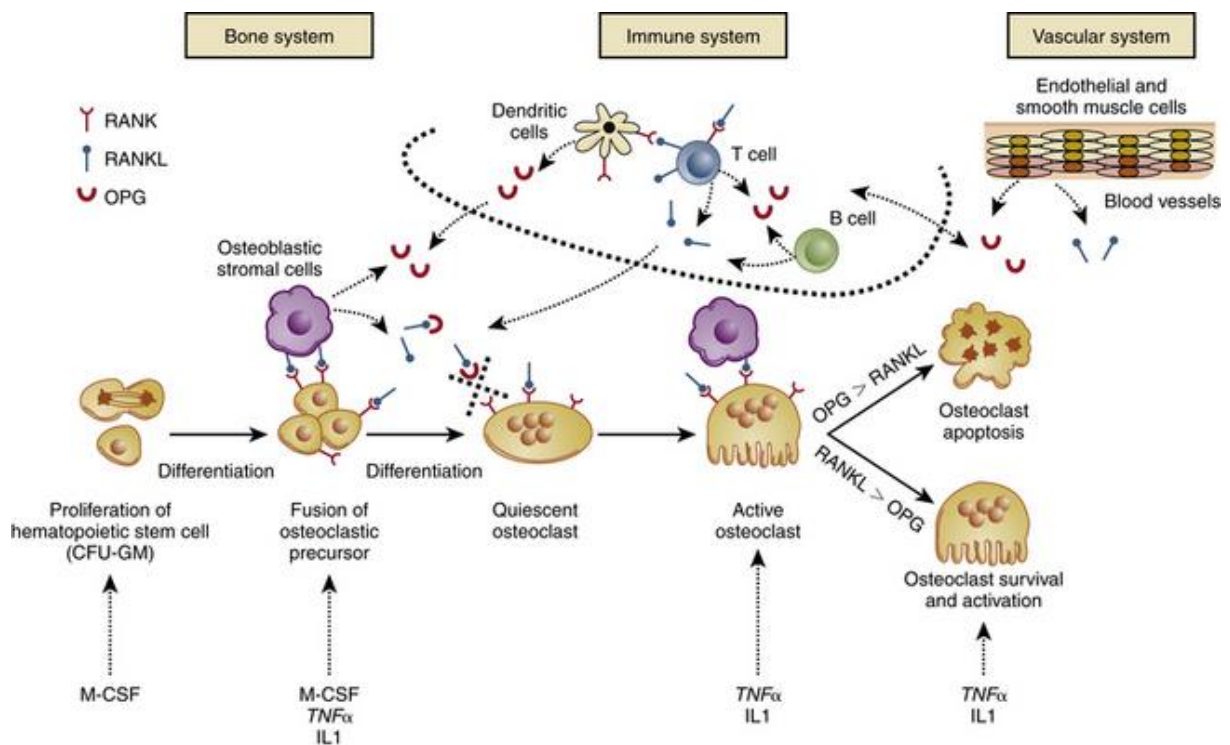


**Figure 2.** The molecular triad OPG/RANK/RANKL [7].

Osteoblasts are derived from the mesenchymal lineage and many factors are required for their differentiation, including transcription factors (*e.g.* runt-related transcription factor-2 and osterix) and components of the canonical Wnt signalling pathway [8]. Mature osteoblasts produce and secrete proteins that constitute the bone matrix, like type I collagen, osteonectin and osteocalcin [9]. In addition, they promote the deposition of hydroxyapatite by regulating local concentrations of calcium and phosphate, which makes them essential for the mineralization of the osteoid matrix [9]. When, over time, osteoblasts become entrapped in their own bone matrix they are called osteocytes, mature bone cells, which express different genes that contribute to bone turnover and the maintenance of bone mineral homeostasis.

## **1.2 IgG glycosylation**

Post translational modifications (PTM) have a crucial impact on the biological function and structure of proteins, altering their stability, activity, localization, and even protein-protein interactions. A direct link in a signalling network between upstream kinases and downstream transcription factors is established by phosphorylation, while after glycosylation, covalently bound sugar moieties provide important recognition epitopes that influence regulatory or effector functions of the protein. Glycosylation is the most complex PTM because (i) there is a large number of enzymatic steps involved in forming a glycan and (ii) it introduces by far the largest number of changes into the proteome, compared to other PTMs. Biological functions of protein glycosylation are numerous; from Fc receptor and pathogen binding, to interaction with complement and resistance to proteases. There are several types of glycosylation in mammals, but N- and O-linked glycosylation are the most common ones. N-linked refers to the glycan attached to the asparagine residue, while O-linked glycosylation introduces the glycan to a hydroxylated amino acid, serine or threonine. The major secretory products of the adaptive immune system, immunoglobulins (Igs), are glycosylated, and both the Fc and the Fab fragments may contain glycans. The sugar moieties attached to immunoglobulins are quite large (around 2 kDa). Since immunoglobulin G accounts for more than 70% of serum Igs, much more is known about this Ig isotype compared to the A, D, M or E classes. The role of IgG glycosylation has been extensively studied in cancer therapy and autoimmunity, linking disease severity to the changes in the composition and location of glycans [10,11,12]. Although most research has been focused on IgG, the link between glycosylation and pathology has been established in other Ig classes as well. Immunoglobulin A (IgA) glycosylation effects have been affirmed in the scope of allergies and IgA nephropathy [13,14] while sialylation influences the

immunomodulatory effects of immunoglobulin M (IgM) on T cells [15]. While glycosylation, as the most common PTM in antibodies, has been a topic of many investigations, rarely studied modifications, such as methionine oxidation, deamidation and disulphide modifications, can all cause potentially immunogenic changes in immunoglobulin structure [16].

Immunoglobulin G is a protein which plays a major role in the humoral immune response regulating the activity of immune cells by binding to the Fc $\gamma$  receptor. It is known that increased bone resorption is connected to the immune system activation in autoimmune or inflammatory diseases. IgG binding to Fc $\gamma$ Rs sends a signal through Fc $\gamma$ R, activating ITAM (immunoreceptor tyrosine-based activation motif) signalization, which is an essential co-stimulatory signal for osteoclast differentiation [17]. Considering that there are positive and negative receptors, the effect of IgG varies between different receptor subtypes. Moreover, monomeric and polymeric IgG forms have different effects, making IgG-Fc $\gamma$ R signalization even more complicated [17].

N-glycan attached to the heavy chain of the Fc moiety of IgG influences its stability and effector functions. The Fab fragment can be glycosylated as well, and 15-20% of IgG has an N-glycan present in its light chain [18]. The N-linked glycan attached to asparagin-297 in the Fc region of IgG is of crucial importance for IgG- Fc $\gamma$ R binding [19] (Figure 3). Fc receptors (FcR) participate in immunity, and their ligands are antibodies expressed by infected cells or pathogens. FcRs are expressed by B lymphocytes, NK cells, macrophages, neutrophils and other immunological cells, as well as osteoclast precursors [20]. FcRs that bind immunoglobulin G (IgG) are called Fc gamma receptors, Fc $\gamma$ R. There are several kinds of Fc $\gamma$  receptors, and they differ in the antibody binding affinity because of their distinct molecular structure: Fc $\gamma$ RI (CD64), Fc $\gamma$ RIIA (CD32), Fc $\gamma$ RIIB (CD32), Fc $\gamma$ RIIIA (CD16a) and Fc $\gamma$ RIIIB (CD16b) [19]. The majority of these receptors act stimulative, while Fc $\gamma$ RIIIB is the only one that acts inhibitory. Osteoclasts are expressing Fc $\gamma$  receptors in quantities similar to those of macrophages and dendritic cells, indicating that immune complexes and immunoglobulin G (IgG) influence their differentiation/activity.

Changes in IgG glycosylation result in changed Fc conformation and influence the affinity of IgG binding to the Fc $\gamma$ R. An addition of terminal sialic acid residues in the IgG glycan has an anti-inflammatory effect, while the lack of it increases the affinity of IgG binding to the receptor, producing a pro-inflammatory response [21]. Negishi-Koga *et al.* have demonstrated that desialylated, but not sialylated, immune complexes enhance osteoclastogenesis *in vitro* and

*in vivo* [22]. *In vitro* osteoclast stimulation with desialylated immune IgG complexes resulted in enhanced osteoclastogenesis with an increase in the number of osteoclasts. On the other hand, stimulation with sialylated IgG complexes did not induce a change in osteoclastogenesis. Mice treated with a sialic acid precursor show increased IgG sialylation and are less prone to inflammatory bone loss, further confirming the protective role of sialylated IgG in the autoimmune loss of bone mass [22]. Furthermore, pathogenic antibodies like ACPA (antibodies against citrullinated proteins) contain less sialic acid in the Fc glycan compared to bodily IgG antibodies, while positively influencing osteoclastogenesis [23]. Therefore, IgG sialylation could be of great importance for the interaction between osteoclasts and the immune system.

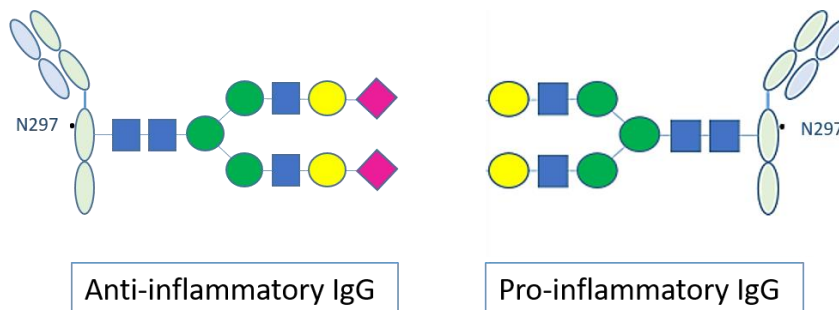


**Figure 3.** IgG sialylation is the key checkpoint that determines the engagement of pro- or anti-inflammatory Fcγ receptors.

### 1.3 Zeolites

Zeolites are hydrated microporous aluminosilicate minerals of volcanic origin. They are crystals with a well-defined tetrahedral structure formed by  $\text{SiO}_4$  and  $\text{AlO}_4$  molecules linked through common oxygen atoms (see Figure 4.) [24]. The ratio between silicon and aluminium varies from 4.0 to 5.3 with a high thermal stability (600–800 °C) [25]. Zeolites' general formula is  $(\text{Mn}^+)_{x/n}[(\text{AlO}_2)_x(\text{SiO}_2)_y \cdot m\text{H}_2\text{O}]$ , where “M” stands for a positively charged metal ion, *e.g.* sodium, potassium, magnesium, calcium [26]. Considering their overall negative charge, they are excellent inorganic cation exchangers, having a stronger selectivity compared to silica and activated charcoal [24]. Zeolites are often called *molecular sieves* since they can exchange one ionic metal in the crystal grid with another, with pore size modulating catalytic properties of





Clinoptilolite is a great source of silicon in the form of orthosilicic acid which protects the body from heavy metals [35]. Lack of silicon in the body leads to a bone defect and there is a positive correlation between an increased silicon intake and mineral hip bone density in premenopausal women [36]. Similar phenomena was observed in female rats [37]. Aluminosilicates are known to have biological activity, and it was also reported that silica, silicates and aluminosilicates act as non-specific immunostimulators by binding to a fraction of the T cell population, inducing their cell death [38]. Moreover, Beck *et al.* showed that silica nanoparticles mediate potent inhibitory effects on osteoclasts and stimulatory effects on osteoblasts *in vitro* [39].

Next to natural zeolites, synthetic zeolite A was shown to positively influence the proliferation and differentiation of human osteoblast like cells *in vitro* [40]. Our preliminary results show an increase in bone density and mineral content in osteoporotic rats treated with clinoptilolite. Considering the clear interconnection between bones, immune system and clinoptilolite, we decided to isolate immunoglobulin G from sera of osteoporotic rats in order to analyse its glycosylation, particularly sialylation, and contribute to our understanding of the mechanisms of osteoporosis.

#### **1.4 Affinity monolith chromatography**

In order to study immunoglobulin structure and function, they first need to be isolated from biological samples. Many commercially available kits for targeted Ig isolation exist, using different specific proteins as purification ligands. However, they can be expensive and do not allow for simultaneous purification of different Ig classes. Chromatographic methods, on the other hand, provide a great platform for concurrent protein isolation, as was shown by Breen *et al.* who successfully isolated both IgG and IgM using protein A affinity chromatography followed by separation on a strong anion-exchange column [41]. High-throughput (HTP) fractionation of human plasma using the same approach allowed for the isolation of IgM from a large number of samples [42]. Generally speaking, affinity chromatography refers to the separation of biomolecules based on their affinity to the molecule immobilized on the chromatographic media. Substances with no or low affinity for the column will have a short retention time and will elute soon after sample application, while those with high affinity are bound so strongly to the column that an eluent has to be added in order to elute them. Elution buffer is in most cases a highly acidic one ( $\text{pH} < 3$ ), and drastic drop in pH weakens protein-protein interactions and leads to an almost immediate dissociation between the ligand and the

analyte. A standard run consist of five steps: (i) the column is equilibrated with the same buffer in which the sample is diluted, allowing for protein-protein interactions to occur in the chromatographic step, (ii) sample is applied in the same buffer and target proteins bind to the ligand; (iii) unbound and weakly bound material is washed away using a buffer with a high salt concentration; (iv) bound proteins are eluted in an elution buffer at a very low pH; (v) the column is re-equilibrated with equilibration buffer to return the pH to a neutral value so that the half-life of ligands immobilized onto the column is prolonged. A typical affinity chromatogram is showed in Figure 6.

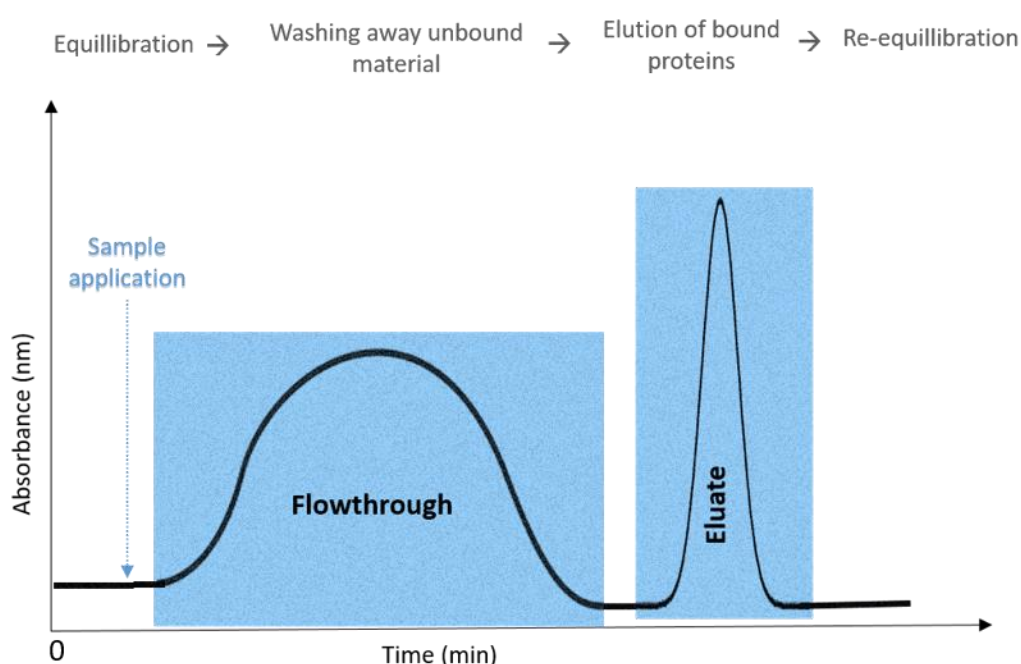


**Figure 6.** A typical affinity chromatography scheme.

Routine chromatographic protocols use particle-based supports, such as inert silica or agarose beads packed into a column. A very efficient alternative are polymethacrylate monolithic supports, which enable rapid and efficient analyses of large biomolecules and nanoparticles [43] (Table 1.) At the end of the 80's, polymer-based monolithic supports were developed by two groups [58-60], firstly called “macroporous membranes” [47] or “continuous polymer beds” [48]. They are porous structures that contain channels and that bear chemically active groups on their surface. In the next step, these active groups can be chemically modified with different ligands. Firstly, successful use of monoliths for fast chromatographic separations of

standard proteins was demonstrated [47,48]. Shortly after the first experimental production of glycidyl-polymethacrylate with ion-exchange ligands, complex biological mixtures were being separated, such as blood plasma and plasma membrane proteins [49], and other small molecules and proteins as potential affinity ligands were immobilized to supports [50]. During the following years, glycidyl-polymethacrylate monoliths became broadly used [51,52]. Monoliths are now widely used for both analytical and preparative separation of biopolymers [49,53,54], as well as for the immobilization of enzymes and fast, in-flow enzymatic conversions [50,54].

It was also demonstrated that miniaturized monolithic columns with immobilized antibodies could be applied for fast isolation of therapeutic proteins by use of affinity chromatography [53,54], as well as for fast detection of potential (glyco)protein biomarkers. The early experiments with the conversion of low and high-molecular weight substrates on monoliths with immobilized enzymes yielded, for the first time, very surprising results, with the conversion rate being faster with a faster flow rate [48,55]. Later investigations confirmed that the material transport in monoliths that contain flow-through channels is based on convection and consequently, it is almost flow-rate independent [52,56]. The low-pressure drop during the separation process on monoliths and their compact structure enabled so-called “conjoint chromatography” by combining columns with different ligands. Such miniaturized units enabled multidimensional separations, such as a combination of affinity chromatography (that enabled removal of some proteins with high abundance, *e.g.* serum albumin) with adsorption chromatography (*e.g.* ion-exchange), that yielded further sample fractionation.

Affinity chromatography on monolithic supports is termed affinity monolith chromatography (AMC). Today, monoliths are usually composed of a polymeric organic, silica, agarose or other substrate that can be chemically modified to bind different ligands [57]. They can be prepared in various formats, from large and middle-sized, columns and discs, to capillaries and microchips [58]. Ligands immobilized to particle-based stationary phases have also been employed in AMC (*e.g.* antibodies, lectins, enzymes, metal ions, dyes). Consequently, AMC can be used for immuno-affinity chromatography, immobilized metal affinity chromatography, dye-ligand affinity chromatography, etc [59]. A monolith does not contain pores but a multitude of longitudinal channels that flow throughout the column, allowing for a large surface area available for reactivity. The continuous bed support displays a higher external porosity compared to chromatographic beads, resulting in increased permeability and lower back pressure at a given flow rate. Furthermore, rapid mass transfer in monoliths is based on convection rather than diffusion and flow rate does not influence protein binding, making them

ideal chromatographic supports when short analysis time is needed, for example HTP drug screening [60]. Affinity monolith chromatography has been used for fast quantification of both IgG and IgM [61,62], as well as for the separation of IgG subclasses [63]. Pucic *et al.* developed a 96 well plate consisting of a monolithic stationary phase with immobilized protein G which enabled HTP isolation and analysis of human IgG of more than 2000 samples in only 12 hours [64].

**Table 1.** Comparison of monoliths and particle-based supports

	Monolith	“Beads”
Large surface area	✗	✓
Increased permeability	✓	✗
Lower back pressure	✓	✗
Unaffected by flow rate	✓	✗
Physically stable	✓	✗

The most common ligands for affinity chromatography are protein G and protein A, isolated from Gram-positive bacteria *Staphylococcus aureus* and *Streptococcus* sp, respectively [65,66]. Both of these ligands interact with immunoglobulins through the Fc fragment. Opposed to that, protein L, a membrane protein from *Peptostreptococcus magnus*, binds with high affinity to the Fab fragment [67] (Figure 7). Specifically, protein L interacts with kappa variable light chain regions of immunoglobulins, which allow for Fab fragment and single domain antibody isolation. It has to be noted that only around 35% of all human Igs contain kappa light chains, irrespective of their class. However, the percentage of rat Igs containing kappa light chains is a higher than 90%.

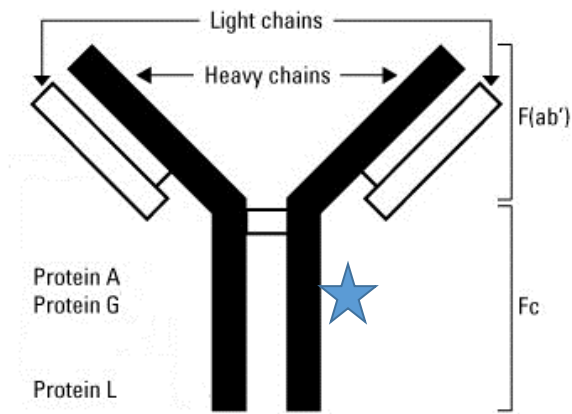


**Figure 7.** Binding sites of protein A, G and L on immunoglobulin G. The star represents N-glycan binding arginine residue.

## 2. RESEARCH GOALS AND HYPOTHESIS

The main goal of this research was to examine the effects of clinoptilolite on IgG glycosylation and liver proteome composition in the osteoporotic rat model. The rationale behind this goal is in already established link between immunoglobulin sialylation and various pathological states. Specifically, we:

1. Developed protocols for a fast, reliable and high-throughput method for IgG isolation from serum, using monolithic columns with immobilized protein L for the isolation of immunoglobulin G from serum of healthy rats, osteoporotic rats and osteoporotic rats supplemented with clinoptilolite.
2. Analysed glycosylation profiles of isolated IgGs.
3. As the main mechanisms of clinoptilolite action is hypothesized to be detoxification in the digestive system, we analysed liver proteomes of healthy rats, osteoporotic rats and osteoporotic rats treated with clinoptilolite.

The results of this thesis are expected to provide novel evidence on clinoptilolite mechanisms of action in a medical device regimen particularly through changes of liver activities as well as through induction of specific glycosylation changes in IgG. We hypothesize that clinoptilolite positively affects the bone status in osteoporotic rats as a consequence of signalling changes in the body, particularly those initiated by the liver and the systemic spread of IgG molecules with higher numbers of sialic acid residues in their glycans.

### 3. MATERIALS AND METHODS

#### 3.1 Experimental animals

Wistar female rats from the Institute of Medical Research and Occupational Health Care in Zagreb were used for these experiments. Animals were bred and maintained according to the Guide for the Care and Use of Laboratory animals: Eight Edition (National Academic Press, 2010). All experimental protocols were approved by the Institutional Animal Care and Use Committee (IACUC). Animals were maintained under pathogen-free conditions in a steady-state micro environment. They were fed with MucedolaRF21 (Mucedola, Settimo Milanese, Italy) food *ab libitum*, with free access to water and altering 12 h light and dark cycles. In order to induce osteopenia, at six months' time, all animals underwent bilateral ovariectomy (OVX) under general anaesthesia, except for one group which was sham operated, meaning that the ovaries were exteriorized and repositioned intact. Administration of tested compounds started after post-operative recovery. Sixty rats were randomly divided into six groups of ten animals, as follows in Table 2.

**Table 2.** Animal groups and treatment

Group	Description	Treatment
0	Healthy control	3 mL H <sub>2</sub> O
1	Sham operated	3 mL H <sub>2</sub> O
2	OVX control	3 mL H <sub>2</sub> O
3	OVX + zeolite A	3 mL suspension of H <sub>2</sub> O and zeolite A (10 gr/kg of b.m./day)
4	OVX + raw clinoptilolite	3 mL suspension of H <sub>2</sub> O and raw clinoptilolite (10 gr/kg of b.m./day)
5	OVX + PMA clinoptilolite	3 mL suspension of H <sub>2</sub> O and PMA clinoptilolite (10 gr/kg of b.m./day)

### **3.2 Tested substances**

Clinoptilolite was provided by Panaceo International Active Mineral Production GmbH (Villach-Gödersdorf, Austria). Synthetic zeolite A was purchased from A. + E. Fischer-Chemie (Karlsruhe, Germany). Natural clinoptilolite was micronized by tribomechanical micronization and PMA (Panaceo Micro Activation) clinoptilolite was produced by technology for double activation adopted from WO00/65486.

### **3.3 Tissue sampling**

At experiment termination, animals were sacrificed by exsanguination under general anaesthesia. Blood was collected, centrifuged and immediately stored as serum at  $-80\text{ }^{\circ}\text{C}$ . Liver tissue was harvested, dipped into liquid nitrogen and stored at  $-80\text{ }^{\circ}\text{C}$ .

### **3.4 Materials and chemicals**

For connection to the high performance liquid chromatography (HPLC) system, a dedicated plastic housing (BIA Separations, Ajdovščina, Slovenia) was used. All chemicals were of analytical grade (Sigma-Aldrich, St. Louis, MO, USA). All buffers were prepared with ultra-pure water ( $\Omega\text{m}\leq 18\text{ S/cm}$ ) and filtered using a 0.22  $\mu\text{m}$  nitrocellulose filter (Millipore, Billerica, MA, USA). Convective interactive media (CIM) r-protein G monolithic disc (0.34 mL) and CIMac r-protein L monolithic column (0.1 mL) were purchased from BIA Separations. These monoliths have a poly (glycidyl methacrylate-co-ethylene dimethacrylate) backbone with immobilized recombinant protein A, G or L produced in *E.coli*. Bicinchoninic acid assay (Thermo Fisher Scientific, Waltham, MA, USA) was used for protein quantification, with bovine serum albumin (BSA) as a standard.

### **3.5 Instrumentation**

Affinity chromatography was performed at room temperature using an HPLC (Knauer, Berlin, Germany) system comprising of a quaternary pump, a solvent degasser, a conductivity/pH monitor, a UV-Vis detector with a 190 to 750 nm wavelength range and a 2 mL sample loop. Operation parameters were fixed and controlled through a computer using ClarityChrom Preparative software version 3.0.5.505 (Knauer).



Mass spectrometric measurements were performed on UltraflexExtreme MALDI TOF TOF instrument (Bruker, Bremen, Germany). The instrument was equipped with a nitrogen laser operating at a wavelength of 337 nm with a 2 kHz frequency in TOF/TOF mode.

### **3.6 Affinity monolith chromatography**

Prior to sample application on a monolithic support, all samples were diluted 10 fold in equilibration buffer, centrifuged and filtered through a 0.22µm filter. Protein G disc was employed using three mobile phases (Buffer A: 0.2M Tris pH 7.2, for equilibration of the column; Buffer B: 0.5M NaCl/50mM Tris-HCl, pH 7.2, for washing of impurities before protein elution; Buffer C: 0.1M glycine-HCl, pH 2, for protein elution). The first two mobile phases were identical when chromatography on protein L column was performed, while the preferred elution buffer was 0.5M acetic acid, without pH adjustment. Elution was performed under isocratic conditions. The flow rate of the mobile phase was 1 mL/min and the column temperature was 25°C. The injection volume of the diluted human serum sample was 2 µL. The eluted proteins were monitored at an absorbance of 280 nm and were rapidly neutralized by addition of a concentrated buffer of 1 M Tris to avoid denaturation. Finally, the system was re-equilibrated with Buffer A.

### **3.7 Protein fractionation**

Liver tissue was lysed and proteins were fractionated using the Subcellular Protein Fractionation Kit for Tissues (Thermo Scientific, Waltham, MA, USA) according to the manufacturer's instructions. 100 mg of tissue was used, and tissues were grinded using a Dounce homogenizer.

### **3.8 Sodium dodecyl sulfate-polyacrylamide gel electrophoresis (SDS-PAGE)**

The composition and purity of eluted protein fractions were tested by vertical SDS-PAGE (Mini Protean Tetracell system, Bio-Rad), using a 12% resolving gel and a 4% stacking gel under reducing conditions. Samples were boiled at 95 °C for 5 minutes. Proteins were separated in the gel for 30min at 200 V. Protein staining was performed with Coomassie Brilliant Blue R-250 (Sigma-Aldrich). Roti-Mark TRICOLOR marker (Carl Roth, Karlsruhe, Germany) was used as a gel standard.

### 3.9 In-gel PNGase F digest, glycan derivatization and glycan enrichment

Protein bands of interest were excised from the gel and cut into 1x1 mm pieces. 250 µl of 100 mM ammonium bicarbonate (ABC), pH 7.8, was added to cover the gel pieces and incubated at RT for 30 minutes, with shaking. Supernatant was removed, and 500 µl of acetonitrile was added and incubated under the same conditions. Again, supernatant was removed, and 250 µl of 100 mM ABC was added and incubated for 30 minutes. To reduce the sample, DTT was used (10 mM DTT, 56 °C, 1 h), and to alkylate it, iodoacetamide (50 mM IAA, RT, 1 h). Samples were washed with 250 µl of 100 mM NaHCO<sub>3</sub> for 30 minutes, followed by 250 µl of acetonitrile for 30 minutes. This step was repeated twice. Samples were then dried in a vacuum concentrator (Eppendorf, Hamburg, Germany). Once completely dried, 5 µl of PNGase F in 20 mM NaHCO<sub>3</sub> per sample was added and incubated for 60 minutes at 37 °C. 20 mM NaHCO<sub>3</sub> was finally added to cover the gel slices and samples were left to incubate O/N at 37 °C. The next day, supernatant was removed, gel pieces were covered with 200 µl of ultra-pure water and each sample was sonified for 30 minutes. The supernatant was stored, and the sonifying step was repeated. Then, gel pieces were covered with 200 µl of 50 % acetonitrile (ACN) and sonified twice, collecting the sup each time. Finally, 100 % ACN was used for sonification, twice. The resulting large volume of collected supernatants amounted to 1200 µl and was dried fully in a vacuum concentrator. When dried, samples were dissolved in 4 µl of pure water, and glycan carboxyethylation was performed. Glycan derivatization leads to sialic acid stabilization when performing MS measurements. 20 µl of ethylation reagent was added to each sample (0.25 M EDC, 0.25 M HOBt, in ethanol) and the reaction was incubated in dark at 37 °C for one hour. 20 µl of ice cold ACN was added to the mixture and incubated at -20 °C for 15 minutes. Cotton HILIC was performed by carefully pipetting 20 µl of solution, thoroughly wetting the cotton, in following order: ultrapure water (3x), 85% ACN (3x), sample (20x), 85% ACN / 1% trifluoroacetic acid (TFA) (3x), 85% ACN (3x). Glycans were eluted in 20 µl ultrapure water and spotted on a MALDI target plate. For glycan analysis, GlycoMod online tool was used.

### 3.10 In-gel digest and ZipTip purification

Protein bands of interest were excised from the gel, cut into 1x1 mm pieces, and each band was de-stained using acetonitrile and 100mM ammonium bicarbonate. Proteins were reduced (with 20mM DTT, 56 °C, 30 minutes) and alkylated (by use of 50mM iodoacetamide, at room temperature for 30 minutes in dark). After washing and further de-staining with acetonitrile and 100mM ABC, samples were dried in a vacuum concentrator (Eppendorf). In-gel tryptic digestion was performed at 4°C for 40 minutes in 50mM ABC containing 400 ng/μL trypsin (sequencing grade, Promega, Madison, WI, USA). Fresh 50mM ABC was then added to the sample, and it was incubated over night at 37 °C. The resulting peptides were re-dissolved in 0.1% TFA and purified via Zip Tip (Millipore, MA, USA) according to the manufacturer's instructions.

### 3.11 MALDI plate sample spotting

Digested peptides were spotted on a MALDI anchor chip plate (Bruker). Sample positions on anchor chip target plates contain "anchors"; hydrophilic patches surrounded by a hydrophobic ring. The "anchor" localizes droplets at the sample position and the hydrophobic ring prevents sample spreading and concentrates the sample into a spot 800 μm in diameter. The concentration effect provides enhanced sensitivity when analyzing dilute samples. Two different matrices were used for spotting peptides and carbohydrates. α- Cyano- 4-hydroxycinnamic acid (HCCA) enables highly sensitive MALDI- TOF- MS measurement of peptides and proteins from 0.7 to 20 kDa. 2,5-Dihydroxybenzoic acid (2,5-DHB), on the other hand, is used for analysis of a wide variety of molecules, including carbohydrates and glycoproteins. When spotting peptides, sample was dissolved in 0.1 % TFA. Matrix solution was prepared by dissolving 1.4 mg/mL HCCA in a solvent mixture containing 85% acetonitrile, 15% water and 0.1% TFA. 1 μL of the sample solution was deposited onto each MALDI target plate position and allow to dry, followed by 1 μL of the matrix solution. For glycans, samples were dissolved in water. Matrix solution was prepared by dissolving 10 mg/mL 2,5-DHB in 30:70 [v/v] acetonitrile : 0.1% TFA : 1 mM NaCl. 0.5 μL of the matrix solution was spotted onto the plate. When dried, 0.5 μL of the sample solution was added. Peptide Calibration Standard II (Bruker) was used for calibration and was dissolved in 125 μL 30:70 [v/v] acetonitrile : 0.1% TFA. One part calibrant solution was mixed with 200 parts HCCA matrix

solution and 1  $\mu\text{L}$  was spotted onto calibrant anchor spots on the anchor chip MALDI target plate.

### **3.12 Synchrotron measurements**

Aluminium and silicone concentrations in the liver were assessed by use of Synchrotron radiation (Elettra Sincrotrone Trieste, Italy, Beamline: TWINMIC). Dried organ samples were cryo-sectioned at  $-23^{\circ}\text{C}$  to 10 micron thick slices and flattened by pre-cooled filter paper. They were freeze-dried and mounted onto Au folding grids for TwinMic spectromicroscope. The brightfield and differential phase contrast acquisition were supplemented by LEXRF emission maps of elements. An area of  $80\ \mu\text{m} \times 80\ \mu\text{m}$  was analysed on all samples, with a spatial resolution of  $1.2\ \mu\text{m}$ .

## 4. RESULTS

### 4.1. Immunoglobulin isolation from human serum

Prior to isolating IgG from rat sera, aware of small volumes of serum obtained from one animal and the accompanying ethical concerns, a protocol for IgG isolation from human sera was optimized, presuming that both rat and human immunoglobulin G bind with similar affinity to the chosen affinity ligand. In this work, carbonyldiimidazole (CDI) –modified monolithic convective interaction media (CIM) columns with 600 nm – 750 nm average pore radius were used for the immobilization of recombinant protein G (Reprokine, Rehovot, Israel) and recombinant protein L (Acro Biosystems, Beijing, China) following similar procedure, as described by Černigoj *et al.* for protein A immobilisation [68]. Measured dynamic binding capacity for protein G column was  $\geq 9,0$  and  $< 15$  mg/mL, with a recovery of  $\geq 90\%$ . Calculated dynamic binding capacity from elution peak for protein L column was  $\geq 9,0$  and  $< 13$  mg/mL, with a recovery of  $\geq 80\%$  (Figure 8).

At the start of the experiment, affinity and selectivity of human serum immunoglobulins (Igs) to protein G and L was compared (Figure 9). Protein G exclusively binds with high affinity to the G class of human immunoglobulins. On the other hand, protein L binds to the kappa light chains of all antibody classes. Under isocratic elution conditions, a similar elution protein profile for protein G and protein L could be obtained, with a noted absence of IgA and IgM in the protein G eluate lane (Figure 9).

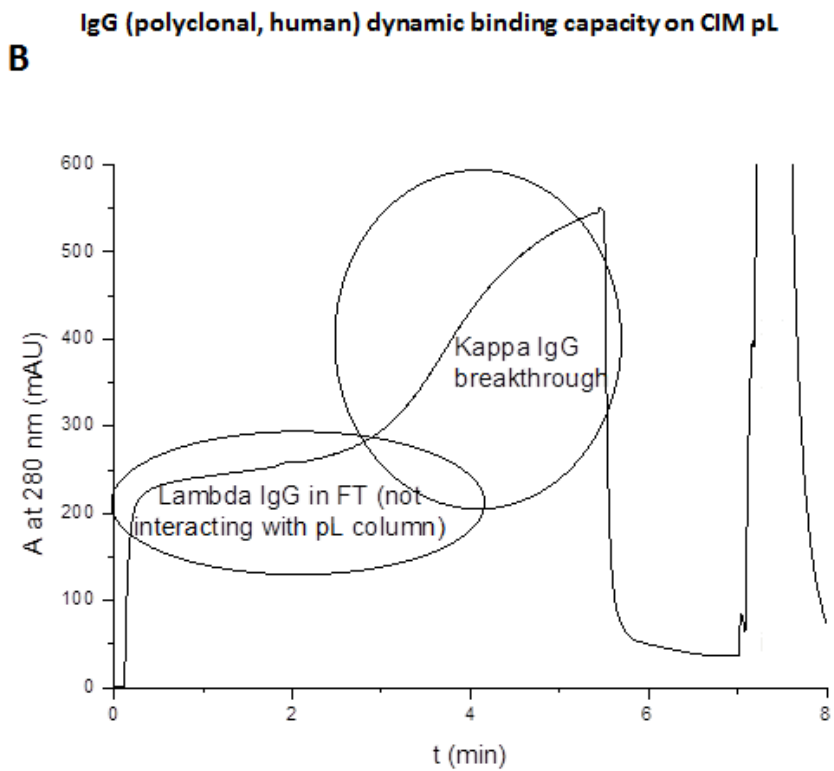
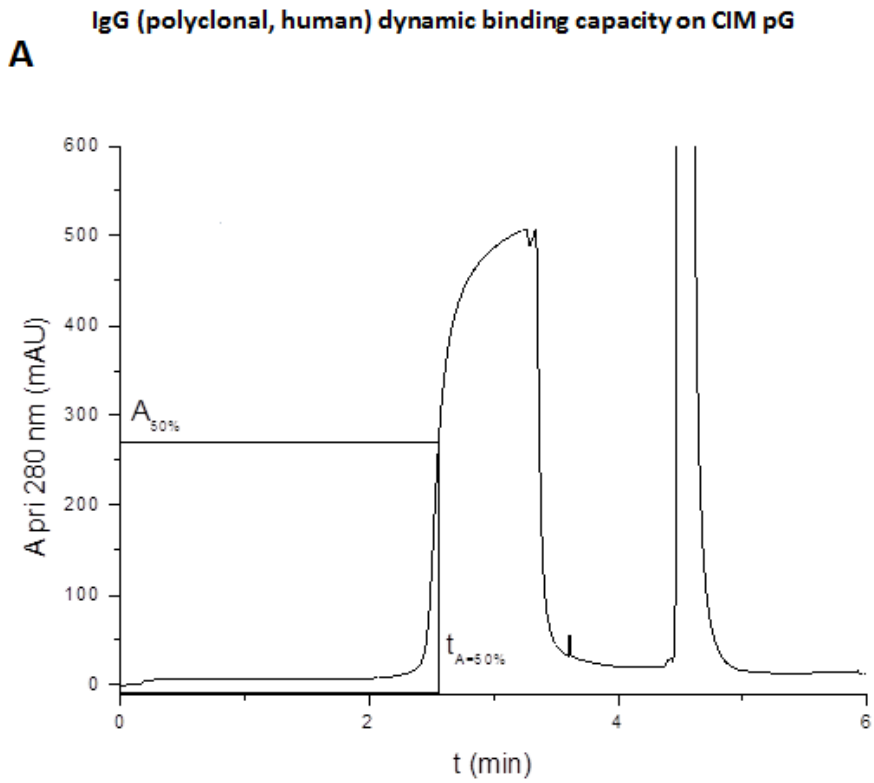


**Figure 8.** IgG dynamic binding capacities of CIM protein G (A) and protein L (B) columns.

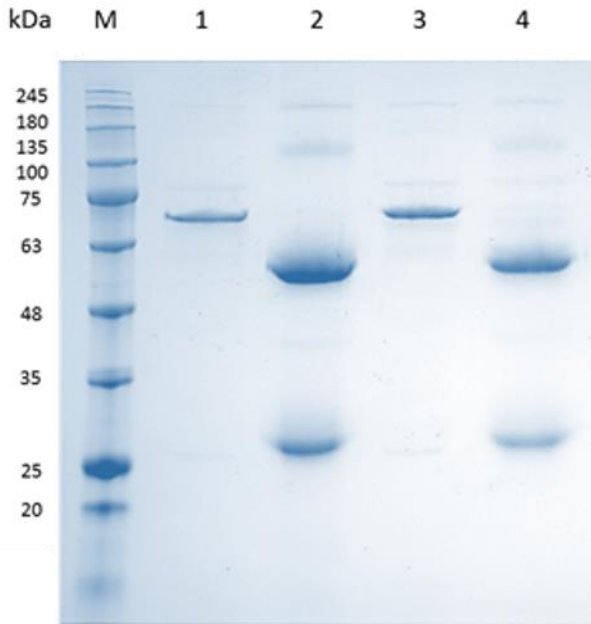


**Figure 9.** SDS PAGE of a comparison of elution patterns between CIM monoliths with immobilized protein G or L. M - Roti-Mark TRICOLOR molecular mass standard. Lanes: (1) pG flow through; (2) pG eluate; (3) pL flow through; (4) pL eluate.

Breen *et al.* optimized a fractionation scheme for fast-throughput isolation of IgM and enrichment of low-abundance proteins [42]. Here, a similar scheme for HTP isolation of IgA, IgM and IgG, using both protein G and protein L, in two distinct and successive chromatographic procedures, is presented. After the first AMC on protein G or L, the unbound proteins are collected and are later applied to the second monolithic column, protein L or G, respectively. This results in the isolation of not only all IgG subclasses (protein G), but of IgA and IgM molecules carrying kappa light chains as well (protein L) (Figure 10). In this way, a broader selection of immunoglobulin classes and subclasses can be purified simultaneously, compared to using only protein G or A for their isolation. Moreover, this experiment is a foundation for isolating IgA and IgM from rat serum, as well.

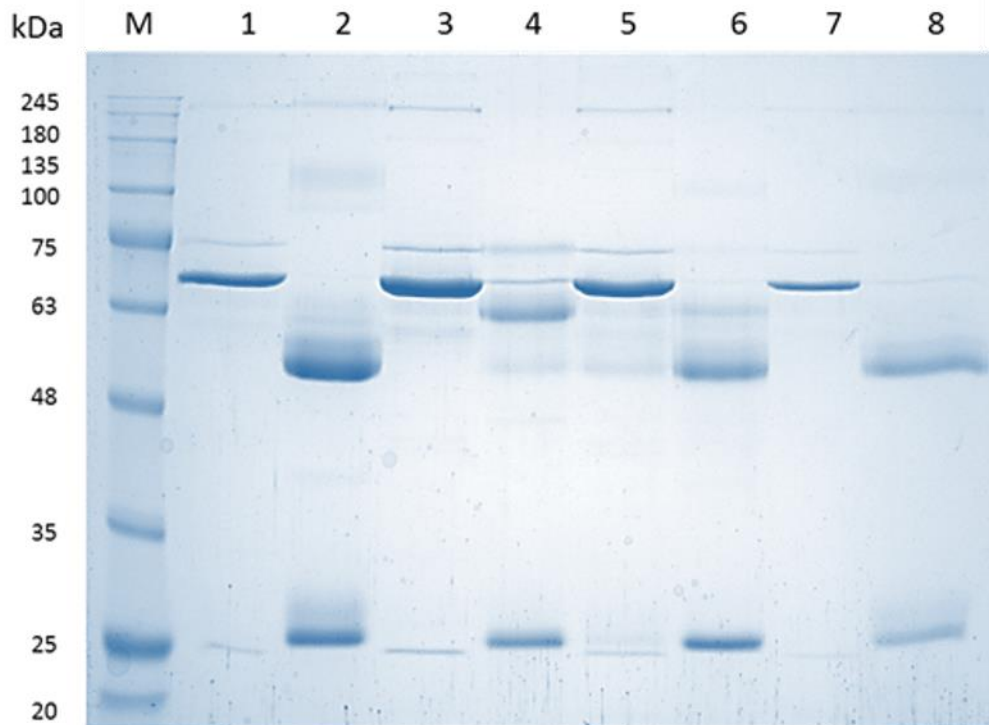


**Figure 10.** SDS PAGE of immunoglobulin A, G and M isolation using affinity monolith chromatography. Lanes marked with \* refer to the second chromatographic step. M - Roti-Mark TRICOLOR molecular mass standard. Lanes: (1) pG flow through; (2) pG eluate; (3) pL flow through\*; (4) pL eluate\*; (5) pL flow through; (6) pL eluate; (7) pG flow through\*; (8) pG eluate\*.

#### 4.1.1 Identification of isolated immunoglobulins

To evaluate whether immunoglobulin A, G and M were successfully isolated and separated, MALDI TOF mass spectrometry was used for their identification. Unbound material and the corresponding eluted fractions were loaded on an SDS PAGE gel and corresponding bands were excised: with an apparent molecular weight of about 55 kDa and 27 kDa for IgG, about 60 and 25 kDa for IgA and about 70 and 25 kDa for IgM (see Figure 10). “In gel” tryptic digestion was performed and peptides were introduced on a MALDI target plate. Mascot online search engine was used for sequence matching, allowing for 2 miscleavages and requiring a minimal accuracy of <20ppm. IgA and IgG heavy and light chains were positively identified, while in the case of IgM, only the heavy chain was recognized. This result is not surprising, considering the low amounts of IgM present in human serum, compared to the other two



examined Ig classes, and also the low visibility of IgM light chain in SDS-PAGE. Protein sequence coverage also correlates with the relative amounts of Ig classes present, with the heavy chain of IgM having the lowest coverage of only 9% (Table 3). Undoubtedly, if a larger amount of total protein in a fraction containing IgM was loaded on an acrylamide gel, the IgM light chain would be successfully identified as well. Taking into consideration the apparent molecular weight of both chains (about 70 and 25 kDa, respectively) and positive identification of the IgM heavy chain, these data are sufficient for a positive identification of this protein.

**Table 3.** MASCOT search results for human IgA, IgG and IgM after tryptic digestion.

Antibody (heavy chain)	Protein sequence coverage	Matched peptides (in red)
IgA	10%	<p>1 ASPTSPKVFV LSLCSTQPDG NVVIACLVQG FFPQEPLSVT WSESGQGVT</p> <p>51 RNFPPSQDAS GDLYTTSSQL TLPATQCLAG KSVTCHVKHY TNPSQDVTVP</p> <p>101 CPVPSTPPTP SPSTPPTPSP SCCHPRLSLH RPALEDLLLG SEANLCTILT</p> <p>151 GLRDASGVTF TWTSSGKSA VQGPPERDLC GCYSVSSVLP GCAEPWNHKG</p> <p>201 TFICTAAYPE SKTPLTATLS KSGNTRPEV HLLPPPSEEL ALNELVLTTC</p> <p>251 LARGFSPKDV LVR<b>WLQGSQE</b> <b>LPREKYLTWA</b> <b>SRQEPSQGT</b> <b>TFAVTSILRV</b></p> <p>301 AAEDWKKGDT FSCMVGHEAL PLAFTQKTID RLAGKPTHVN VSVVMAEVDG</p> <p>351 TCY</p>
IgG	23%	<p>1 ASTKGPSVFP LAPSSKSTSG GTAALGCLVK DYFPEPVTVS WNSGALTSGV</p> <p>51 HTFPAVLQSS GLYLSVVVT VPSSSLGTQT YICNVNHKPS NTKVDKKEVP</p> <p>101 KSCDKTHTCP PCPAPELLGG PSVFLFPPKP <b>KDTLMISRTP</b> <b>EVTCCVVVDVS</b></p> <p>151 <b>HEDPEVKFNW</b> <b>YVDGVEVHNA</b> <b>KTKPREEQYN</b> STYRVVSVLT VLHQDWLNGK</p> <p>201 EYKCKVSNKA <b>LPAIEKTIS</b> <b>KAKGQPREPQ</b> <b>VYTLPPSRDE</b> <b>LTKNQVSLTC</b></p> <p>251 <b>LVKGFYPSDI</b> AVEWESNGQP ENNYKTTPPV LDSDGSFFLY SKLTVDKSRW</p> <p>301 QQGNVFSCSV MHEALHNYHT QKSLSLSPGK</p>
IgM	9%	<p>1 DIQMTQSPST LSASVGDRT <b>ITCRASQSN</b> TWLAWYQQKP <b>GKAPKLLMYK</b></p> <p>51 ASSLESGVPS RFIGSGSGTE FILTISSLQP DDFATYYCQQ YNSDSKMFQ</p> <p>101 GTKVEVKGTV AAPSVFIFPP SDEQLK<b>SGTA</b> <b>SVCLLNIFY</b> <b>PREAKVQWKV</b></p> <p>151 DNALQSGNSQ ESVTEQDSKD STYLSSTILT LSKADYEK<b>HK</b> <b>VYACEVTHQG</b></p> <p>201 <b>LSSPVTKSFN</b> <b>RGEC</b></p>

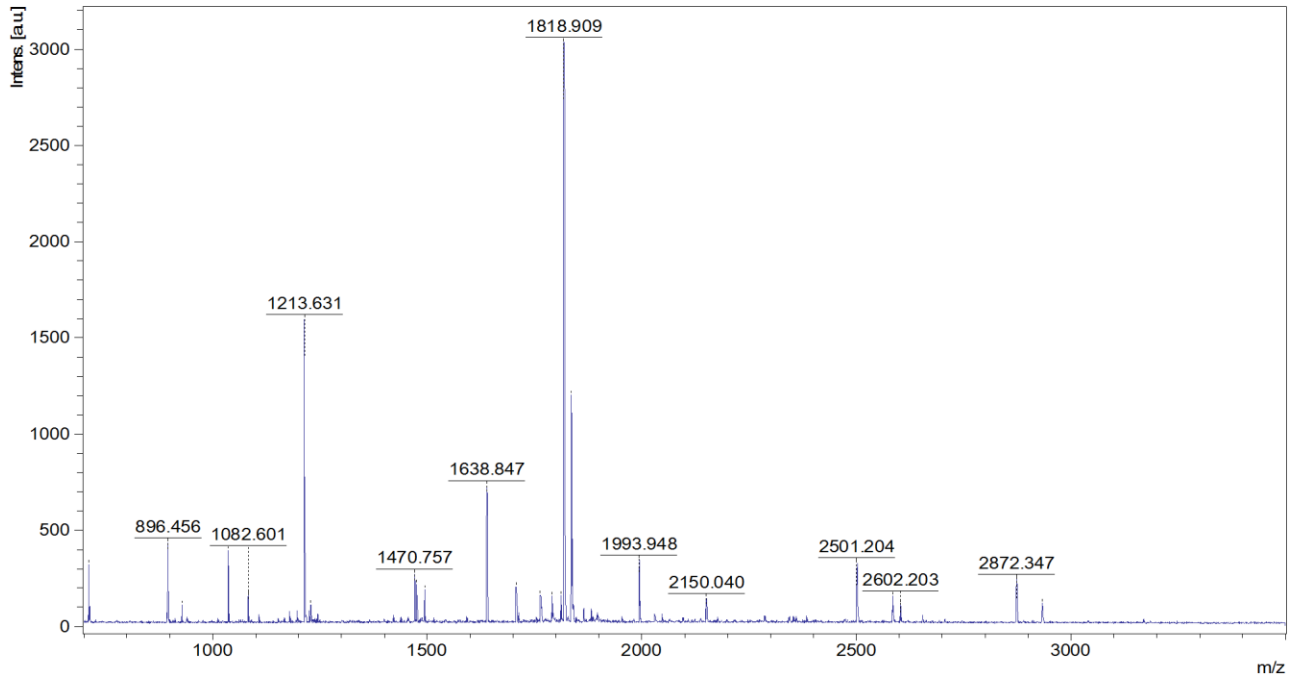


**Figure 11.** A MALDI TOF fingerprint spectrum of the human IgA heavy chain.

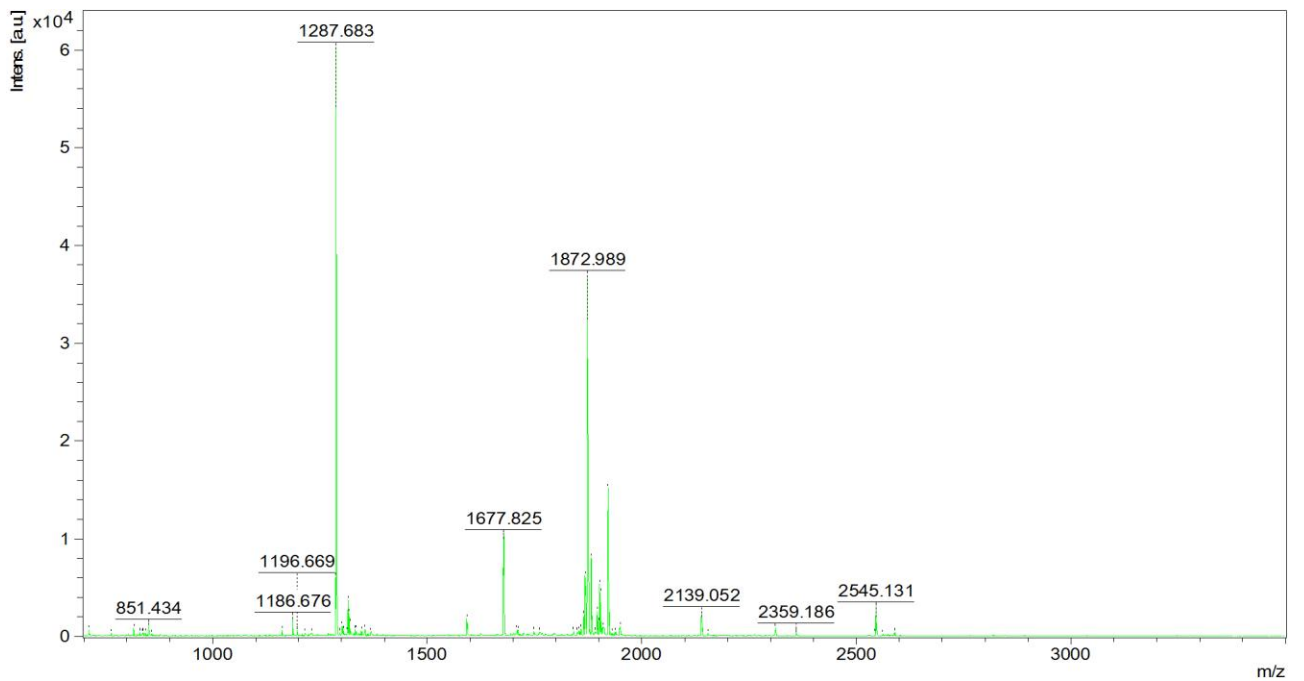


**Figure 12.** A MALDI TOF fingerprint spectrum of the human IgG heavy chain.

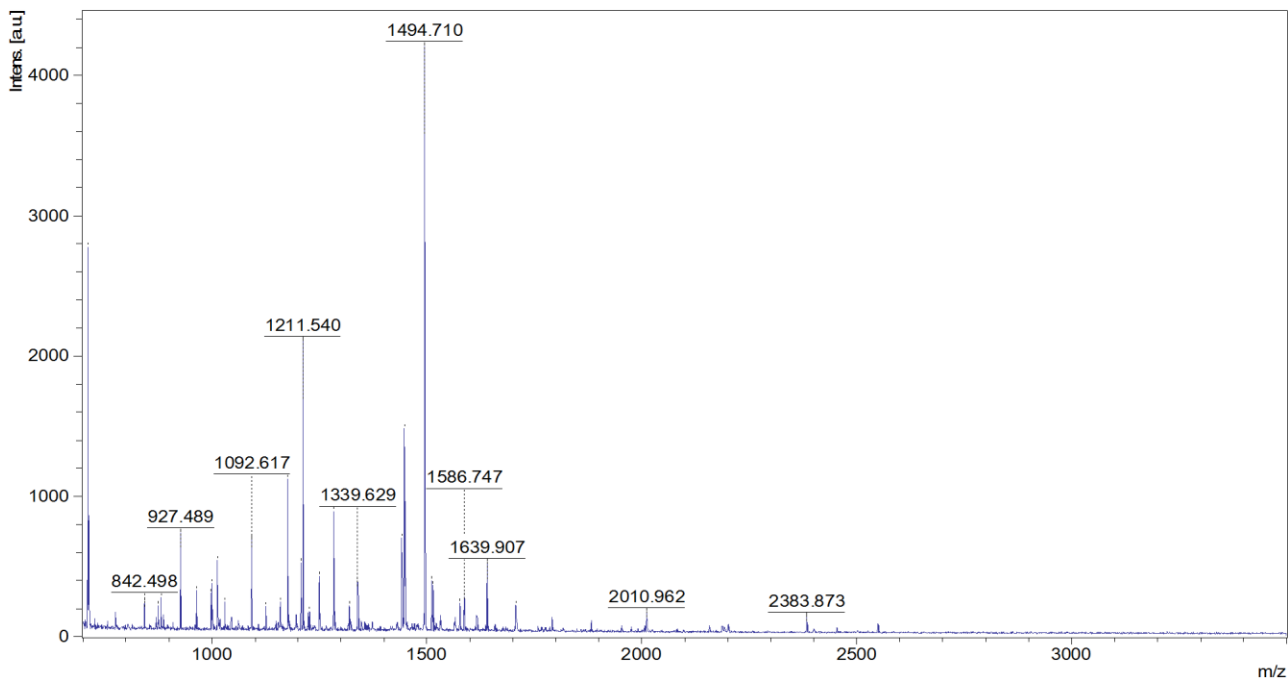


**Figure 13.** A MALDI TOF fingerprint spectrum of the human IgM heavy chain.

#### 4.1.2 High-throughput automation of immunoglobulin isolation

The continuous structure of a monolith results in high external porosity, leading to increased permeability, which lowers the back pressure to a minimum. Since high flow rates can easily be applied and analysis time can be very short, monoliths are perfect supports for HTP screening. A semi-high-throughput isolation of human fibrinogen using monolithic supports with immobilized monoclonal anti-human fibrinogen antibodies was successfully performed [69]. Another group used monoliths for HTP isolation of transferrin from human plasma by use of anti-transferrin monoclonal antibodies immobilized on monoliths [70]. Pucić *et al.* developed a 96 well-plate consisting of a monolithic stationary phase with immobilized protein G which enabled HTP isolation and analysis of human IgG [64]. Similarly, we designed a HTP 96 well-plate with mounted monolithic units with immobilized protein L (Figure 14). The average binding capacity of the column for IgG is 9.4 mg/mL. Thus, the immunoglobulin purification scheme that we present in this article can be adapted for a HTP and simultaneous Ig isolation from 96 samples. A fully automated liquid handling system, namely the Tecan Genesis WorkStation 200, is needed to perform HTP experiments using the 96 well-plate. It is a robot

for automating pipetting tasks, equipped with two arms: the liquid handler, an 8 channel pipetting arm and the robot manipulator, an arm that picks up and moves objects on the workstation. We programmed its software and adapted it to our experimental design for HTP Ig purification.

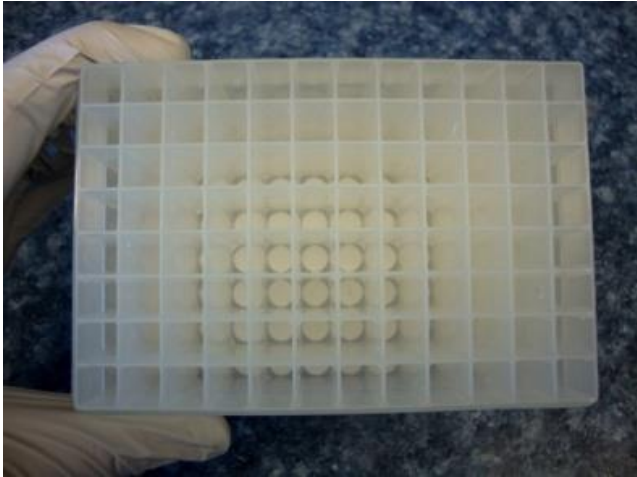


**Figure 14.** A 96-well plate with mounted small monolithic columns for HTP sample preparation (BIA Separations).

#### **4.2 IgG isolation from rat serum**

Once the protocol for the isolation of human IgG was established, the same conditions were used to isolate IgG from rat serum in order to look at the changes in IgG sialylation patterns in osteoporotic rats. Firstly, a method for rat IgG isolation was optimized using healthy control samples. Rat serum diluted in equilibration buffer was injected onto a monolithic column with immobilized protein L. In parallel, and under the same conditions, commercially available human IgG and IgM were loaded onto the column as control samples, both separately and as a 1:1 mixture. After extensive washing, proteins were eluted in glycine, pH 2. As expected, rat IgG binds to protein L with high affinity since almost 100% of rat immunoglobulins contain kappa light chains (Table 4). Two distinct bands were noted at a molecular weight of around 50 kDa, corresponding to different rat IgG subclasses, namely IgG1, IgG2a, IgG2b and IgG2c (Figure 15).

**Table 4.** Immunoglobulin concentrations in rat and human.

Species	IgG (mg/ml)	IgM (mg/ml)	IgA (mg/ml)	% $\kappa/\lambda$
Rat	Total: 5-7	0.6-1.0	0.1-0.2	99/1
	IgG1: ~5.85			
	IgG2a: 6.7 - 8.0			
	IgG2b: ca. 0.9			
	IgG2c: ~2.6			
Human	Total: 7.5-22	0.2-2.8	0.5-3.6	67/33
	IgG1: 5 - 9.5			
	IgG2: 2.2 - 4.8			
	IgG3: 0.4 - 1.0			
	IgG4: 0.1 - 0.6			

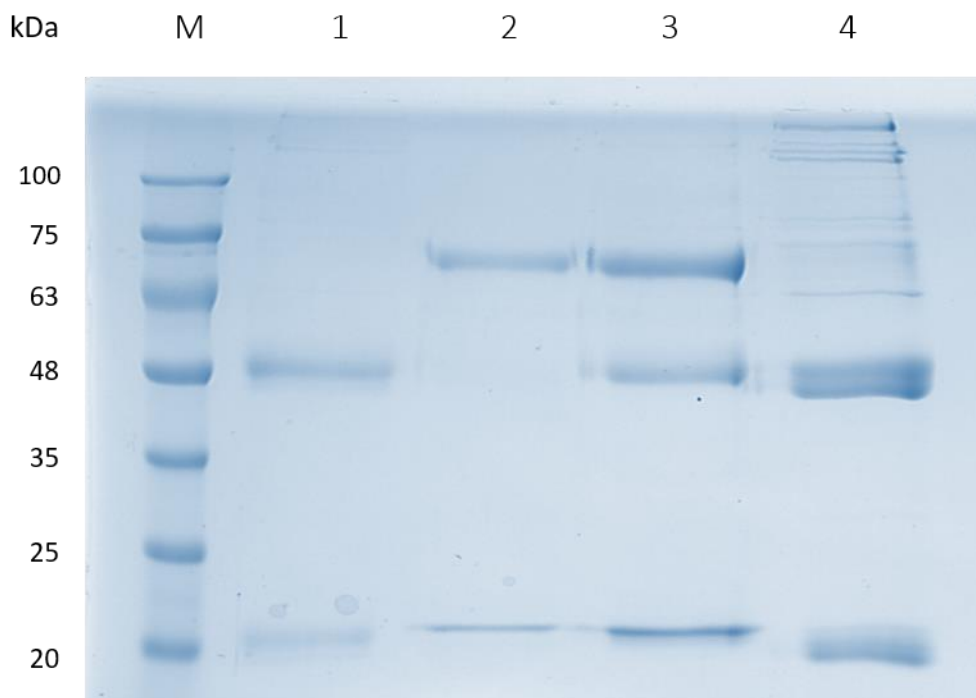


**Figure 15.** CIM monolith with immobilized pL binds rat IgG. M - Roti-Mark TRICOLOR molecular mass standard. Lanes: (1) control, human IgG; (2) control, human IgM; (3) control, human IgG and IgM; (4) pL eluate.

An experimental rat model was set up, and following groups of animals were analysed: healthy control, sham control (ovaries were exteriorized and repositioned intact), ovariectomized control (OVX), OVX supplemented with synthetic zeolite, OVX supplemented with natural clinoptilolite and OVX supplemented with micro activated clinoptilolite (Table 2). Using the affinity monolith chromatography protocol previously optimized for 200  $\mu$ L of healthy rat serum, IgG was isolated from three animals from each group, yielding triplicate samples for validation and statistical purposes. Although the obtained eluate contained a mixture of proteins rather than pure IgG, its concentration, compared to other eluted proteins, is extremely high and sufficient for both in-gel and in-solution digestion followed by successful analysis and protein validation on a mass spectrometer. An example of IgG isolation from six different animals, each belonging to a different group, is shown in Figure 15. Following 6 figures (Figure 16-21) show chromatograms of AMC methods that resulted in rat IgG isolation from three control and three treated samples, respectively. Protocol was identical to the one previously described for isolating IgG from human serum.

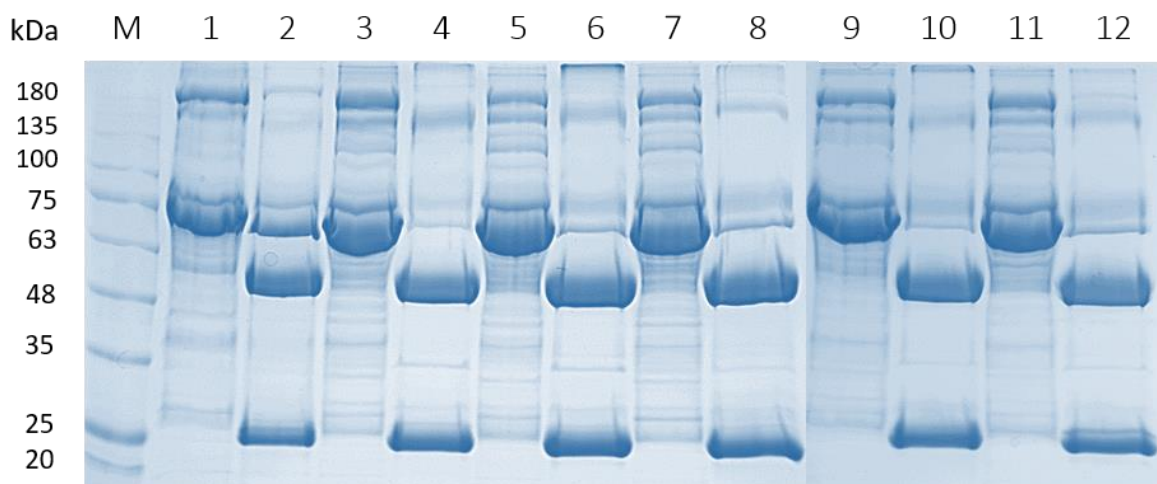


**Figure 16.** IgG isolation from rat sera. CIM monolith with immobilized pL binds rat IgG. M - Roti-Mark TRICOLOR molecular mass standard. Lanes: (1) group 0 flowthrough (FT); (2) group 0 eluate (E); (3) group 1 FT; (4) group 1 E; (5) group 2 FT; (6) group 2 E; (7) group 3 FT; (8) group 3 E; (9) group 4 FT; (10) group 4 E; (11) group 5 FT; (12) group 5 E.

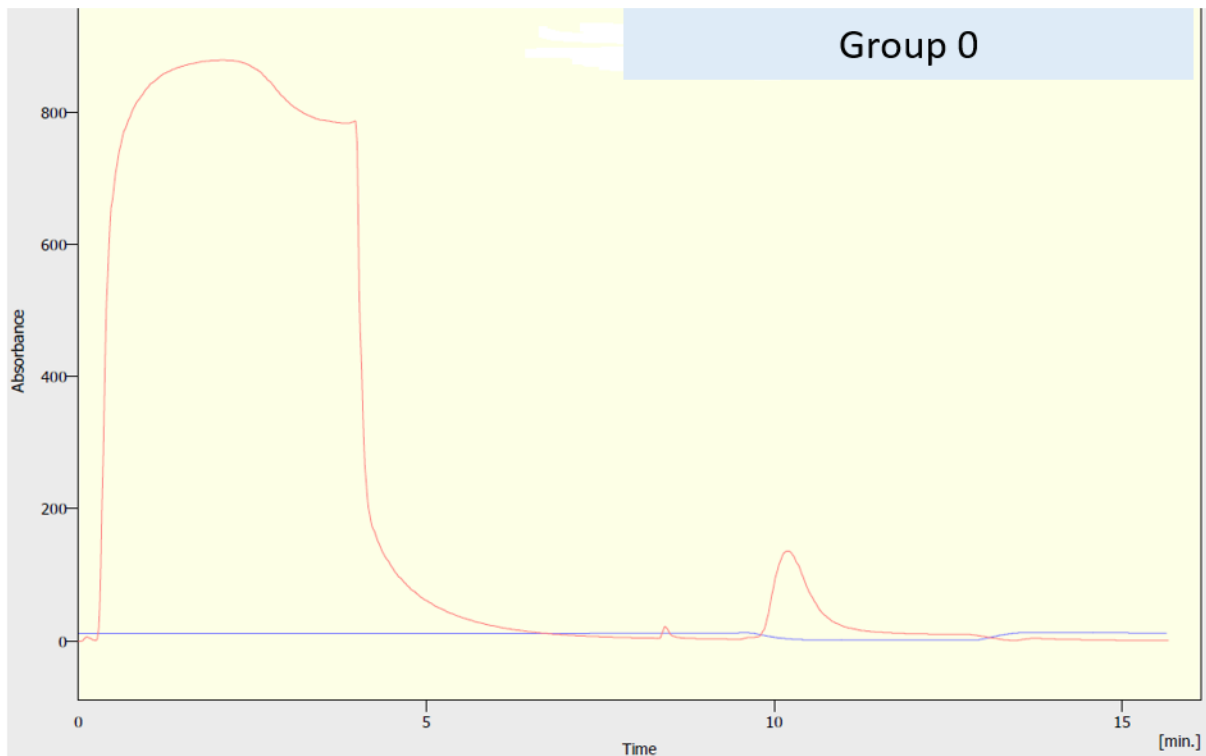


**Figure 17.** A chromatogram of IgG elution, sample: 0-1, healthy control. The first peak represents unbound material, while the second, smaller peak, represents proteins bound and then eluted from the column (IgG).

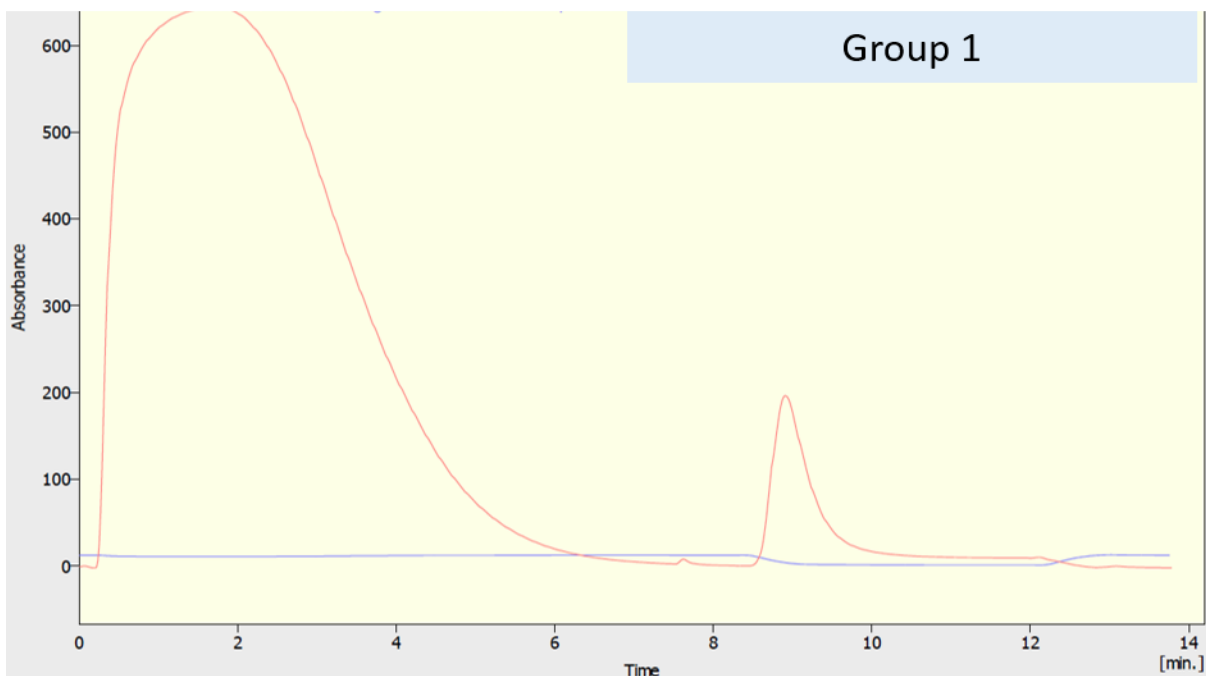


**Figure 18.** A chromatogram of IgG elution, sample: 1-1, sham. The first peak represents unbound material, while the second, smaller peak, represents proteins bound and then eluted from the column (IgG).

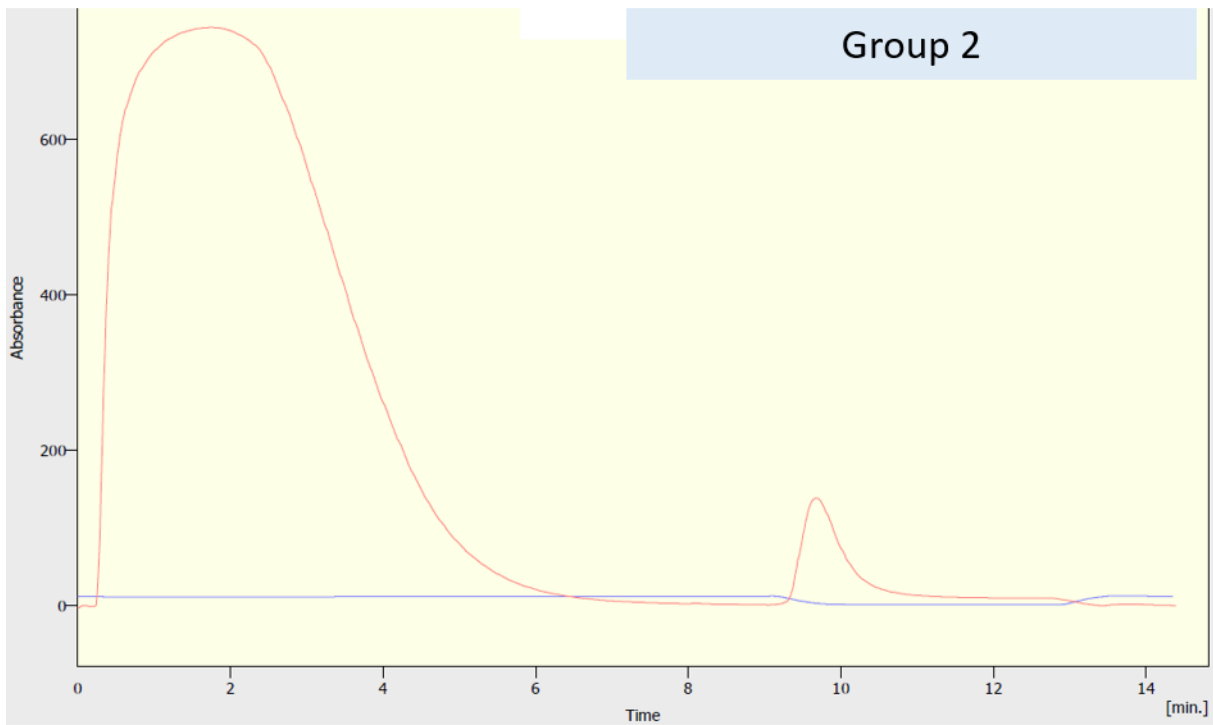


**Figure 19.** A chromatogram of IgG elution, sample: 2-1, OVX control. The first peak represents unbound material, while the second, smaller peak, represents proteins bound and then eluted from the column (IgG).

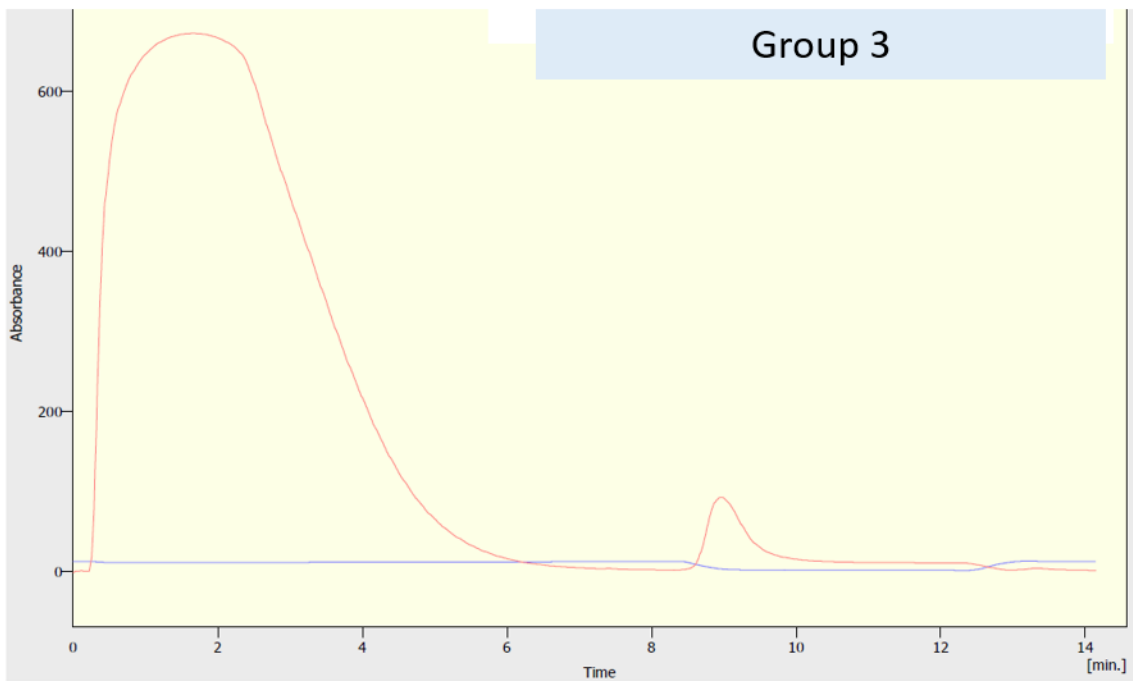


**Figure 20.** A chromatogram of IgG elution, sample: 3-1, zeolite A. The first peak represents unbound material, while the second, smaller peak, represents proteins bound and then eluted from the column (IgG).



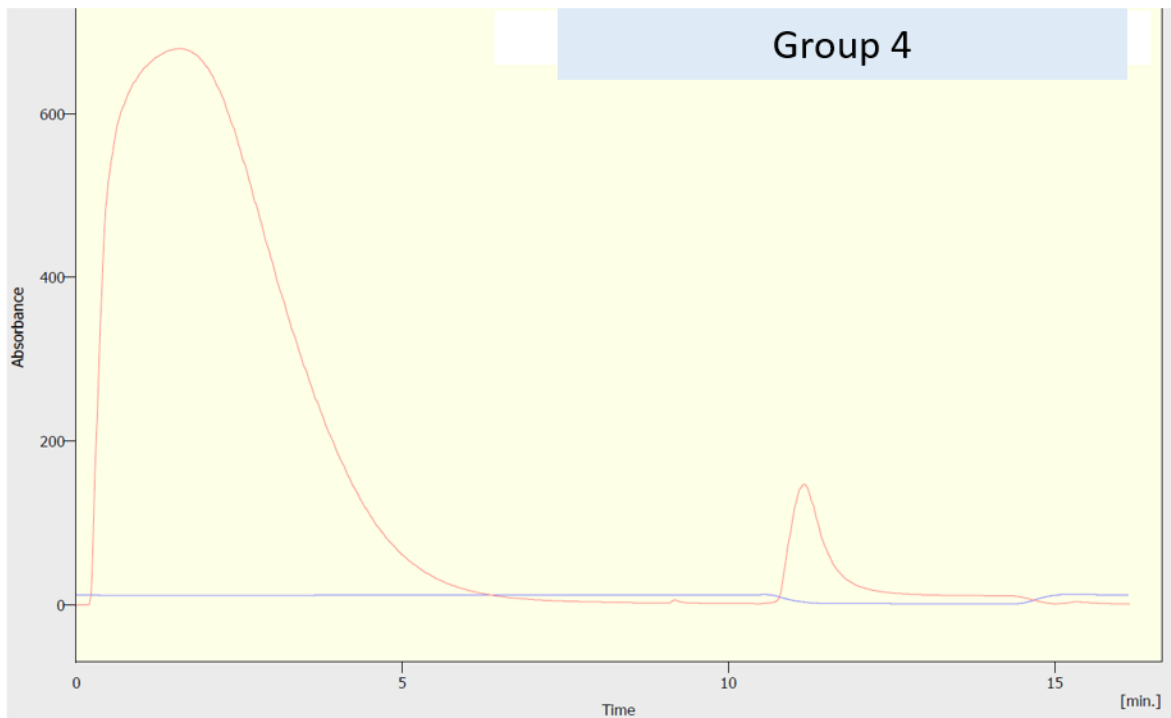


**Figure 21.** A chromatogram of IgG elution, sample: 4-1, clinoptilolite. The first peak represents unbound material, while the second, smaller peak, represents proteins bound and then eluted from the column (IgG).

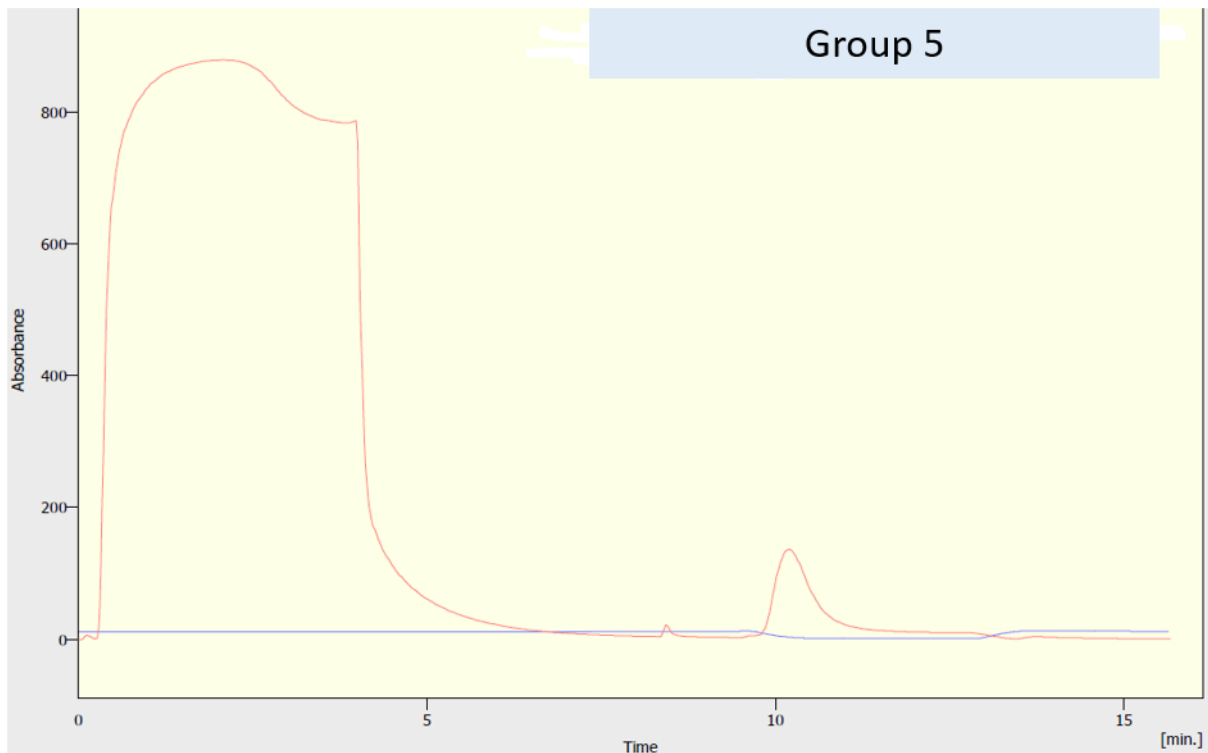


**Figure 22.** A chromatogram of IgG elution, sample: 5-1, PMA clinoptilolite. The first peak represents unbound material, while the second, smaller peak, represents proteins bound and then eluted from the column (IgG).

#### 4.2.1 Validation of rat IgG isolation

Affinity chromatography on a serum sample using protein L as a ligand is expected to result in successful purification of all immunoglobulins containing kappa light chains, if performed under the right conditions. Gel electrophoretic separation of proteins by their molecular weight serves as a further chromatographic step that confirms Ig isolation. As an extra validation step, mass spectrometry was used to confirm that the protein isolated from rat serum and excised from an SDS PAGE gel (Mw ~ 50 kDa) is indeed immunoglobulin G. After “in gel” tryptic digestion of IgG isolated from three animals from each of the six groups, peptides were spotted onto a MALDI anchor chip plate and samples were analysed on a MALDI TOF instrument. Mascot online search engine was used for sequence matching, allowing for 2 miscleavages and requiring a minimal accuracy of <25ppm.

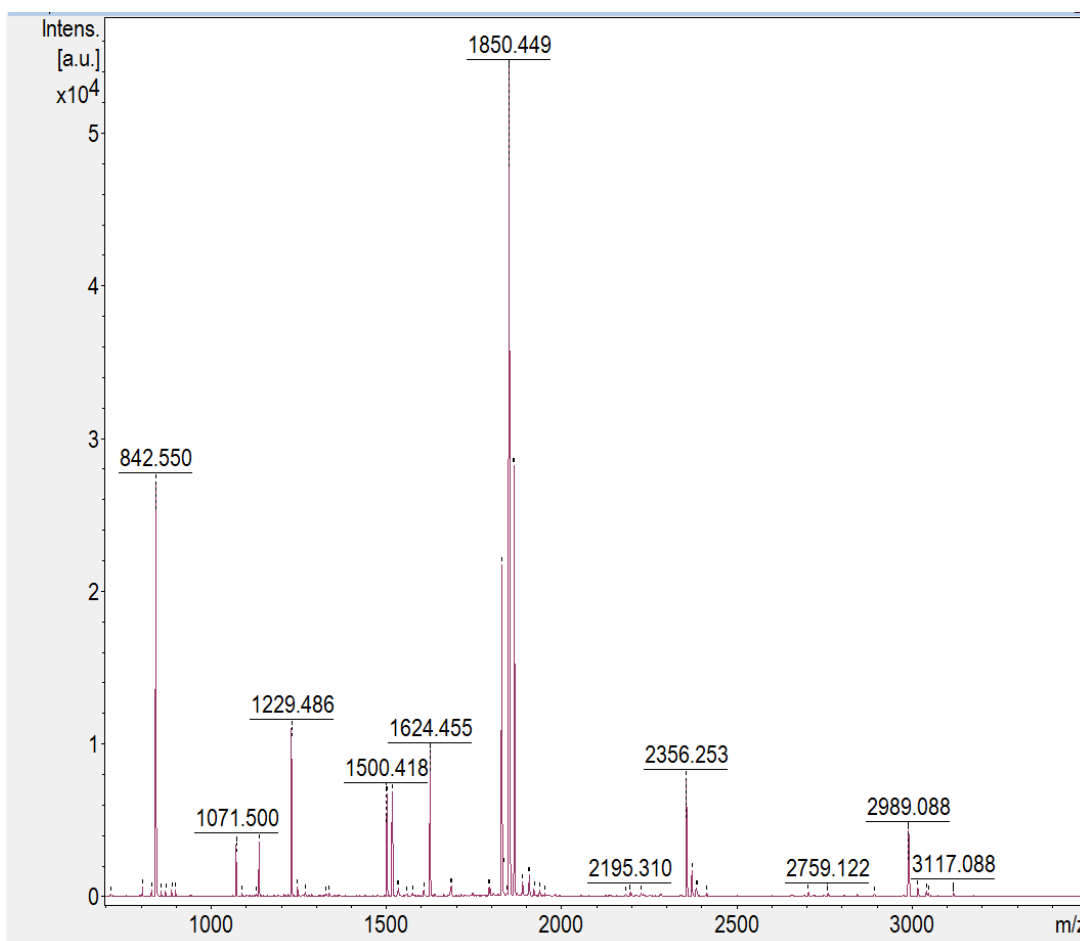


**Figure 23.** A MALDI TOF fingerprint spectrum of the rat IgG heavy chain.

Figure 23 represents an example of a rat IgG m/z spectrum with a Mascot score of 68 and protein sequence coverage of 48%. Matched peptides are shown in red.

1	AETTAPSVYP	LAPGTALKSN	SMVTLGCLVK	GYFPEPVTVT	WNSGALSSGV
51	HTFPAVLQSG	LYTLTSSVTV	PSSTWSSQAV	TCNVAHPASS	TKVDKKIVPR
101	<b>ECNPCGCTGS</b>	<b>EVSSVFIFPP</b>	<b>KT</b> KDVLITIL	<b>TPK</b> VTCVVVD	<b>ISQ</b> NDPEVRF
151	<b>SW</b> FIDDVEVH	<b>TAQ</b> THAPEKQ	SNSTLR <b>SVSE</b>	<b>LPIV</b> HRDWLN	<b>GKIF</b> KCKVNS
201	<b>GA</b> FPAPIEKS	<b>IS</b> KPEGIPRG	<b>PQ</b> VYTMAPPK	<b>EEM</b> TQSQVSI	<b>TC</b> MVKGFPYP
251	<b>DIY</b> TEWKMNG	QPQENYKNIP	<b>P</b> TMDIDGSYF	<b>LYS</b> KLNVKKE	TWQQGNTFTC
301	SVLHEGLHNS	HTEKSLSHSP	GK		

Since MS identification of IgG was effective for all samples, and not to list all gathered spectra, Figure 24 represents a comparison of MALDI TOF spectra of trypsinized rat IgG from all analysed samples, namely one animal from each group (0-6). Clearly the peak pattern is overall very similar, confirming that IgG was successfully identified in all samples, validating the efficiency of our purification method.

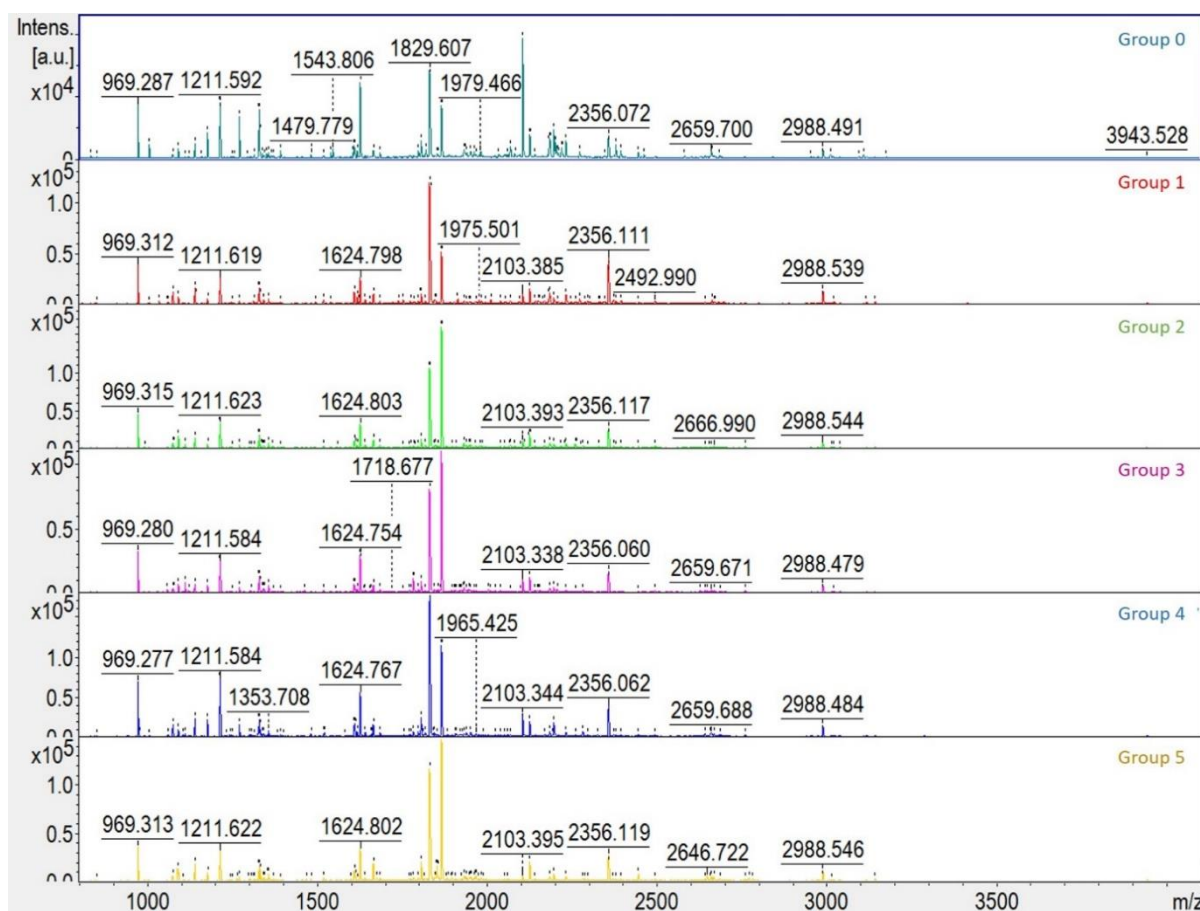


**Figure 24.** A comparison of MALDI TOF spectra of trypsinized rat IgG peptides from all analysed groups (0-6).

### 4.3 Rat serum IgG glycosylation

In order to examine the effects of zeolite on IgG glycosylation in osteoporosis, we analysed N-linked glycans enzymatically released from the protein. Representative sampling and adequate sample preparation are key factors for successful performance of further steps in any analysis, as well as for correct data interpretation- When it comes to glycan analysis, it is of great importance to optimize a protocol for derivatization of sialic acid, since this molecule is known to easily hydrolyse from the glycan moiety that it is attached to. Glycan carboxyethylation reaction leads to sialic acid stabilization in MALDI TOF reflectron mode measurements. N-Acetylneuraminic acid (NeuAc) residues are modified depending on their linkage positions. 2,6-linked NeuAc is ethyl esterified at the carboxyl group, while 2,3-linked NeuAc forms an internal lactone. Unmodified NeuAc residues have a mass of 291.10 Da, while the 2,6-linked and 2,3-linked NeuAc, after the derivatization reaction, have masses of 319.13 Da and 273.08 Da, respectively.

To the author's knowledge, this is the first semiquantitative analysis of rat's IgG glycome. We successfully identified sialic acid signals in all of our samples, and a comparison of spectra of glycans released from all analysed groups (0-6) can be found in Figure 25. Overall m/z values and signal intensities are similar throughout all spectra, since possible changes in IgG glycan composition are expected to be minute, and thus not easily detected. It has to be noted that the presented assay is a semi quantitative one, and we can only judge the amount of sialic acid (or any other glycan moieties) present in a sample by peak intensity. Moreover, because of variations introduced during sample preparation, especially cotton HILIC for which pipette tips were manually filled with cotton, there is a discrepancy in peak intensities throughout all samples. To be able to give a quantitative evaluation, we compared the ratio between the main reference peak (1485 Da), which is the peak with the most intensity in all samples, to other peaks (Figure 25). An in depth analysis of each glycan MS spectrum revealed various glycoforms to be present, and they are all represented in Figures 26-31, along with their corresponding tables listing MALDI TOF measured glycan experimental masses, glycans' exact glycoform mass, the difference between experimental and glycoform masses expressed in Daltons, and the suggested glycan structures in the sample (Tables 5-10). Experimental mass is the mass measured on a mass spectrometer during an experiment and it does not represent the actual mass of the analysed molecule. When measuring glycan masses, one has to take into account sodium adducts that get formed from the addition of NaOH during the glycan enrichment process (22.989 Da). Next to that, the derivative mass of the free reducing end has

to be noted (18.011 Da). Finally, since sialic acid residues were carboxyethylated during sample preparation, when investigating potential sialic acid peaks, another 273.08 Da or 319.13 Da have to be accounted for, depending on the linkage of NeuAc. Thus, the difference between the exact glycoform mass and the experimental mass is expressed in  $\Delta$  Da.

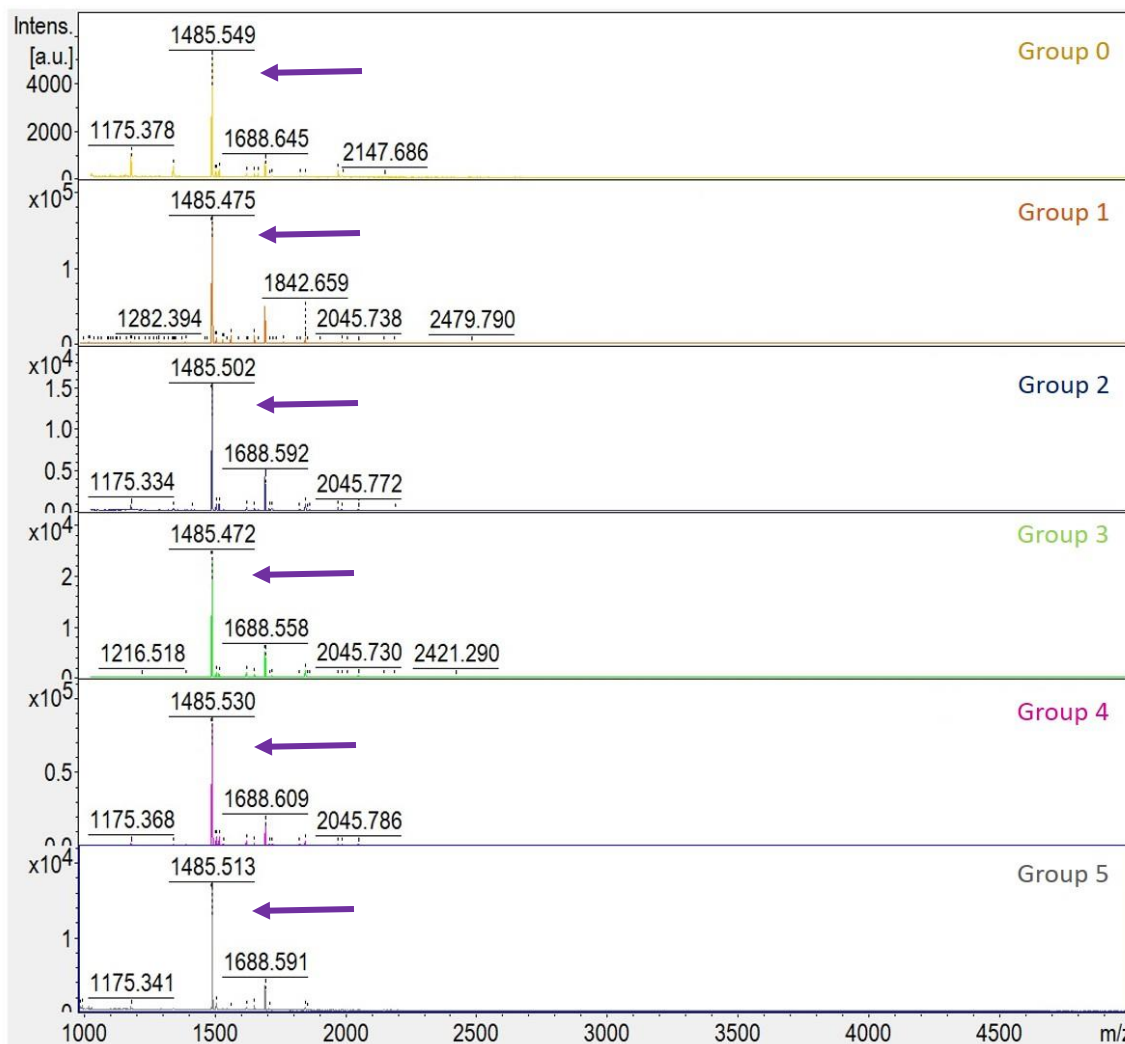


**Figure 25.** A comparison of MALDI TOF spectra of glycans released from all analysed groups (0-6) clearly showing the presence of a master reference peak across all spectra (1485 Da), marked with an arrow.

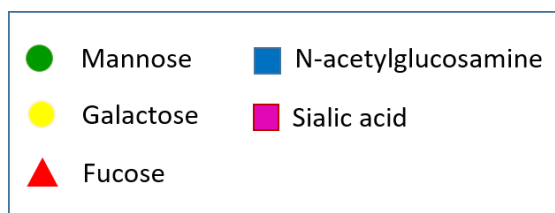


**Figure 26.** Glycan legend

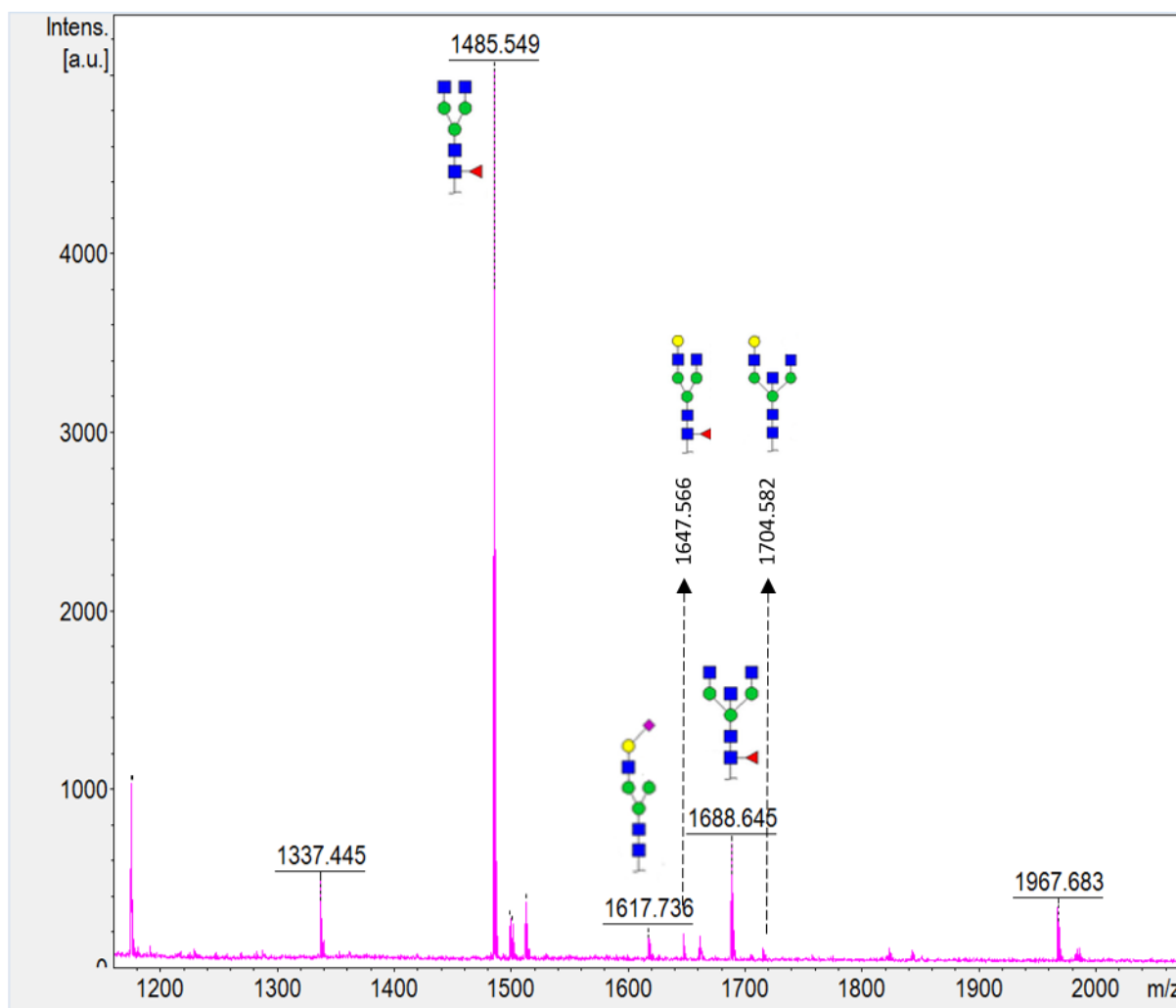


**Figure 27.** MALDI TOF spectrum of glycans released from rat IgG (group 0 – control).

**Table 5.** A list of MALDI TOF measured glycan experimental masses, glycans' exact glycoform mass, the difference between experimental and glycoform masses expressed in Daltons, and the suggested glycan structures for samples from the control group (0).

**Control N-glycans (group 0)**

Experimental mass (m/z)	Glycoform mass (m/z)	Glycan structure	$\Delta$ mass (Dalton)
1485.549	1444.534	(HexNAc) <sub>2</sub> (Deoxyhexose) <sub>1</sub> + (Man) <sub>3</sub> (GlcNAc) <sub>2</sub>	-0.015
1617.736	1257.449	(NeuAc $\alpha$ 2-6) (Hex) <sub>1</sub> (HexNAc) <sub>1</sub> + (Man) <sub>3</sub> (GlcNAc) <sub>2</sub>	-0.157

1647.556	1606.587	(Hex) <sub>1</sub> (HexNAc) <sub>2</sub> (Deoxyhexose) <sub>1</sub> + (Man) <sub>3</sub> (GlcNAc) <sub>2</sub>	-0.032
1688.645	1647.613	(HexNAc) <sub>3</sub> (Deoxyhexose) <sub>1</sub> + (Man) <sub>3</sub> (GlcNAc) <sub>2</sub>	0.032
1704.582	1663.608	(Hex) <sub>1</sub> (HexNAc) <sub>3</sub> + (Man) <sub>3</sub> (GlcNAc) <sub>2</sub>	0.023

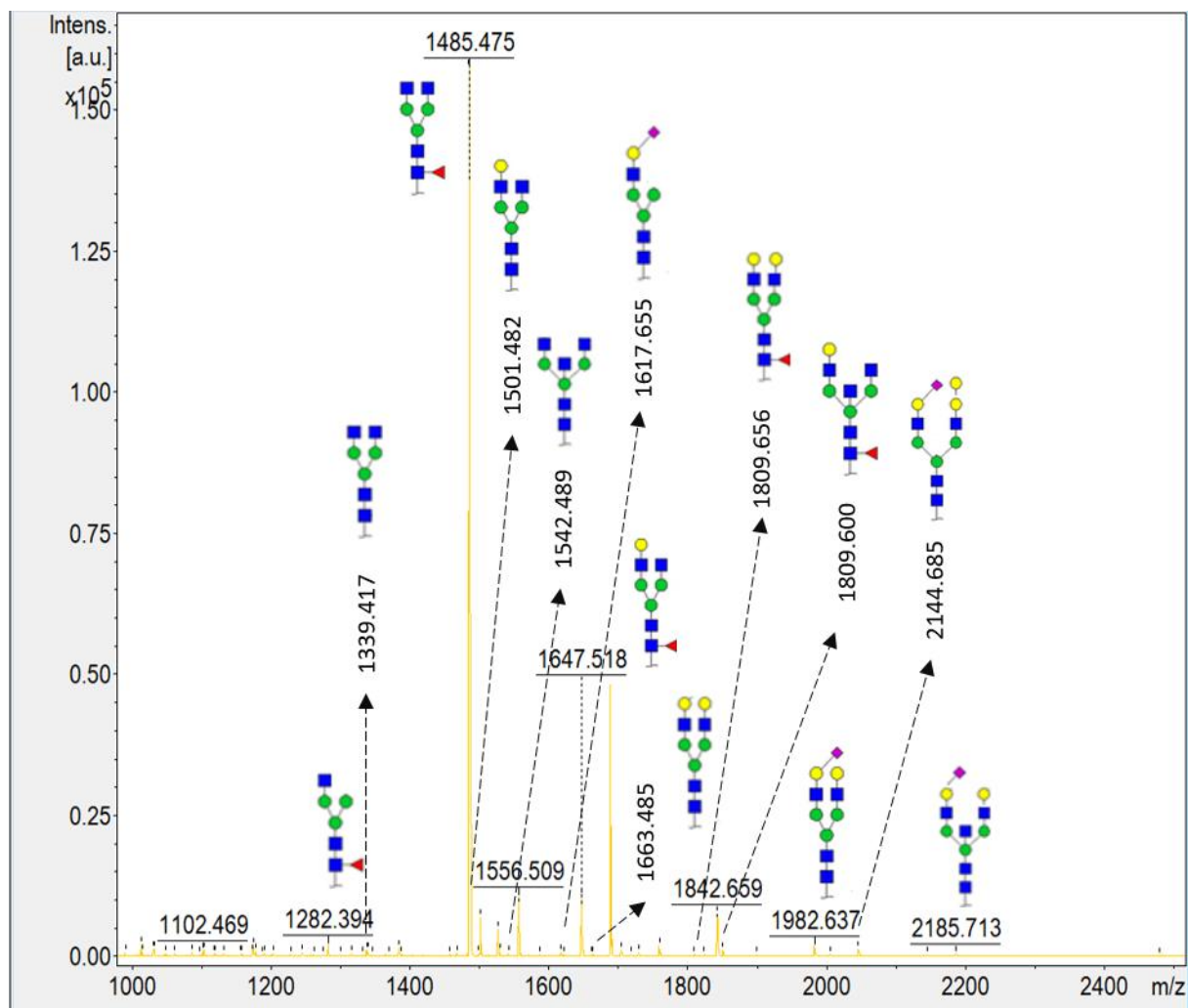


**Figure 28.** MALDI TOF spectrum of glycans released from rat IgG (group 1 – sham operated).

**Table 6.** A list of MALDI TOF measured glycan experimental masses, glycans' exact glycoform mass, the difference between experimental and glycoform mass expressed in Daltons, and the suggested glycan structure for samples from the sham group (1).

**Sham operated N-glycans (group 1)**

<b>Experimental mass (m/z)</b>	<b>Glycoform mass (m/z)</b>	<b>Glycan structure</b>	<b><math>\Delta</math>mass (Dalton)</b>
1282.394	1241.455	(HexNAc) <sub>1</sub> (Deoxyhexose) <sub>1</sub> + (Man) <sub>3</sub> (GlcNAc) <sub>2</sub>	-0.06
1339.417	1298.476	(HexNAc) <sub>2</sub> + (Man) <sub>3</sub> (GlcNAc) <sub>2</sub>	-0.058
1485.475	1444.534	(HexNAc) <sub>2</sub> (Deoxyhexose) <sub>1</sub> + (Man) <sub>3</sub> (GlcNAc) <sub>2</sub>	-0.058
1501.459	1460.529	(Hex) <sub>1</sub> (HexNAc) <sub>2</sub> + (Man) <sub>3</sub> (GlcNAc) <sub>2</sub>	-0.069
1542.489	1501.555	(HexNAc) <sub>3</sub> + (Man) <sub>3</sub> (GlcNAc) <sub>2</sub>	-0.065
1617.655	1257.449	(NeuAc $\alpha$ 2-6) (Hex) <sub>1</sub> (HexNAc) <sub>1</sub> + (Man) <sub>3</sub> (GlcNAc) <sub>2</sub>	0.076
1647.518	1606.587	(Hex) <sub>1</sub> (HexNAc) <sub>2</sub> (Deoxyhexose) <sub>1</sub> + (Man) <sub>3</sub> (GlcNAc) <sub>2</sub>	-0.068
1663.485	1622.582	(Hex) <sub>2</sub> (HexNAc) <sub>2</sub> + (Man) <sub>3</sub> (GlcNAc) <sub>2</sub>	-0.096
1809.565	1768.64	(Hex) <sub>2</sub> (HexNAc) <sub>2</sub> (Deoxyhexose) <sub>1</sub> + (Man) <sub>3</sub> (GlcNAc) <sub>2</sub>	-0.074
1850.600	1809.666	(Hex) <sub>1</sub> (HexNAc) <sub>3</sub> (Deoxyhexose) <sub>1</sub> + (Man) <sub>3</sub> (GlcNAc) <sub>2</sub>	-0.065
1982.637	1622.582	(NeuAc $\alpha$ 2-6)(Hex) <sub>2</sub> (HexNAc) <sub>2</sub> + (Man) <sub>3</sub> (GlcNAc) <sub>2</sub>	-0.074
2144.685	1784.634	(NeuAc $\alpha$ 2-6)(Hex) <sub>3</sub> (HexNAc) <sub>2</sub> + (Man) <sub>3</sub> (GlcNAc) <sub>2</sub>	-0.078
2185.713	1825.661	(NeuAc $\alpha$ 2-6)(Hex) <sub>2</sub> (HexNAc) <sub>3</sub> + (Man) <sub>3</sub> (GlcNAc) <sub>2</sub>	-0.077



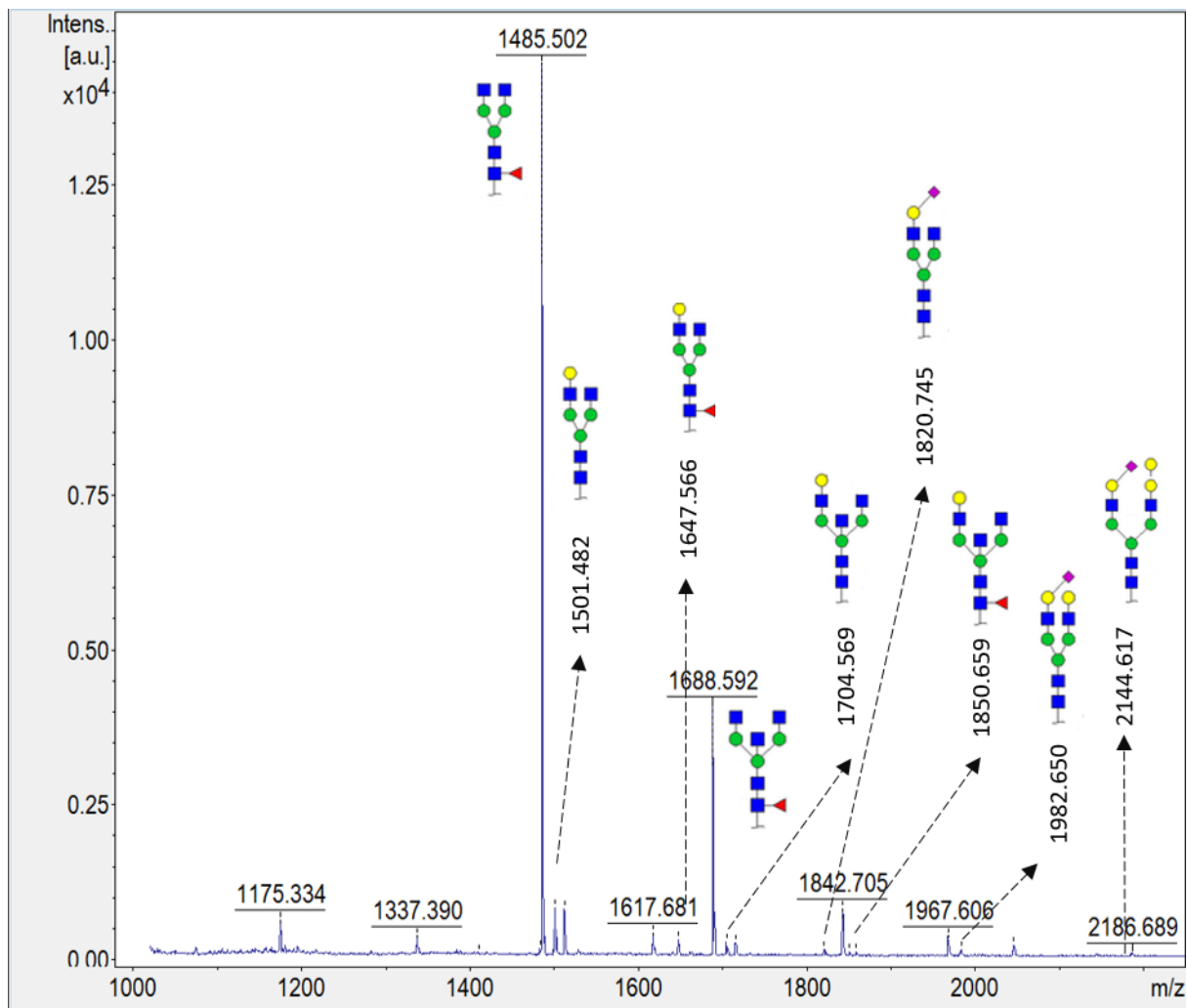


**Figure 29.** MALDI TOF spectrum of glycans released from rat IgG (group 2 – OVX).

**Table 7.** A list of MALDI TOF measured glycan experimental masses, glycans' exact glycoform mass, the difference between experimental and glycoform mass expressed in Daltons, and the suggested glycan structure for samples from the OVX group (2).

#### OVX N-glycans (group 2)

Experimental mass (m/z)	Glycoform mass (m/z)	Glycan structure	$\Delta$ mass (Dalton)
1485.502	1444.534	(HexNAc) <sub>2</sub> (Deoxyhexose) <sub>1</sub> + (Man) <sub>3</sub> (GlcNAc) <sub>2</sub>	-0.061
1501.482	1460.529	(Hex) <sub>1</sub> (HexNAc) <sub>2</sub> + (Man) <sub>3</sub> (GlcNAc) <sub>2</sub>	-0.064
1647.566	1606.587	(Hex) <sub>1</sub> (HexNAc) <sub>2</sub> (Deoxyhexose) <sub>1</sub> + (Man) <sub>3</sub> (GlcNAc) <sub>2</sub>	-0.053
1688.592	1647.613	(HexNAc) <sub>3</sub> (Deoxyhexose) <sub>1</sub> + (Man) <sub>3</sub> (GlcNAc) <sub>2</sub>	-0.053

1704.569	1663.608	$(\text{Hex})_1 (\text{HexNAc})_3 + (\text{Man})_3 (\text{GlcNAc})_2$	-0.069
1820.745	1460.529	$(\text{NeuAc } \alpha 2-6)(\text{Hex})_1 (\text{HexNAc})_2 + (\text{Man})_3 (\text{GlcNAc})_2$	0.067
1850.659	1809.666	$(\text{Hex})_1 (\text{HexNAc})_3 (\text{Deoxyhexose})_1 + (\text{Man})_3 (\text{GlcNAc})_2$	-0.084
1982.650	1622.582	$(\text{NeuAc } \alpha 2-6)(\text{Hex})_2 (\text{HexNAc})_2 + (\text{Man})_3 (\text{GlcNAc})_2$	-0.051
2144.617	1784.634	$(\text{NeuAc } \alpha 2-6)(\text{Hex})_3 (\text{HexNAc})_2 + (\text{Man})_3 (\text{GlcNAc})_2$	-0.136

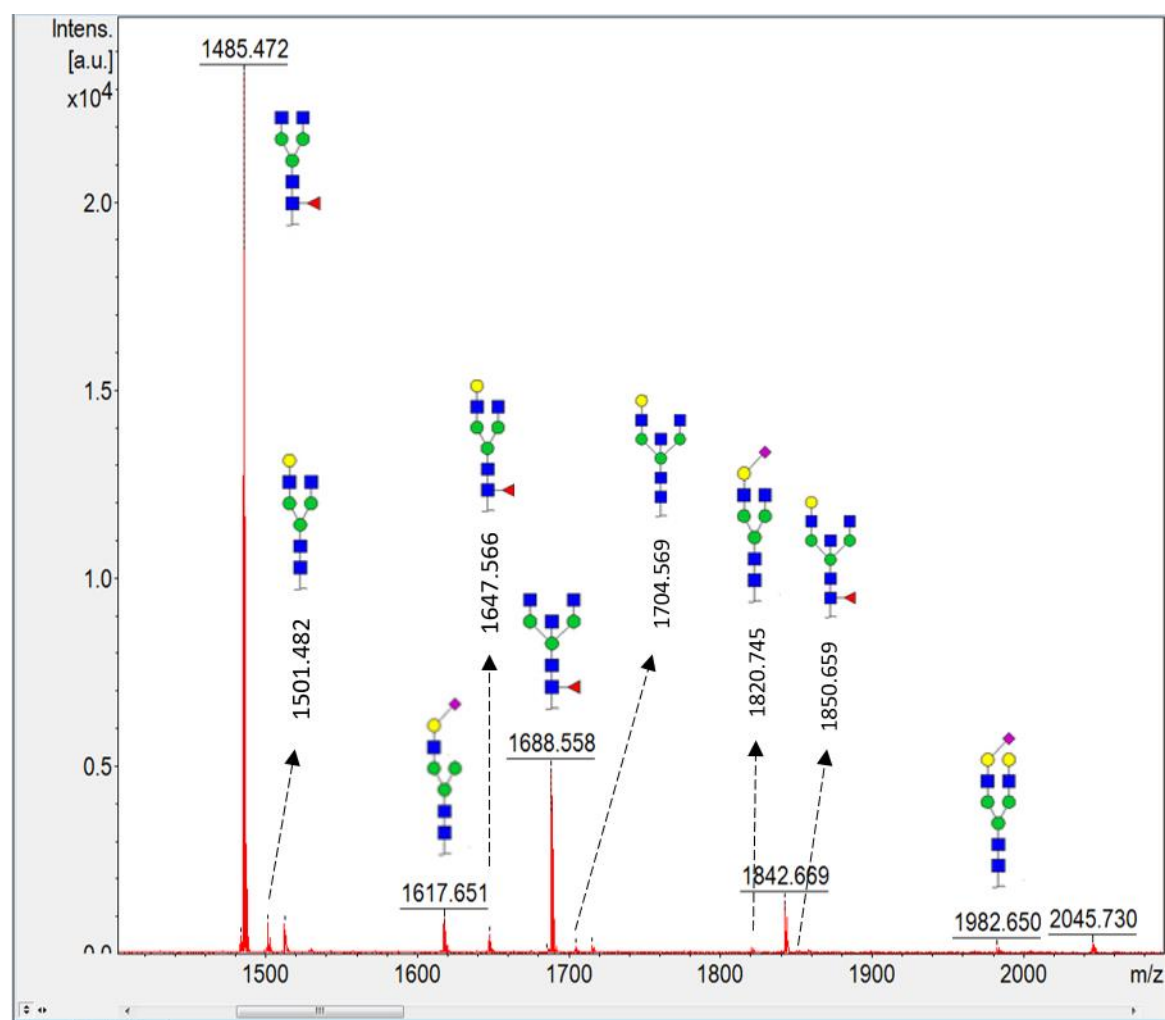


**Figure 30.** MALDI TOF spectrum of glycans released from rat IgG (group 3 – OVX supplemented with zeolite A).

**Table 8.** A list of MALDI TOF measured glycan experimental masses, glycans' exact glycoform mass, the difference between experimental and glycoform mass expressed in Daltons, and the suggested glycan structure for samples from the OVX group supplemented with zeolite A (3).

**Zeolite A OVX N-glycans (group 3)**

<b>Experimental mass (m/z)</b>	<b>Glycoform mass (m/z)</b>	<b>Glycan structure</b>	<b><math>\Delta</math>mass (Dalton)</b>
1485.502	1444.534	(HexNAc) <sub>2</sub> (Deoxyhexose) <sub>1</sub> + (Man) <sub>3</sub> (GlcNAc) <sub>2</sub>	-0.031
1501.482	1460.529	(Hex) <sub>1</sub> (HexNAc) <sub>2</sub> + (Man) <sub>3</sub> (GlcNAc) <sub>2</sub>	-0.046
1617.651	1257.449	(NeuAc $\alpha$ 2-6) (Hex) <sub>1</sub> (HexNAc) <sub>1</sub> + (Man) <sub>3</sub> (GlcNAc) <sub>2</sub>	-0.072
1647.566	1606.587	(Hex) <sub>1</sub> (HexNAc) <sub>2</sub> (Deoxyhexose) <sub>1</sub> + (Man) <sub>3</sub> (GlcNAc) <sub>2</sub>	-0.02
1688.592	1647.613	(HexNAc) <sub>3</sub> (Deoxyhexose) <sub>1</sub> + (Man) <sub>3</sub> (GlcNAc) <sub>2</sub>	-0.02
1704.569	1663.608	(Hex) <sub>1</sub> (HexNAc) <sub>3</sub> + (Man) <sub>3</sub> (GlcNAc) <sub>2</sub>	-0.038
1820.745	1460.529	(NeuAc $\alpha$ 2-6)(Hex) <sub>1</sub> (HexNAc) <sub>2</sub> + (Man) <sub>3</sub> (GlcNAc) <sub>2</sub>	0.096
1850.659	1809.666	(Hex) <sub>1</sub> (HexNAc) <sub>3</sub> (Deoxyhexose) <sub>1</sub> + (Man) <sub>3</sub> (GlcNAc) <sub>2</sub>	-0.006
1982.650	1622.582	(NeuAc $\alpha$ 2-6) (Hex) <sub>2</sub> (HexNAc) <sub>2</sub> + (Man) <sub>3</sub> (GlcNAc) <sub>2</sub>	-0.061

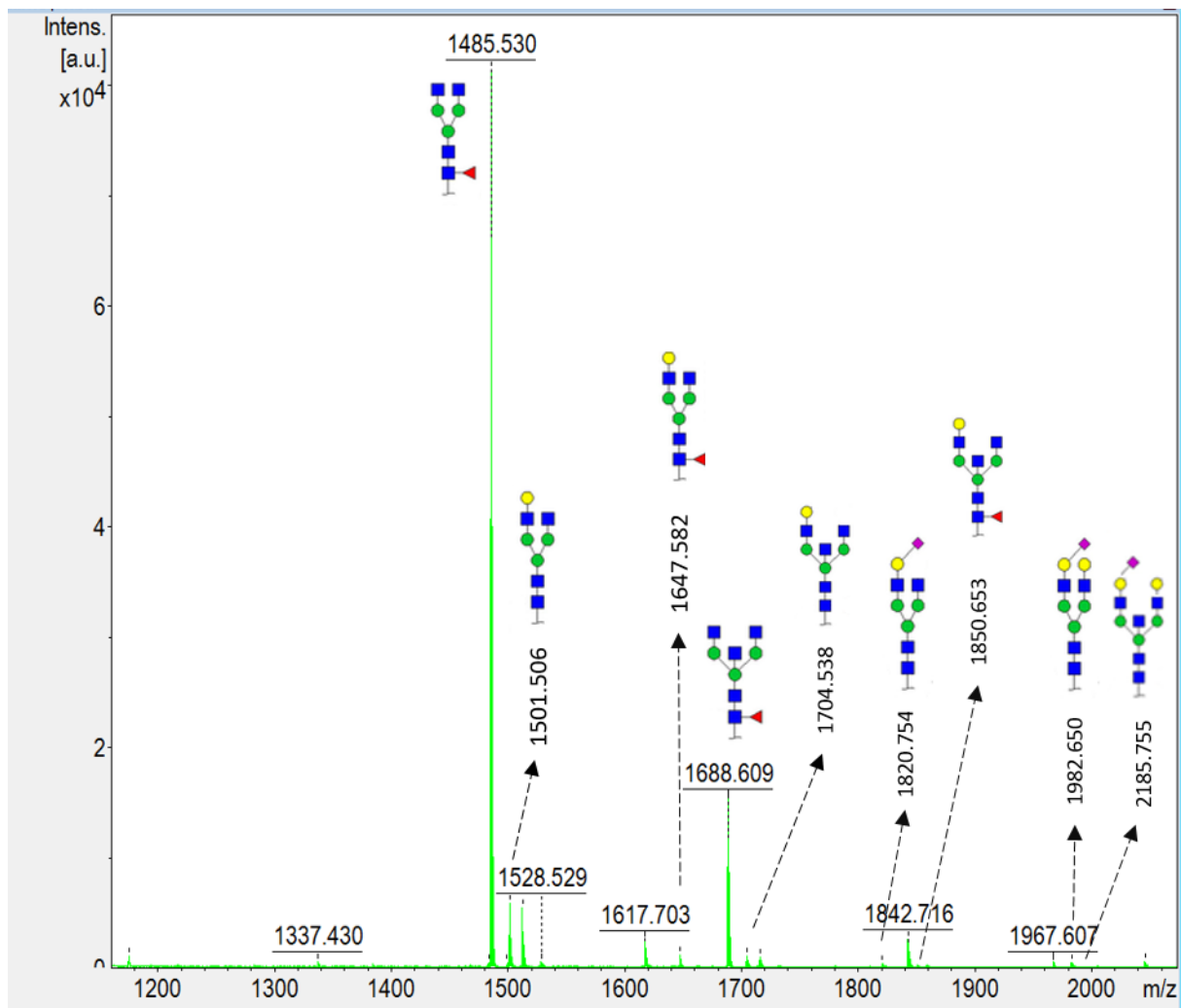


**Figure 31.** MALDI TOF spectrum of glycans released from rat IgG (group 4 – OVX supplemented with clinoptilolite).

**Table 9.** A list of MALDI TOF measured glycan experimental masses, glycans' exact glycoform mass, the difference between experimental and glycoform mass expressed in Daltons, and the suggested glycan structure for samples from the OVX group supplemented with clinoptilolite (4).

#### Clinoptilolite OVX N-glycans (group 4)

Experimental mass (m/z)	Glycoform mass (m/z)	Glycan structure	$\Delta$ mass (Dalton)
1485.530	1444.534	(HexNAc) <sub>2</sub> (Deoxyhexose) <sub>1</sub> + (Man) <sub>3</sub> (GlcNAc) <sub>2</sub>	-0.003
1501.506	1460.529	(Hex) <sub>1</sub> (HexNAc) <sub>2</sub> + (Man) <sub>3</sub> (GlcNAc) <sub>2</sub>	-0.022
1647.582	1606.587	(Hex) <sub>1</sub> (HexNAc) <sub>2</sub> (Deoxyhexose) <sub>1</sub> + (Man) <sub>3</sub> (GlcNAc) <sub>2</sub>	-0.004

1688.609	1647.613	(HexNAc) <sub>3</sub> (Deoxyhexose) <sub>1</sub> + (Man) <sub>3</sub> (GlcNAc) <sub>2</sub>	-0.025
1704.538	1663.608	(Hex) <sub>1</sub> (HexNAc) <sub>3</sub> + (Man) <sub>3</sub> (GlcNAc) <sub>2</sub>	-0.069
1820.754	1460.529	(NeuAc α2-6)(Hex) <sub>1</sub> (HexNAc) <sub>2</sub> + (Man) <sub>3</sub> (GlcNAc) <sub>2</sub>	0.105
1850.653	1809.666	(Hex) <sub>1</sub> (HexNAc) <sub>3</sub> (Deoxyhexose) <sub>1</sub> + (Man) <sub>3</sub> (GlcNAc) <sub>2</sub>	-0.012
1982.650	1622.582	(NeuAc α2-6)(Hex) <sub>2</sub> (HexNAc) <sub>2</sub> + (Man) <sub>3</sub> (GlcNAc) <sub>2</sub>	-0.008
2185.755	1825.661	(NeuAc α2-6)(Hex) <sub>2</sub> (HexNAc) <sub>3</sub> + (Man) <sub>3</sub> (GlcNAc) <sub>2</sub>	-0.025

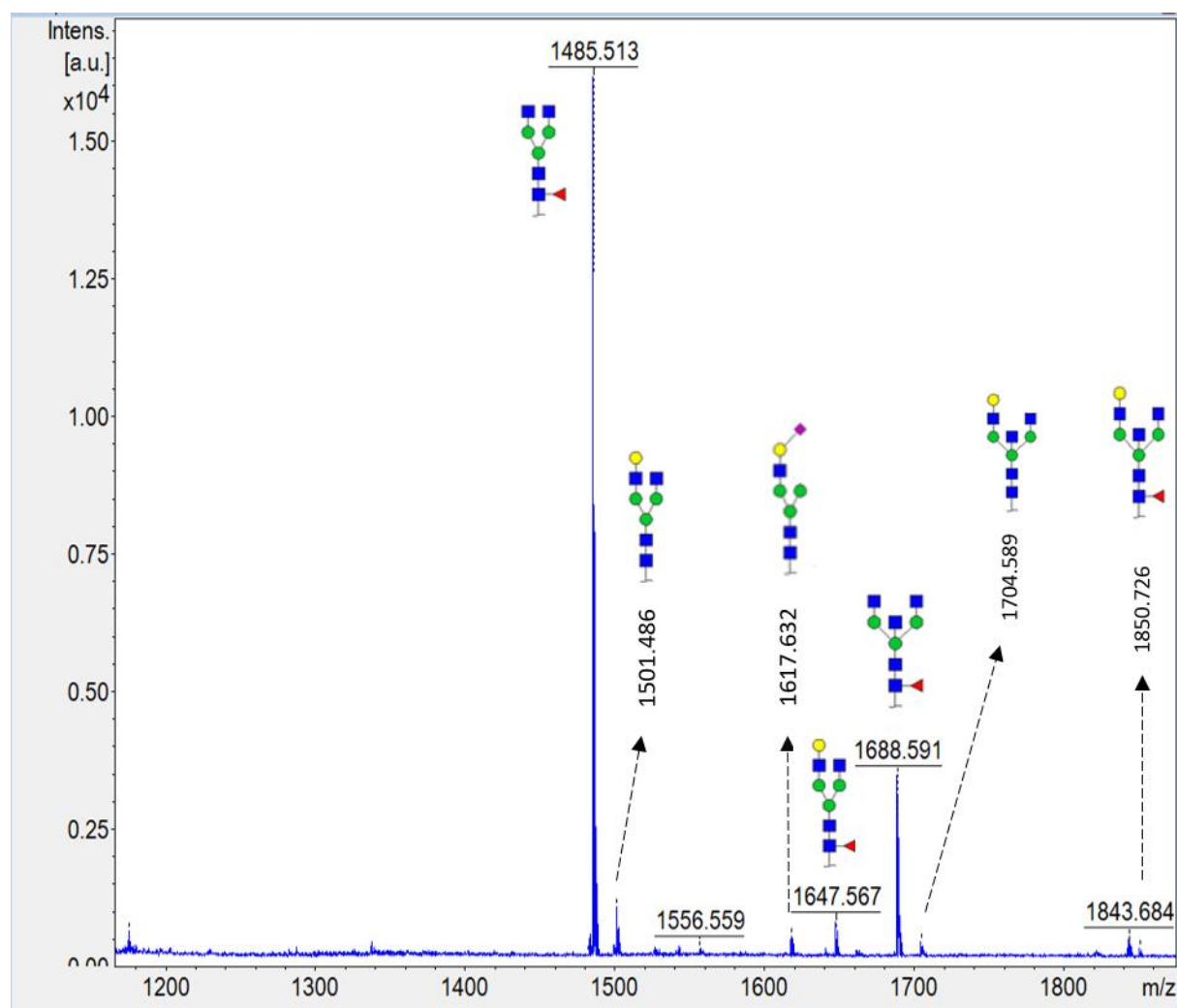


**Figure 32.** MALDI TOF spectrum of glycans released from rat IgG (group 5 – OVX supplemented with PMA clinoptilolite).

**Table 10.** A list of MALDI TOF measured glycan experimental masses, glycans' exact glycoform mass, the difference between experimental and glycoform mass expressed in Daltons, and the suggested glycan structure for samples from the OVX group supplemented with PMA clinoptilolite (5).

**PMA OVX N-glycans (group 5)**

<b>Experimental mass (m/z)</b>	<b>Glycoform mass (m/z)</b>	<b>Glycan structure</b>	<b><math>\Delta</math>mass (Dalton)</b>
1485.513	1444.534	(HexNAc) <sub>2</sub> (Deoxyhexose) <sub>1</sub> + (Man) <sub>3</sub> (GlcNAc) <sub>2</sub>	-0.02
1501.486	1460.529	(Hex) <sub>1</sub> (HexNAc) <sub>2</sub> + (Man) <sub>3</sub> (GlcNAc) <sub>2</sub>	-0.042
1617.632	1257.449	(NeuAc $\alpha$ 2-6)(Hex) <sub>1</sub> (HexNAc) <sub>1</sub> + (Man) <sub>3</sub> (GlcNAc) <sub>2</sub>	0.053
1647.567	1606.587	(Hex) <sub>1</sub> (HexNAc) <sub>2</sub> (Deoxyhexose) <sub>1</sub> + (Man) <sub>3</sub> (GlcNAc) <sub>2</sub>	-0.019
1688.591	1647.613	(HexNAc) <sub>3</sub> (Deoxyhexose) <sub>1</sub> + (Man) <sub>3</sub> (GlcNAc) <sub>2</sub>	-0.021
1704.589	1663.608	(Hex) <sub>1</sub> (HexNAc) <sub>3</sub> + (Man) <sub>3</sub> (GlcNAc) <sub>2</sub>	-0.058
1850.726	1809.666	(Hex) <sub>1</sub> (HexNAc) <sub>3</sub> (Deoxyhexose) <sub>1</sub> + (Man) <sub>3</sub> (GlcNAc) <sub>2</sub>	0.06

As one can infer from the glycan peaks detected, the majority of the most intensive peaks are spotted in all samples. However, in some samples a higher number of glycans was detected than in others (Table 11). Sugars that are not mutually shared, but specific for one or more analysed groups, are depicted in Table 12.

**Table 11.** A list of all detected peaks and detected glycan structures for each sample.

<b>Sample</b>	<b>Number of detected peaks</b>	<b>Number of detected glycan structures</b>
0	17	5
1	70	13
2	20	9
3	13	9
4	18	9
5	12	7

**Table 12.** A table depicting all detected glycan structures in all samples (groups 0 to 5). Composite glycans are shown in black; glycans with sialic acid residues are shown in green.

0	1	2	3	4	5
(HexNAc) <sub>2</sub> (Deoxyhexose) <sub>1+</sub> (Man) <sub>3</sub> (GlcNAc) <sub>2</sub>	(HexNAc) <sub>2</sub> (Deoxyhexose) <sub>1+</sub> (Man) <sub>3</sub> (GlcNAc) <sub>2</sub>	(HexNAc) <sub>2</sub> (Deoxyhexose) <sub>1+</sub> (Man) <sub>3</sub> (GlcNAc) <sub>2</sub>	(HexNAc) <sub>2</sub> (Deoxyhexose) <sub>1+</sub> (Man) <sub>3</sub> (GlcNAc) <sub>2</sub>	(HexNAc) <sub>2</sub> (Deoxyhexose) <sub>1+</sub> (Man) <sub>3</sub> (GlcNAc) <sub>2</sub>	(HexNAc) <sub>2</sub> (Deoxyhexose) <sub>1+</sub> (Man) <sub>3</sub> (GlcNAc) <sub>2</sub>
(HexNAc) <sub>3</sub> (Deoxyhexose) <sub>1+</sub> (Man) <sub>3</sub> (GlcNAc) <sub>2</sub>		(HexNAc) <sub>3</sub> (Deoxyhexose) <sub>1+</sub> (Man) <sub>3</sub> (GlcNAc) <sub>2</sub>	(HexNAc) <sub>3</sub> (Deoxyhexose) <sub>1+</sub> (Man) <sub>3</sub> (GlcNAc) <sub>2</sub>	(HexNAc) <sub>3</sub> (Deoxyhexose) <sub>1+</sub> (Man) <sub>3</sub> (GlcNAc) <sub>2</sub>	(HexNAc) <sub>3</sub> (Deoxyhexose) <sub>1+</sub> (Man) <sub>3</sub> (GlcNAc) <sub>2</sub>
(Hex) <sub>1</sub> (HexNAc) <sub>3</sub> + (Man) <sub>3</sub> (GlcNAc) <sub>2</sub>			(Hex) <sub>1</sub> (HexNAc) <sub>3</sub> + (Man) <sub>3</sub> (GlcNAc) <sub>2</sub>	(Hex) <sub>1</sub> (HexNAc) <sub>3</sub> + (Man) <sub>3</sub> (GlcNAc) <sub>2</sub>	(Hex) <sub>1</sub> (HexNAc) <sub>3</sub> + (Man) <sub>3</sub> (GlcNAc) <sub>2</sub>
	(Hex) <sub>1</sub> (HexNAc) <sub>2</sub> + (Man) <sub>3</sub> (GlcNAc) <sub>2</sub>	(Hex) <sub>1</sub> (HexNAc) <sub>2</sub> + (Man) <sub>3</sub> (GlcNAc) <sub>2</sub>	(Hex) <sub>1</sub> (HexNAc) <sub>2</sub> + (Man) <sub>3</sub> (GlcNAc) <sub>2</sub>	(Hex) <sub>1</sub> (HexNAc) <sub>2</sub> + (Man) <sub>3</sub> (GlcNAc) <sub>2</sub>	(Hex) <sub>1</sub> (HexNAc) <sub>2</sub> + (Man) <sub>3</sub> (GlcNAc) <sub>2</sub>
(Hex) <sub>1</sub> (HexNAc) <sub>2</sub> (Deoxyhexose) <sub>1+</sub> (Man) <sub>3</sub> (GlcNAc) <sub>2</sub>			(Hex) <sub>1</sub> (HexNAc) <sub>2</sub> (Deoxyhexose) <sub>1+</sub> (Man) <sub>3</sub> (GlcNAc) <sub>2</sub>	(Hex) <sub>1</sub> (HexNAc) <sub>2</sub> (Deoxyhexose) <sub>1+</sub> (Man) <sub>3</sub> (GlcNAc) <sub>2</sub>	(Hex) <sub>1</sub> (HexNAc) <sub>2</sub> (Deoxyhexose) <sub>1+</sub> (Man) <sub>3</sub> (GlcNAc) <sub>2</sub>
	(Hex) <sub>1</sub> (HexNAc) <sub>3</sub> (Deoxyhexose) <sub>1+</sub> (Man) <sub>3</sub> (GlcNAc) <sub>2</sub>	(Hex) <sub>1</sub> (HexNAc) <sub>3</sub> (Deoxyhexose) <sub>1+</sub> (Man) <sub>3</sub> (GlcNAc) <sub>2</sub>	(Hex) <sub>1</sub> (HexNAc) <sub>3</sub> (Deoxyhexose) <sub>1+</sub> (Man) <sub>3</sub> (GlcNAc) <sub>2</sub>	(Hex) <sub>1</sub> (HexNAc) <sub>3</sub> (Deoxyhexose) <sub>1+</sub> (Man) <sub>3</sub> (GlcNAc) <sub>2</sub>	(Hex) <sub>1</sub> (HexNAc) <sub>3</sub> (Deoxyhexose) <sub>1+</sub> (Man) <sub>3</sub> (GlcNAc) <sub>2</sub>
	(NeuAc α2-6) (Hex) <sub>2</sub> (HexNAc) <sub>2+</sub> (Man) <sub>3</sub> (GlcNAc) <sub>2</sub>	(NeuAc α2-6) (Hex) <sub>2</sub> (HexNAc) <sub>2+</sub> (Man) <sub>3</sub> (GlcNAc) <sub>2</sub>	(NeuAc α2-6) (Hex) <sub>2</sub> (HexNAc) <sub>2+</sub> (Man) <sub>3</sub> (GlcNAc) <sub>2</sub>	(NeuAc α2-6) (Hex) <sub>2</sub> (HexNAc) <sub>2+</sub> (Man) <sub>3</sub> (GlcNAc) <sub>2</sub>	
(NeuAc α2-6) (Hex) <sub>1</sub> (HexNAc) <sub>1</sub> + (Man) <sub>3</sub> (GlcNAc) <sub>2</sub>	(NeuAc α2-6) (Hex) <sub>1</sub> (HexNAc) <sub>1</sub> + (Man) <sub>3</sub> (GlcNAc) <sub>2</sub>		(NeuAc α2-6) (Hex) <sub>1</sub> (HexNAc) <sub>1</sub> + (Man) <sub>3</sub> (GlcNAc) <sub>2</sub>		(NeuAc α2-6) (Hex) <sub>1</sub> (HexNAc) <sub>1</sub> + (Man) <sub>3</sub> (GlcNAc) <sub>2</sub>
	(NeuAc α2-6) (Hex) <sub>2</sub> (HexNAc) <sub>3</sub> + (Man) <sub>3</sub> (GlcNAc) <sub>2</sub>	(NeuAc α2-6) (Hex) <sub>2</sub> (HexNAc) <sub>3</sub> + (Man) <sub>3</sub> (GlcNAc) <sub>2</sub>		(NeuAc α2-6) (Hex) <sub>2</sub> (HexNAc) <sub>3</sub> + (Man) <sub>3</sub> (GlcNAc) <sub>2</sub>	
		(NeuAc α2-6) (Hex) <sub>1</sub> (HexNAc) <sub>2</sub> + (Man) <sub>3</sub> (GlcNAc) <sub>2</sub>	(NeuAc α2-6) (Hex) <sub>1</sub> (HexNAc) <sub>2</sub> + (Man) <sub>3</sub> (GlcNAc) <sub>2</sub>	(NeuAc α2-6) (Hex) <sub>1</sub> (HexNAc) <sub>2</sub> + (Man) <sub>3</sub> (GlcNAc) <sub>2</sub>	
	(Hex) <sub>1</sub> (HexNAc) <sub>2</sub> (Deoxyhexose) <sub>1+</sub> (Man) <sub>3</sub> (GlcNAc) <sub>2</sub>	(Hex) <sub>1</sub> (HexNAc) <sub>2</sub> (Deoxyhexose) <sub>1+</sub> (Man) <sub>3</sub> (GlcNAc) <sub>2</sub>			

0	1	2	3	4	5
	(NeuAc $\alpha$ 2-6) (Hex) <sub>3</sub> (HexNAc) <sub>2</sub> + (Man) <sub>3</sub> (GlcNAc) <sub>2</sub>	(NeuAc $\alpha$ 2-6) (Hex) <sub>3</sub> (HexNAc) <sub>2</sub> + (Man) <sub>3</sub> (GlcNAc) <sub>2</sub>			
	(HexNAc) <sub>1</sub> (Deoxyhexose) <sub>1</sub> + (Man) <sub>3</sub> (GlcNAc) <sub>2</sub>				
	(HexNAc) <sub>2</sub> + (Man) <sub>3</sub> (GlcNAc) <sub>2</sub>				
	(HexNAc) <sub>3</sub> + (Man) <sub>3</sub> (GlcNAc) <sub>2</sub>				
	(Hex) <sub>2</sub> (HexNAc) <sub>7</sub> + (Man) <sub>3</sub> (GlcNAc) <sub>2</sub>				
	(Hex) <sub>2</sub> (HexNAc) <sub>7</sub> (Deoxyhexose) <sub>1</sub> + (Man) <sub>3</sub> (GlcNAc) <sub>2</sub>				
		(Hex) <sub>1</sub> (HexNAc) <sub>3</sub> + (Man) <sub>3</sub> (GlcNAc) <sub>2</sub>			

Considering that the rat IgG glycome was not previously researched, we decided to compare the analysed IgG carbohydrate profile with already published human and murine IgG glycome (Figures 33 and 34). Most of the peaks detected in rat IgG spectra were identical to the most intense peaks in human and mouse IgG (Table 13). Next, we compared relative intensities of that peak in rat, human and mouse IgG glycan spectra (Figure 35). Furthermore, we compared relative intensities of mutual glycan peaks detected in rat, mouse and human IgG, relative to the same reference peak in rat IgG glycome (Figure 36). Finally, we investigated relative intensities of mutual glycan peaks detected in samples from animal groups 1 (healthy control), 2 (sham operated) and 5 (PMA OVX), relative to the reference peak (Figure 37).



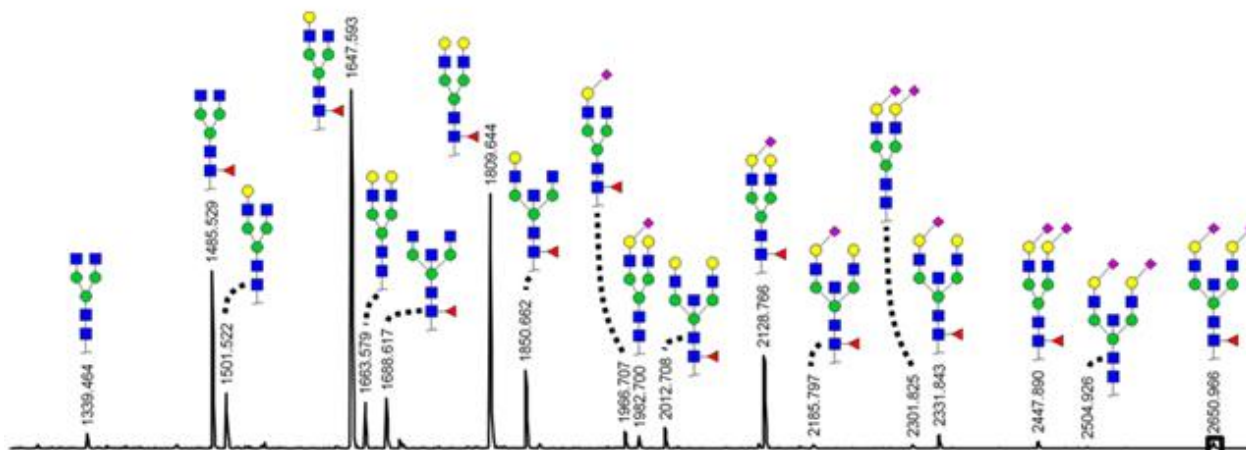


**Figure 33.** A MALDI TOF MS spectrum of the human IgG glycome [71].

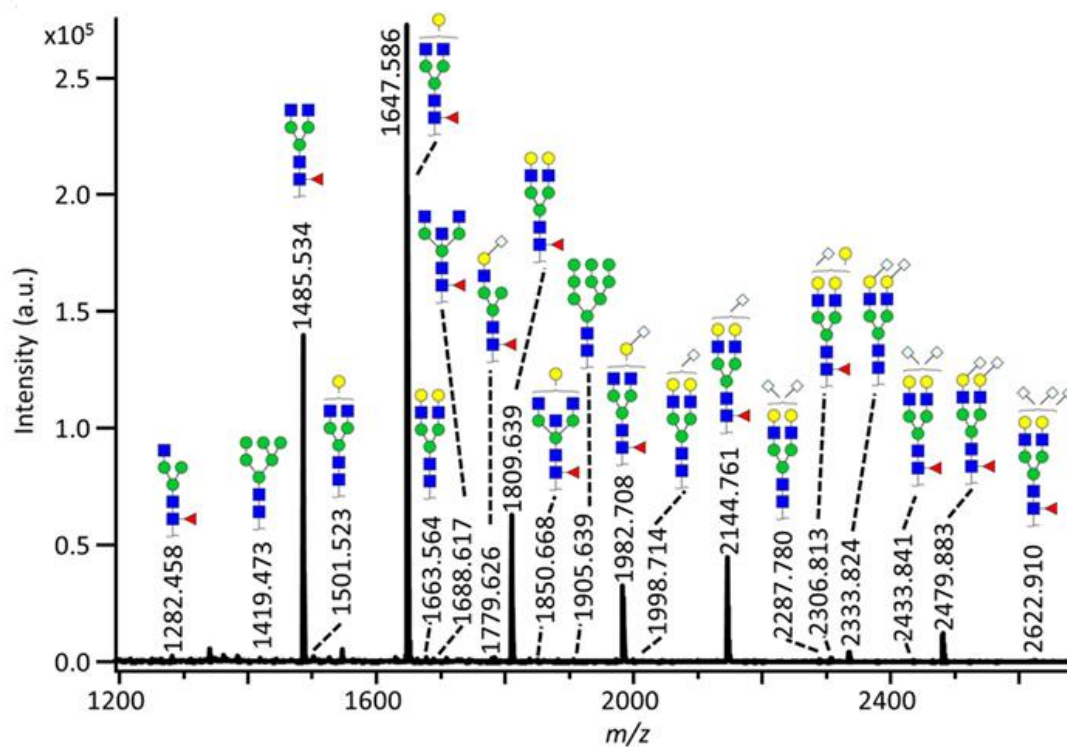


**Figure 34.** The 20 most abundant released glycans of total mouse fragment crystallizable (Fc)-region IgG analyzed by MALDI-TOF-MS after linkage-specific sialic acid derivatization [18].

**Table 13.** Comparison between measured rat IgG glycan peaks and human and rat IgG glycan peaks from literature. Peaks highlighted in blue are detected across all three species, peaks shared between rat and human or rat and mouse are shown in green and yellow, respectively.

Human IgG glycan peaks (m/z) (ref)	Rat IgG glycan peaks (m/z)	Mouse IgG glycan peaks (m/z)
	1282.394	1282.458
1339.464	1339.417	
1485.529	1485.529	1485.534
1501.522	1501.459	1501.523
	1617.736	
1647.593	1647.556	1647.586
1633.579	1663.485	1663.564
1688.617	1688.645	1688.617
	1704.582	
1809.644	1809.565	1809.639
	1820.745	
1850.662	1850.600	1850.668
1966.707		
1982.700	1982.650	1982.708
		1998.714
2012.708		
2128.766		
	2144.685	2144.761
2185.797	2185.713	

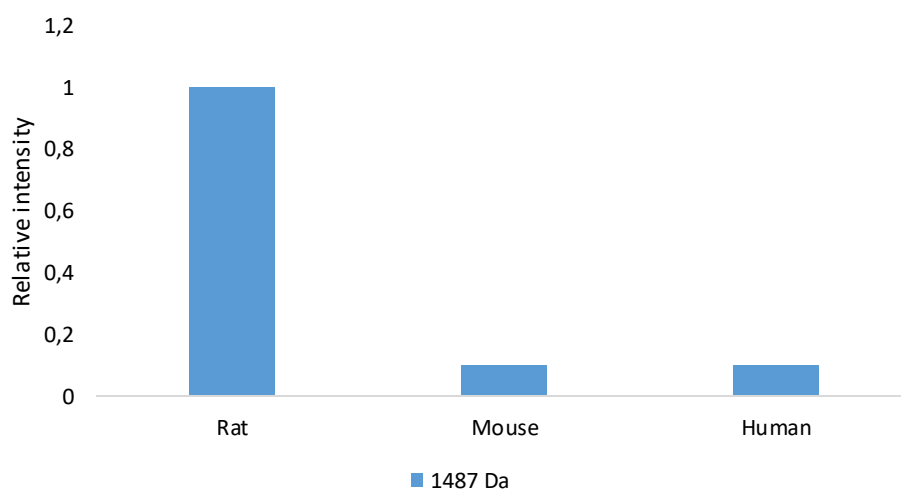


**Figure 35.** A graphical representation of the relative intensity of the most prominent peak in rat IgG glycome (1485 Da) detected in rat, mouse and human.

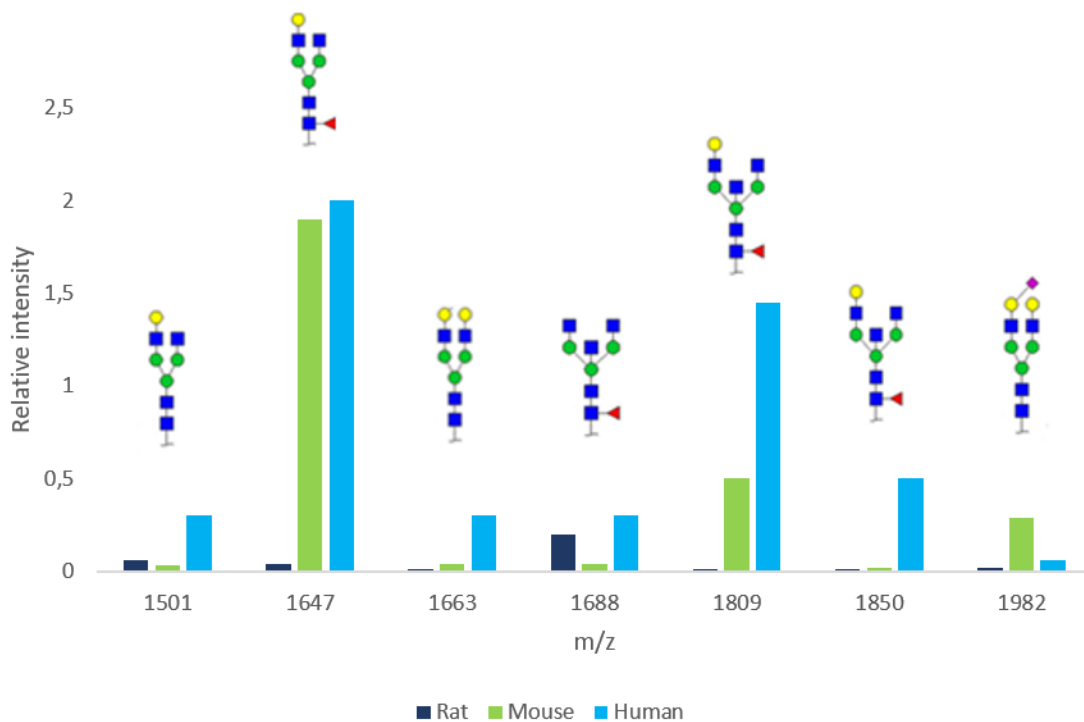


**Figure 36.** A graphical representation of the intensity of mutual glycan peaks detected in rat, mouse and human IgG, relative to the reference peak in rat IgG glycome (1485 Da) whose value is considered to be 1.

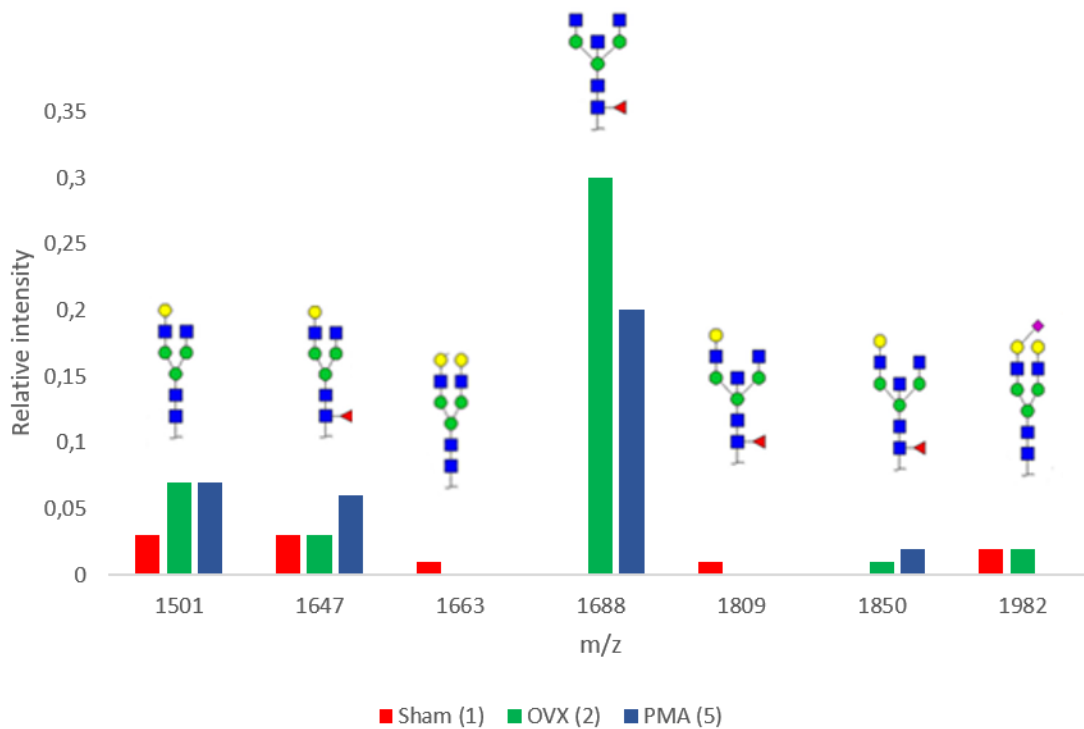


**Figure 37.** A graphical representation of the intensity of mutual glycan peaks detected in samples from groups 1, 2 and 5, relative to the reference peak in rat IgG glycome (1485 Da) whose value is considered to be 1.

#### 4.4 Rat liver fractionation

Considering that the liver is the main metabolic organ, and the main mechanisms of clinoptilolite action is hypothesized to be detoxification in the digestive system, we decided to investigate liver proteomes of all six animal groups (Table 2.). Using a commercial kit that fractionates proteins based on their hydrophobicity, rat liver proteins were separated into five fractions, namely (i) cytoplasmic, (ii) membrane, (iii) soluble nuclear, (iv) chromatin-bound nuclear and (v) cytoskeletal fraction. Firstly, by disrupting the cell membrane, cytoplasmic contents are released. Tissue debris is removed through a tissue strainer before the second buffer dissolves everything but nuclear membranes. A third buffer yields the soluble nuclear fraction. Addition of micrococcal nuclease releases the chromatin-bound fraction. The resulting pellet is finally exposed to a buffer that exposes cytoskeletal proteins. Figures 32 to 36 show SDS PAGE gels containing isolated liver proteins in a certain protein fraction (1-6) from six animals, one from each experimental group. On a one dimensional scale, there seems to be no great difference in protein expression in these fractions. However, some qualitative differences are present in fractions 3, 4 and 5 (see Figures 32,33,34), containing mostly proteins that are not very soluble. This experiment is a basis for further proteomic analyses. In order to dig deeper into the proteome, gel bands will be excised, trypsinized, and containing proteins will be identified by mass spectrometry. Alternatively, each fraction can be trypsinized (without SDS PAGE), separated by reverse phase HPLC and analysed by electrospray ionization MS/MS (LC-ESI-MS/MS).

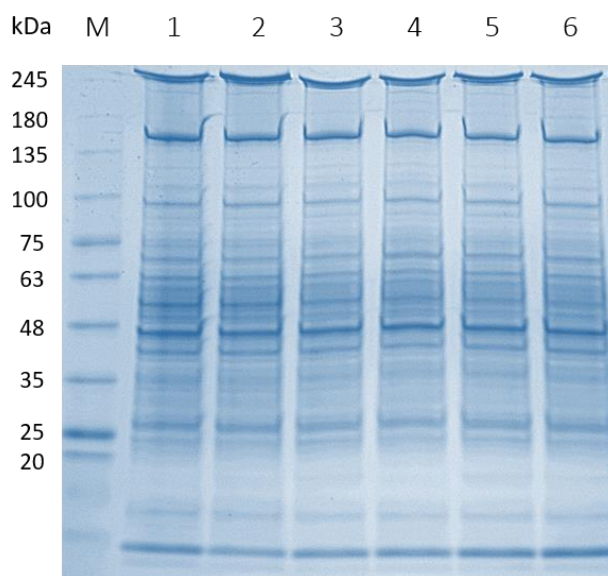


**Figure 38.** Rat liver fractionation – SDS PAGE of fraction I. Lanes: (1) group 0; (2) group 1; (3) group 2; (4) group 3; (5) group 4; (6) group 5.

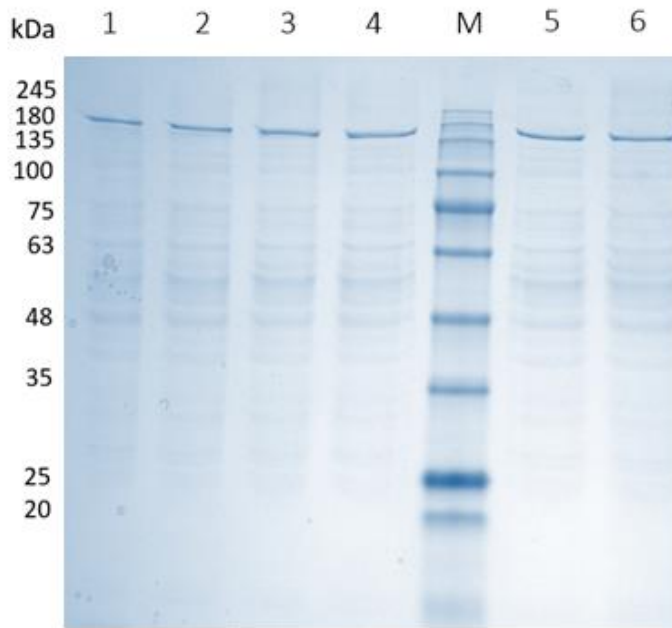


**Figure 39.** Rat liver fractionation – SDS PAGE of fraction II. Lanes: (1) group 0; (2) group 1; (3) group 2; (4) group 3; (5) group 4; (6) group 5.

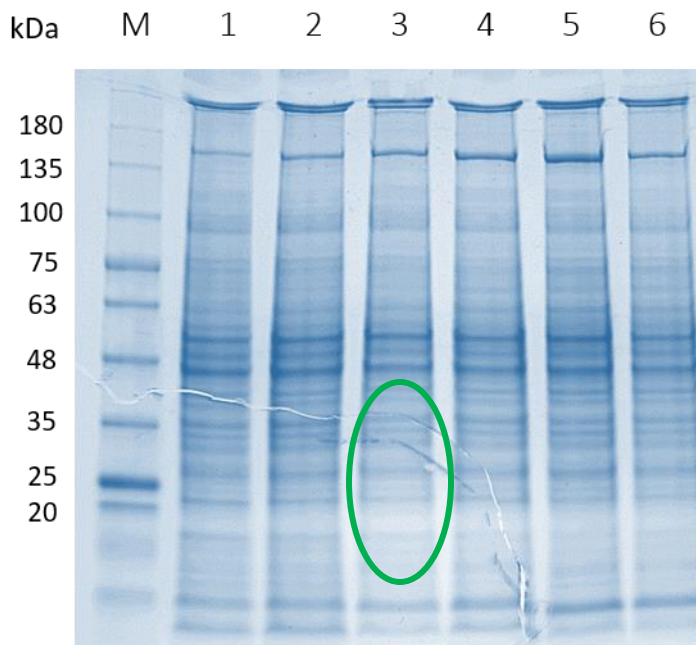


**Figure 40.** Rat liver fractionation – SDS PAGE of fraction III. Lanes: (1) group 0; (2) group 1; (3) group 2; (4) group 3; (5) group 4; (6) group 5.

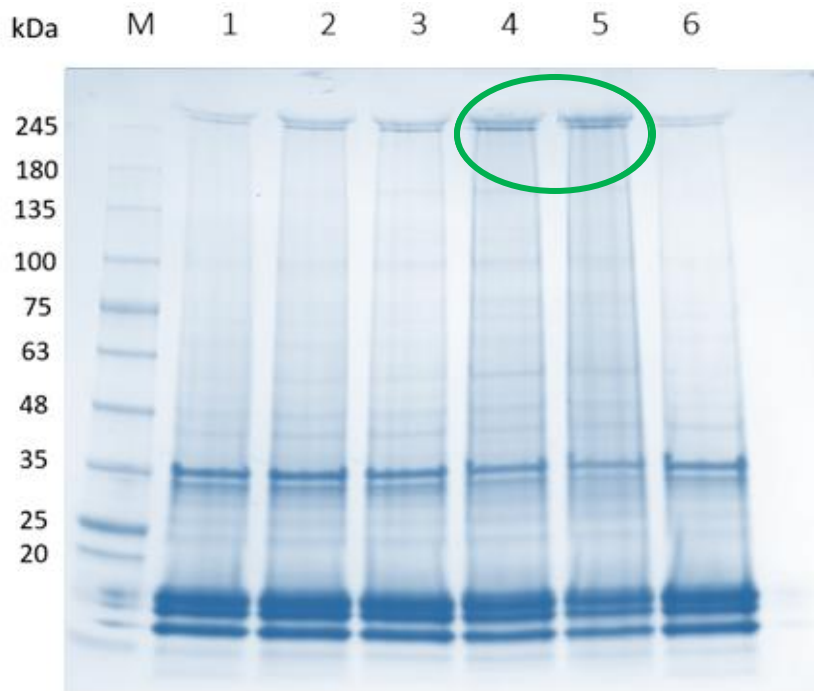


**Figure 41.** Rat liver fractionation – SDS PAGE of fraction IV. Lanes: (1) group 0; (2) group 1; (3) group 2; (4) group 3; (5) group 4; (6) group 5.

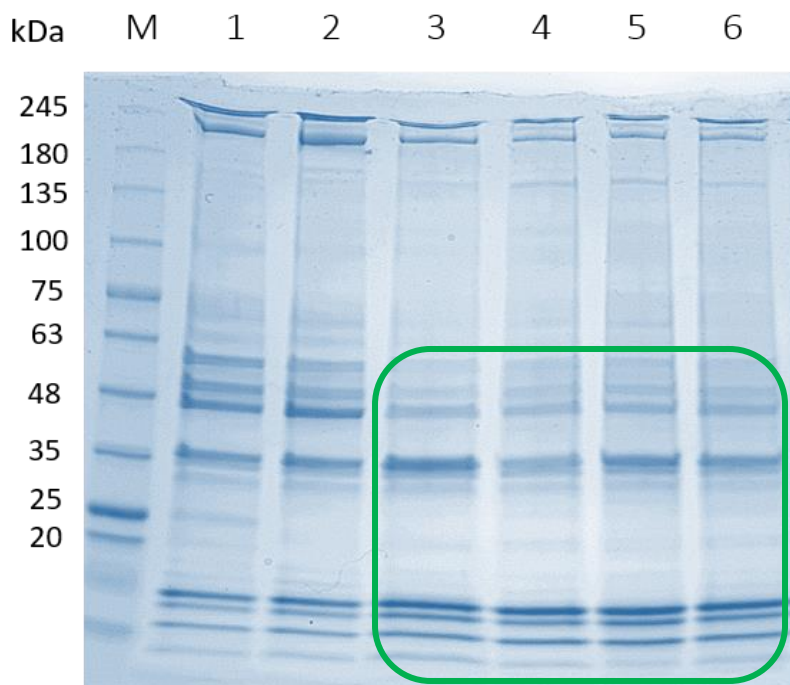


**Figure 42.** Rat liver fractionation – SDS PAGE of fraction V. Lanes: (1) group 0; (2) group 1; (3) group 2; (4) group 3; (5) group 4; (6) group 5.

#### 4.5 Presence of aluminium and silicone in rat liver

Aluminium and silicone concentrations in the livers of animals (groups 2, 3 and 5) were assessed by use of Synchrotron radiation. The aluminium background signal is the same in all samples, with no substantial differences between groups 3 and 5, but certain hot spots (1-2  $\mu\text{m}$ ) in group 3 (zeolite A) show a much higher Al content compared to the other two samples. These spots are most likely nano-aluminosilicate particles generated during the breakdown of zeolite A's crystal structure in the digestive tract, entering the bloodstream. Moreover, silicone seems to be co-localized with aluminium in these hot spots.

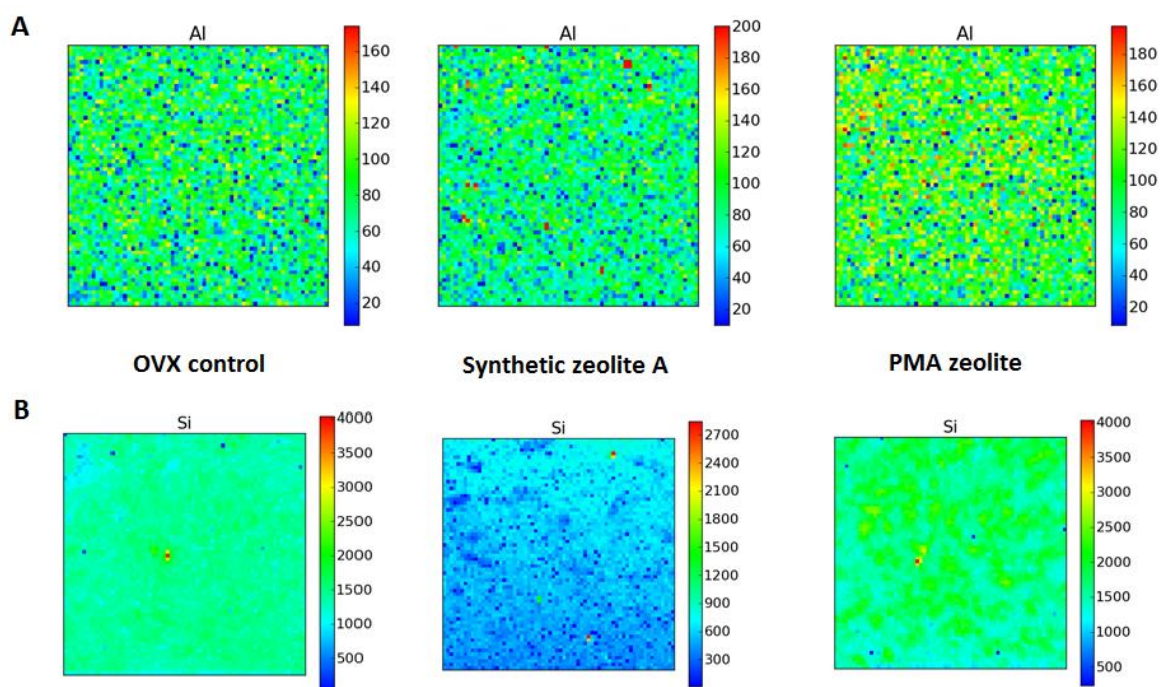


**Figure 43.** Presence of aluminium (A) and silicone (B) in liver slices of healthy ovariectomized (OVX) rats, OVX rats treated with synthetic zeolite A, and OVX rats treated with PMA clinoptilolite.

## 5. DISCUSSION

In this work, we developed a protocol based on polymethacrylate monolithic supports with immobilized recombinant protein G and protein L ligands for simultaneous isolation of immunoglobulins A, G and M from human serum. In opposite to both protein A and protein G that bind to the Fc fragment, protein L binds with high affinity to the kappa variable light chain regions of immunoglobulins. This different interaction allows isolation of Fab fragments of antibodies, but also complete antibody molecules that do not bind to protein A and protein G. However, only around 35% of human IgGs contain kappa light chain. A fractionation scheme for fast throughput isolation of IgM and enrichment of low-abundance proteins was published by Breen *et al.* [42]. It involves two different fractionation steps, namely protein A fractionation, resulting in the enrichment of immunoglobulins, and anion exchange chromatography, resulting in two separate fractions containing IgG or IgM. Similarly, we developed a protocol for high throughput isolation of IgA, IgM and IgG, using both protein G and protein L, in two distinct and successive chromatographic procedures. After the first affinity monolith chromatography on protein G or L, unbound proteins are collected and are later applied to the second monolithic column, protein L or G, respectively. This results in the isolation of not only all IgG subclasses (protein G), but of IgA and IgM molecules carrying kappa light chains as well (protein L) (Figure 10). In this way, a broader selection of immunoglobulin classes and subclasses can be purified simultaneously, compared to using only protein G or A for their isolation. Isolation scheme that is presented here can be applied for high-throughput isolation of immunoglobulins, and further analysis of their glycosylation changes as possible diagnostic and prognostic biomarkers. Miniaturized disks carrying affinity ligands can be mounted into ELISA plates and applied for simultaneous isolation of antibodies by use of laboratory robotics. Moreover, this experiment is a foundation for isolating IgA and IgM from rat serum, as well.

Upon successful method development, we optimized the protocol for isolation of rat IgG using protein L affinity monolith chromatography. Rats are used as important model organisms and the lack of methodological approaches hampers the analysis of their serum IgG glycosylation patterns. Rat immunoglobulins mostly have lambda light chains and are therefore perfect ligands for protein L. Rat IgG was consequently successfully isolated from six groups of animals, followed by the analysis of its glycosylation pattern by MALDI TOF mass spectrometry. In particular, changes in glycosylation were studied in relation to osteoporosis



and zeolite supplementation. Interestingly, we detected the fewest number of glycans in the healthy control sample (only five), while the largest number was found in the sham control sample (thirteen), which corresponds to animals undergoing surgery. The number of detected glycan structures in ovariectomized animals and OVX animals treated with zeolites is somewhat lower, but still rather high considering the total number of peaks detected in spectra in these samples, 17 on average, versus 70 detected in the sham sample. Most of the glycans that were detected only in the sham sample are not fucosylated. The detected changes in the glycosylation patterns of sham operated rats could simply be a consequence of inflammation resulting from operation. Novokmet *et al.* analysed the composition of IgG N-glycomes in 107 patients undergoing cardiac surgery and found the same pattern of changes in the first 72 h in nearly all individuals [72]. In another study, rapid alterations in transferrin sialylation during sepsis were detected [73]. Taken together, these results point to imminent changes in glycosylation patterns after inflammation. It has to be noted that we isolated and analysed IgG from only three animals from each group, and due to the small sample number, for conclusive statements, preferably IgG from sera from 10 animals per group should be analysed.

Glycosylation of human and murine immunoglobulins is quite extensively researched, yet there is no information available on the glycome of rat immunoglobulins. Thus, we compared the analysed IgG carbohydrate profile with already published human and murine IgG glycomes (Figures 33 and 34). Most of the peaks detected in rat IgG spectra were identical to the most intense peaks in human and mouse IgG (Table 13). This was expected, since all three species are mammals, possessing the same cellular glycosylation machinery. However, there is an obvious difference between m/z spectra of rat IgG compared to the other two species. Human and murine samples share several most intensive peaks, with the peak with the highest intensity in both spectra being 1647 Da. The same peak is barely detectable in all of our rat IgG spectra, while the most intensive peak of 1485 Da is the most prominent in all rat samples, chosen as a reference peak for semiquantitative evaluation. Thus, we compared relative intensities of that peak in rat, human and mouse IgG glycan spectra (Figure 35). A consistent almost 100 % fold increase in intensity is found in rat samples compared to both human and mouse, revealing a significant inter species difference. Next, we compared relative intensities of mutual glycan peaks detected in rat, mouse and human IgG, relative to the same reference peak in rat IgG glycome, revealing three glycoforms that had significantly different signal intensities: 1647 Da, 1809 Da and 1809 Da, all three having the highest intensities in human samples (Figure 36). This finding further stands to show differences in glycan expression between species. The

analysis of relative intensities of mutual glycan peaks detected in samples from animal groups 1 (healthy control), 2 (sham operated) and 5 (PMA OVX), relative to the reference peak, exposed a glycan  $(\text{HexNAc})_3(\text{Deoxyhexose})_1 + (\text{Man})_3(\text{GlcNAc})_2$  (1688 Da) that is barely detected in sham operated animal, has a threefold higher intensity in ovariectomized sample, while PMA clinoptilolite treatment lowered the signal by one third (Figure 37). This particular glycan could well be a potential therapeutic marker. Tested zeolites expectedly exerted different effects on IgG glycosylation as these materials differ in structure (artificial zeolite A vs. natural clinoptilolite, as shown in Figure 5) and active surface area. Raw clinoptilolite has a lower active surface in comparison to PMA clinoptilolite which was prepared by tribomechanical double micronization [26]. It is possible that the local zeolite effect in the gut affects the immune system through plasma cells in the Peyer's patches, which are organized lymphoid follicles located in the lowest portion of the small intestine.

Human IgG contains glycans with N-acetylneuraminic acid (NeuAc), while rat IgG contains glycans with both NeuAc and N-glycolylneuraminic acid (NeuGc), found in most non-human mammals [74]. They differ only by a single oxygen atom, but our derivatization protocol targeted towards sialic acid does not work for NeuGc. Unfortunately, NeuGc gets hydrolysed during sample preparation and by use of this protocol we could not detect this isoform in present samples. A solution could be a parallel experiment in which NeuGc, and not NeuAc, is derivatized and measured. As for NeuAc sialic acid, we detected five different species, and their presence varied from sample to sample. Surprisingly, only one sialic acid glycoform,  $(\text{NeuAc } \alpha 2-6) (\text{Hex})_1 (\text{HexNAc})_1 + (\text{Man})_3 (\text{GlcNAc})_2$ , was found in ovariectomized rats treated with PMA clinoptilolite (group 5). The same structure was detected in groups 0 (healthy control), 1 (sham control) and 3 (zeolite A), but not in groups 2 (OVX) and 4 (raw clinoptilolite). In order to confirm this finding, glycan analysis should be done on a larger number of samples. It is possible that that particular glycoform is lost upon inflammation and stress [72,73], but is reintroduced when treated with PMA clinoptilolite or zeolite A, but not raw clinoptilolite. Another glycan with a sialic acid residue,  $(\text{NeuAc } \alpha 2-6) (\text{Hex})_2 (\text{HexNAc})_2 + (\text{Man})_3 (\text{GlcNAc})_2$ , is detected in all MS spectra, except in healthy control samples and samples treated with PMA clinoptilolite. This finding supports our previous premise that treatment with PMA clinoptilolite affects IgG glycosylation, returning it to its normal physiological state, in this case accomplished by the loss of a sialic acid residue. Moreover, the presence of  $(\text{NeuAc } \alpha 2-6) (\text{Hex})_1 (\text{HexNAc})_2 + (\text{Man})_3 (\text{GlcNAc})_2$  glycan in groups 2, 3 and 4 indicates that ovariectomy resulted in the introduction of a glycan on which zeolite A and raw clinoptilolite had no effect,

opposed to PMA clinoptilolite after whose treatment the glycan is not detectable, just like it is not detectable in the healthy control sample. There are two structures,  $(\text{Hex})_1 (\text{HexNAc})_3 + (\text{Man})_3 (\text{GlcNAc})_2$  and  $(\text{Hex})_1 (\text{HexNAc})_2 (\text{Deoxyhexose})_1 + (\text{Man})_3 (\text{GlcNAc})_2$  that were detected in healthy control and all treated samples, but not in sham operated or ovariectomized animals, allowing for the possibility that next to PMA clinoptilolite, raw clinoptilolite and zeolite A also have an effect on the IgG glycome.

We still do not know whether the changes in IgG sialylation are a cause or a consequence of different pathologies. For example, there is a clear link between decreased IgG glycosylation levels and autoimmune diseases. Patients with progressive rheumatoid arthritis have poorly galactosylated and sialylated IgG compared with patients with less severe disease or those in remission [75]. Degalactosylated IgG enhance pathogenic activity in several autoimmune disease models [76,77]. Moreover, galactosylated IgG counteract complement mediated inflammation, supporting the concept that galactosylation levels influence the pathogenic potential of IgG [78]. Anthony *et al.* reported that the sialylated fraction of intravenous immunoglobulin G (IVIg) is effective in its anti-inflammatory activity [79]. Therefore, modulation of glycosylation on pathologic IgG might be vital to develop an immunomodulatory therapy that selectively targets pathologic autoimmune reactions. However, some recent research challenges the persistent view on the importance of sialylation in autoimmune disorders, and provides different and even provocative answers. For example, murine immune thrombocytopenia was ameliorated via intravenous IgG and the effects of IVIg were independent of sialylation of the Fc regions of IVIg [80], proving that a sialylation independent mechanism is responsible for the positive outcome. One has to keep in mind that IVIg is a pluripotent and complex drug, and combined with the pathogenic heterogeneity of autoimmune diseases, remains still highly unexplored and does not allow for a simplistic perspective on its modes of action. To understand the contribution of each N-glycan component on antibody effector function, with a focus on sialic acid and fucose, Li *et al.* engineered homogenous IgG1 glycoforms using a chemo-enzymatic approach and performed side-by-side *in vitro* binding, antibody dependent cell mediated cytotoxicity (ADCC) and *in vivo* IgG mediated cell depletion assays [81]. The results showed that core fucosylation exerted a significant adverse effect on all three experiments, regardless of sialylation status. In contrast, the effect of sialylation on ADCC was dependent on the status of core fucosylation. Sialylation in the context of core fucosylation significantly decreased

ADCC in vitro and suppressed antibody mediated cell killing in vivo. However, in the absence of fucosylation, sialylation did not adversely impact ADCC.

There is only a limited amount of information available about the regulatory mechanisms of IgG sialylation within B cells. Sialylation of IgG Fc is carried out by sialyltransferases, namely beta-galactoside alpha-2,6-sialyltransferase (ST6Gal1) and beta-galactoside alpha-2,6-sialyltransferase 2 (ST6Gal2), that catalyse the transfer of a sialic acid to galactose with  $\alpha$ -2,6 linkage. Cytidine-5'-monophospho-N-acetylneuraminic acid (CMP-SA) is the substrate for both enzymes. ST6Gal1 sialylates all glycoproteins in the body; only those in the central nervous system are sialylated by ST6Gal2 [82]. ST6Gal1 can be used to modulate IgG sialylation levels clinically. It is ubiquitously expressed in many cell types, including plasma cells. However, it is important to note that ST6Gal1 expression in plasma cells is influenced by the types of antigens and immunization techniques [83]. In particular, antigens or immunization regimes that do not activate T cells maintain ST6Gal1 expression in plasma cells, leading to the production of highly sialylated IgG, whereas B cell activation in the presence of T cells turns off the expression of this enzyme [84].

The classically defined secretory pathway of glycoproteins in B cells implies glycoproteins exiting the endoplasmic reticulum and travelling through the Golgi apparatus where N-glycans are folded into their final structure. This entails that IgG sialylation depends on the secretory pathway in B cells and on metabolic circumstances of a specific cell. Recently, Jones et al. made a remarkable discovery when they showed B cell independent sialylation of IgG [85]. Creation and analysis of a B cell specific knockout of ST6Gal1 revealed that IgG sialylation may occur independently of the B cell secretory pathway and within the bloodstream after IgG secretion. There was no difference in the percentage of sialylated IgG between wild-type and knockout animals, demonstrating that B cell expression of ST6Gal1 is dispensable for the synthesis of sialylated IgG. ST6Gal1 is known to be secreted/cleaved from the Golgi membrane which normally anchors the enzyme [86], and Western blots showed that the liver is the primary source of cleaved ST6Gal1, produced by cells lining the central veins [85]. CMP-SA is a nucleotide monophosphate sugar which donates N-acetylneuraminic acid to the terminal sugar of a glycoprotein, thus acting as a substrate for ST6Gal1. It has never been found in the circulation and its reported half-life is outside of a cell is extremely short [85]. However, already in 1981, a paper was published demonstrating that the half-life of extracellular CMP-SA in a rat brain is around 4 hours [87]. Jones *et al.* showed that the nucleotide sugar donor is at least partially supplied by activated platelets [85]. Taken

together, these findings support a paradigm for exogenous PTM modification of glycoproteins, providing the immune system to modulate circulatory IgG in a dynamic fashion without relying only upon de novo IgG synthesis.

Because of its extremely low Si/Al ratio and the resulting highly charged membrane, synthetic zeolite A easily breaks down in the stomach, unlike other zeolites that only pass through the digestive system. We detected hotspots of aluminium co-localized with silicone in liver slices of rats fed with Zeolite A, but not in rats fed with clinoptilolite, confirming the abovementioned fact (Figure 43). Since liver is a detoxification organ, one can presume that clinoptilolite exerts some of its, if not all, beneficial properties via the liver as well. To investigate zeolite's detoxification effects, rats were intoxicated with aluminium chloride, and consequently fed with one of four types of zeolites and colloidal silica as control. Al concentrations expectedly increased in the plasma, liver and bone [24]. All tested zeolites effectively decreased Al concentrations in the liver of intoxicated animals, while no significant changes in the liver Al concentrations were observed for colloidal silica-supplemented animals [24]. These results confirm the fact that zeolites do exert an effector function on the liver, further supporting the idea that clinoptilolite interacts with the liver-secreted sialylase, resulting in at least partially increased sialylation of IgG. This is probably due to the release of soluble silica into the blood in the form of orthosilicic acid which protects the body from heavy metals [35]. The finding that orthosilicic acid stimulates collagen type 1 synthesis and osteoblastic differentiation in human osteoblast-like cells *in vitro* [88], offers another plausible zeolite's mechanism of action on bone architecture through soluble silica, independent of immunoglobulin glycosylation. To provide more evidence to the fact that clinoptilolite positively affect bone status in osteoporotic rats as a consequence of signalling changes in the body, particularly those initiated by the liver and the systemic spread of IgG molecules with higher numbers of sialic acid residues in their glycans, further complex proteomic studies of the liver should be performed.

## 6. CONCLUSIONS

The main goal of this research was to examine the effects of clinoptilolite on IgG glycosylation in the osteoporotic rat model. The rationale behind this goal is in an already established link between immunoglobulin sialylation and various pathologies. We developed protocols for a fast, reliable and high-throughput method for IgG isolation from human and rat serum, using polymethacrylate monolithic columns with immobilized protein L for the isolation of immunoglobulin G from serum of healthy rats, osteoporotic rats and osteoporotic rats supplemented with clinoptilolite. Furthermore, we analysed glycosylation profiles of isolated IgGs, with a specific focus on sialic acid residues. Finally, we analysed liver proteomes of healthy rats, osteoporotic rats and osteoporotic rats treated with clinoptilolite, since the main mechanisms of clinoptilolite action is hypothesized to be detoxification in the digestive system. The results of this thesis provide novel evidence on clinoptilolite mechanisms of action in a medical device regimen particularly through changes of liver activities as well as through induction of specific glycosylation changes in IgG. Present results give us the evidence that the developed HTP protocols for analysis of glycosylation of rat immunoglobulins, namely IgG, IgA and IgM, as well as the protocol for quantitative proteomic investigations of rat liver proteome, give us the fundament for further investigations by use of a larger number of experimental animals. We suggest that clinoptilolite positively affects bone status in osteoporotic rats as a consequence of signalling changes in the body, particularly those initiated by the liver and the systemic spread of IgG molecules.

## 7. LITERATURE

1. Hernlund E, Svedbom A, Ivergard M, Compston J, et. al. Osteoporosis in the European Union: Medical Management, Epidemiology and Economic Burden. A report prepared in collaboration with the International Osteoporosis Foundation (IOF) and the European Federation of Pharmaceutical Industry Associations (EFPIA). *Arch. Osteoporos.* 2013, 8, 136.
2. Raisz LG. Pathogenesis of osteoporosis: concepts, conflicts, and prospects. *J. Clin. Invest.* 2005, 115, 3318-25.
3. Kapinas K, Delany AM. MicroRNA biogenesis and regulation of bone remodeling. *Arthritis Res Ther.* 2011, 13, 220.
4. Boyce BF, Xing L. Biology of RANK, RANKL, and osteoprotegerin. *Arthritis Res. Ther.* 2007, 9, Suppl 1:S1.
5. Takahata M, Iwasaki N, Nakagawa H, Abe Y, Watanabe T, Ito M, Majima T, Minami A. Sialylation of cell surface glycoconjugates is essential for osteoclastogenesis. *Bone.* 2007, 41, 77-86.
6. Crockett JC, Rogers MJ, Coxon FP, Hocking LJ, Helfrich MH. Bone remodelling at a glance. *J. Cell Sci.* 2011, 124(Pt 7), 991-8.
7. Theoleyre S, Wittrant Y, Kwan Tat S, et al. The molecular triad OPG/RANK/RANKL: involvement in the orchestration of pathophysiological bone remodelling. *Cytokine Growth Factor Rev.* 2004, 15, 457–475.
8. Yavropoulou MP, Yovos JG. The role of the Wnt signaling pathway in osteoblast commitment and differentiation. *Hormones (Athens)* 2007, 6, 279-94.
9. Swisher JF, Feldman GM. The many faces of Fc $\gamma$ RI: implications for therapeutic antibody function. *Immunol. Rev.* 2015, 268, 160-74.
10. Yu X, Marshall MJE, Cragg MS, Crispin M. Improving Antibody-Based Cancer Therapeutics Through Glycan Engineering. *BioDrugs* 2017, 31, 151-166.
11. Huang C, Liu Y, Wu H, Sun D, Li Y. Characterization of IgG glycosylation in rheumatoid arthritis patients by MALDI-TOF-MSn and capillary electrophoresis. *Anal. Bioanal. Chem.* 2017, 409, 3731-3739.
12. Mittermayr S, Lê GN, Clarke C, Millán Martín S, Larkin AM, O'Gorman P, Bones, JJ. Polyclonal Immunoglobulin G N-Glycosylation in the Pathogenesis of Plasma Cell Disorders. *Proteome Res.* 2017, 16, 748-762.

13. Epp A, Sullivan KC, Herr AB, Strait RT. Immunoglobulin Glycosylation Effects in Allergy and Immunity. *Curr. Allergy Asthma Rep.* 2016, 16, 79.
14. Novak J, Julian BA, Mestecky J, Renfrow MB. Glycosylation of IgA1 and pathogenesis of IgA nephropathy. *Semin. Immunopathol.* 2012, 34, 365-82.
15. Colucci M, Stöckmann H, Butera A, Masotti A, Baldassarre A, Giorda E, Petrini S, Rudd PM, Sitia R, Emma F, Vivarelli MJ. Sialylation of N-linked glycans influences the immunomodulatory effects of IgM on T cells. *Immunol.* 2015, 194, 151-7.
16. Hayes JM, Wormald MR, Rudd PM, Davey GP. Fc gamma receptors: glycobiology and therapeutic prospects. *J. Inflamm. Res.* 2016, 9, 209-219.
17. Hmiel LK, Brorson KA, Boyne MT. Post-translational structural modifications of immunoglobulin G and their effect on biological activity. *Anal. Bioanal. Chem.* 2015, 407, 79-94.
18. de Haan N, Reiding KR, Krišćić J, Hipgrave Ederveen AL, Lauc G, Wuhler M. The N-Glycosylation of Mouse Immunoglobulin G (IgG)-Fragment Crystallizable Differs Between IgG Subclasses and Strains. *Front. Immunol.* 2017, 8, 608.
19. Nimmerjahn F, Ravetch JV. Fc gamma receptors as regulators of immune responses. *Nat. Rev. Immunol.* 2008, 8, 34-47.
20. Stavros C. Manolagas. Birth and Death of Bone Cells: Basic Regulatory Mechanisms and Implications for the Pathogenesis and Treatment of Osteoporosis, *Endocrine Reviews* 2000, 21, 115–137.
21. Harre U, Lang SC, Pfeifle R, Rombouts Y, Frühbeißer S, Amara K, Bang H, Lux A, Koeleman CA, Baum W, Dietel K, Gröhn F, Malmström V, Klareskog L, Krönke G, Kocjan R, Nimmerjahn F, Toes RE, Herrmann M, Scherer HU, Schett G. Glycosylation of immunoglobulin G determines osteoclast differentiation and bone loss. *Nat. Commun.* 2015, 6, 6651.
22. Negishi-Koga T, Gober HJ, Sumiya E, Komatsu N, Okamoto K, Sawa S, Suematsu A, Suda T, Sato K, Takai T, Takayanagi H. Immune complexes regulate bone metabolism through FcR $\gamma$  signalling. *Nat. Commun.* 2015, 6, 6637.
23. Harre U, Georgess D, Bang H, Bozec A, Axmann R, Ossipova E, Jakobsson PJ, Baum W, Nimmerjahn F, Szarka E, Sarmay G, Krumbholz G, Neumann E, Toes R, Scherer HU, Catrina AI, Klareskog L, Jurdic P, Schett G. Induction of osteoclastogenesis and bone loss by human autoantibodies against citrullinated vimentin. *J. Clin. Invest.* 2012, 122, 1791-802.



24. Laurino C, Palmieri B. Zeolite: „The magic stone“; main nutritional, environmental, experimental and clinical fields of application. *Nutr. Hosp.* 2015, 32, 573-81.
25. Kowalczyk P, Sprynskyy M, Terzyk AP, Lebedynets M, Namieśnik J, Buszewski B. Porous structure of natural and modified clinoptilolites. *J. Colloid Interface Sci.* 2006, 297, 77-85.
26. Kraljević Pavelić A, Micek V, Filošević A, Gumbarević D et al. Novel, oxygenated clinoptilolite material efficiently removes aluminium from aluminium chloride-intoxicated rats in vivo, In *Microporous Mesoporous Mater.* 2017, 249, 146-156.
27. Yeritsyan H, Sahakyan A, Harutyunyan V, Nikoghosyan S, Hakhverdyan E, Grigoryan N, et al. Radiation-modified natural zeolites for cleaning liquid nuclear waste (irradiation against radioactivity). *Sci. reports* 2013, 3, 2900.
28. Ambrozova P, Kynicky J, Urubek T, Nguyen VD. Synthesis and Modification of Clinoptilolite. *Molecules.* 2017, 22.
29. Grce M, Pavelić K. Antiviral properties of clinoptilolite. *Microporous Mesoporous Mater.* 2005, 79, 165–169.
30. Tomečková, V.; Reháková, M.; Mojžišová, G.; Magura, J.; Wadsten, T.; Zelenáková, K. Modified natural clinoptilolite with quercetin and quercetin dihydrate and the study of their anticancer activity. *Microporous Mesoporous Mater.* 2012, 147, 59–67.
31. Cerri, G.; de' Gennaro, M.; Bonferoni, M.C.; Caramella, C. Zeolites in biomedical application: Zn-exchanged clinoptilolite-rich rock as active carrier for antibiotics in anti-acne topical therapy. *Appl. Clay Sci.* 2004, 27, 141–150
32. Alireza, N.-E.; Sanaz, T.-G. Effect of a nano-sized natural clinoptilolite modified by the hexadecyltrimethyl ammonium surfactant on cephalexin drug delivery. *Comptes, Rendus. Chim.* 2014, 17, 49–61.
33. Joshi JT. A review on micronization techniques. *J. Pharmaceutical Sci. Technol.* 2011, 3, 651-681.
34. Palubinskaite D, Kantautas A. Influence of tribomechanical milling and activation of primary mixtures on the synthesis of calcium silicate hydrates. *Materials Science-Poland.* 2006, 24.
35. Martin KR. Silicon: the health benefits of a metalloid. *Met. Ions Life Sci.* 2013, 13, 451-73.
36. Jugdaohsingh R, Tucker KL, Qiao N, Cupples LA, Kiel DP, Powell JJ. Dietary silicon intake is positively associated with bone mineral density in men and premenopausal women of the Framingham Offspring cohort. *J. Bone Miner. Res.* 2004, 19, 297-307.

37. Jugdaohsingh R, Watson AI, Bhattacharya P, van Lenthe GH, Powell JJ. Positive association between serum silicon levels and bone mineral density in female rats following oral silicon supplementation with monomethylsilanetriol. *Osteoporos. Int.* 2015, 26, 1405-15.
38. Ueki A, Yamaguchi M, Ueki H, Watanabe Y, Ohsawa G, Kinugawa K, Kawakami Y, Hyodoh F. Polyclonal human T-cell activation by silicate in vitro. *Immunology.* 1994, 82, 332-5.
39. Beck GR Jr, Ha SW, Camalier CE, Yamaguchi M, Li Y, Lee JK, Weitzmann MN. Bioactive silica-based nanoparticles stimulate bone-forming osteoblasts, suppress bone-resorbing osteoclasts, and enhance bone mineral density in vivo. *Nanomedicine.* 2012, 8, 93-803.
40. Schütze N, Oursler MJ, Nolan J, Riggs BL, Spelsberg TC. Zeolite A inhibits osteoclast-mediated bone resorption in vitro. *J. Cell Biochem.* 1995, 58, 39-46.
41. Breen LD, Pučić-Baković M, Vučković F, Reiding K, Trbojević-Akmačić I, Šrajer Gajdošik M, Cook MI, Lopez MJ, Wuhler M, Camara LM, Andjelković U, Dupuy DE, Josić D. IgG and IgM glycosylation patterns in patients undergoing image-guided tumor ablation. *Biochim. Biophys. Acta.* 2016, 1860, 1786-94.
42. Breen, L., Cao, L., Eom, K., Srajer Gajdosik, M., Camara, L., Giacometti, J., Dupuy, D.E., Josic, D. High-throughput fractionation of human plasma for fast enrichment of low- and high-abundance proteins. *Blood Transfus.* 2012, 10, Suppl 2:s89-100.
43. Barut, M., Podgornik, A., Urbas, L., Gabor, B., Brne, P., Vidic, J., Plevcak, S., Strancar, A. Methacrylate-based short monolithic columns: enabling tools for rapid and efficient analyses of biomolecules and nanoparticles. *J. Sep. Sci.* 2008, 31, 1867-80.
44. Svec F. Monolithic columns: A historical overview. *Electrophoresis.* 2017, 38, 22-23.
45. Tennikova TB, Svec F, Belenkii BG. High-performance membrane chromatography. A novel method of protein separation. *J. Liquid Chromatogr.* 1990 13, 63-70.
46. Hjertén S, Liao JL, Zhang R. High-performance liquid chromatography on continuous polymer beds. *J. Chromatogr. A.* 1989, 273-275.
47. Krajačić M, Ravnikar M, Štrancar A, Gutierrez Aguirre, I. Application of monolithic chromatographic supports in virus research. *Electrophoresis.* 2017, 38, 2827-2836.
48. Josić Dj, Löster K, Baum O, Reutter W. High-performance membrane chromatography of serum and plasma membrane proteins. *J. Chromatogr. A* 1992, 590, 59-76.

49. Abou-Rebyeh H., Körber F., Schubert-Rehberg K., Reusch J., Josic, Dj. Carrier membrane as stationary phase for affinity chromatography and kinetic studies of membrane-bound enzymes. *J. Chromatogr. B* 1991, 586, 341-350.
50. Svec, F, Fréchet, J. M. J. Molded rigid monolithic porous polymers: an inexpensive, efficient, and versatile alternative to beads for the design of materials for numerous applications. *Ind. Eng. Chem. Res.* 1999, 38, 34-48.
51. Josić, Dj. Štrancar, A. Application of membranes and compact, porous units for separation of biopolymers, *Ind. Eng. Chem. Res.* 1999, 38, 333-342.
52. Štrancar, A., Koselj, P., Schwinn, H., Josić, Dj. Application of Compact Porous Disks for Fast Separation of Biopolymers and In-Process Control in Biotechnology, *Anal. Chem.* 1996, 68, 3486-3488.
53. Peters, E. C., Svec, F., Fréchet, J. M. J. Rigid macroporous polymer monoliths, *Adv. Mat.* 1999, 11, 1169-1181.
54. Vlakh, E, Tappe, A, Kasper, K., Tennikova, T. B. Monolithic peptidyl sorbents for comparison of affinity properties of plasminogen activators, *J. Chromatogr. B* 2004, 810, 15-23.
55. Švec F., Lv Y. Advances and Recent Trends in the Field of Monolithic Columns for Chromatography, *Anal. Chem.* 2015, 87, 250-273.
56. Josić Dj., Buchacher A. Application of monoliths as supports for affinity chromatography and fast enzymatic conversion. *J Biochem Biophys Methods* 2001, 49, 153-174.
57. Tetala KKR, Van Beek TA. Bioaffinity chromatography on monolithic supports. *J. Sep. Sci.* 2010; 33:422–438.
58. Monolithic Materials Preparation, Properties and Applications, Edited by Svec F, Tennikova TB, Deyl Z. *J. Chromatogr. Library.* 67, 2003, 1-733.
59. Pfaunmiller EL, Paulemond ML, Dupper CM, Hage DS. Affinity monolith chromatography: a review of principles and recent analytical applications. *Anal Bioanal Chem.* 2013, 405, 2133-45.
60. Gustavsson PE, Larsson PO. In: Handbook of Affinity Chromatography. 2nd edn. Hage DS, editor. Boca Raton: CRC Press; 2006. Chap 2.
61. Tscheliessnig, A., Jungbauer, A. High-performance monolith affinity chromatography for fast quantitation of immunoglobulin G. *J. Chromatogr. A.* 2009, 1216, 2676-82.
62. Neff, S., Jungbauer, A. Monolith peptide affinity chromatography for quantification of immunoglobulin M. *J. Chromatogr. A.* 2011, 1218, 2374-80.

63. Leblebici, P., Leblebici, M.E., Ferreira-da-Silva, F., Rodrigues, A.E., Pais, L.S. Separation of human immunoglobulin G subclasses on a protein A monolith column. *J. Chromatogr. B Analyt. Technol. Biomed. Life. Sci.* 2014, 962, 89-93.
64. Pucić, M., Knezević, A., Vidic, J., Adamczyk, B., Novokmet, M., Polasek, O., Gornik, O., Supraha-Goreta, S., Wormald, M.R., Redzić, I., Campbell, H., Wright, A., Hastie, N.D., Wilson, J.F., Rudan, I., Wuhrer, M., Rudd, P.M., Josić, D., Lauc, G. High throughput isolation and glycosylation analysis of IgG-variability and heritability of the IgG glycome in three isolated human populations. *Mol. Cell. Proteomics.* 2011, 10, M111.010090.
65. Langone, J.J. Protein A of *Staphylococcus aureus* and related immunoglobulin receptors produced by streptococci and pneumococci. *Adv. Immunol.* 1982, 32, 157-252.
66. Björck, L., Kronvall, G. Purification and some properties of streptococcal protein G, a novel IgG-binding reagent. *J. Immunol.* 1984, 133, 969-74.
67. Björck, L. Protein L. A novel bacterial cell wall protein with affinity for Ig L chains. *J. Immunol.* 1988, 140, 1194-7.
68. Černigoj, U., Vidic, U., Nemeč, B., Gaspersic, J., Vidic, J., Krajnc, N.L., Strancar, A., Podgornik, A. Characterization of methacrylate chromatographic monoliths bearing affinity ligands. *J. Chromatogr. A.* 2016, 1464, 72–78.
69. Vidič, U., Trbojević-Akmačić, I., Černigoj, U., Albers, M., Gašperšič, J., Pučić-Baković, M., Vidič, J., Štrancar, A., Lauc, G. Semi-high-throughput isolation and N-glycan analysis of human fibrinogen using monolithic supports bearing monoclonal anti-human fibrinogen antibodies. *Electrophoresis.* 2017, 38, 2922-2930.
70. Trbojević-Akmačić, I., Nemeč, B., Vidic, U., Malić, S., Miklić, K., Černigoj, U., Vidič, J., Lendero Krajnc, N., Štrancar, A., Lauc, G., Lenac Roviš, T., Pučić-Baković, M. Chromatographic Monoliths for High-Throughput. Immunoaffinity Isolation of Transferrin from Human Plasma. *Croatica Chemica Acta.* 2016, 89, doi:10.5562/cca2815
71. Bondt A, Rombouts Y, Selman MH, Hensbergen PJ, Reiding KR, Hazes JM, Dolhainn RJ, Wuhrer M. Immunoglobulin G (IgG) Fab glycosylation analysis using a new mass +spectrometric high-throughput profiling method reveals pregnancy-associated changes. *Mol Cell Proteomics.* 2014, 13, 3029-39.
72. Novokmet M, Lukić E, Vučković F, et al. Changes in IgG and total plasma protein glycomes in acute systemic inflammation. *Scientific Reports.* 2014, 4, 4347.
73. Piagnerelli M, Boudjeltia KZ, Nuyens V, De Backer D, Su F, Wang Z, Vincent JL, Vanhaeverbeek M. Rapid alterations in transferrin sialylation during sepsis. *Shock* 2005, 24, 48-52.

74. Raju TS, Briggs JB, Borge SM, Jones AJ. Species-specific variation in glycosylation of IgG: evidence for the species-specific sialylation and branch-specific galactosylation and importance for engineering recombinant glycoprotein therapeutics. *Glycobiology*. 2000, 10, 477-86.
75. Scherer H. u. et al. Glycan profiling of anti-citrullinated protein antibodies isolated from human serum and synovial fluid. *Arthritis Rheum*. 2010, 62, 1620-1629.
76. Rademacher TW, Williams P & Dwek RA. Agalactosyl glycoforms of IgG autoantibodies are pathogenic. *Proc. Natl Acad. Sci. USA* 1994, 91, 6123-36127.
77. Ito K. et al. Lack of galactosylation enhances the pathogenic activity of IgG1 but not IgG2a anti-erythrocyte autoantibodies. *J. Immunol*. 2014, 192, 581-588.
78. Karsten, C. M. et al. Anti-inflammatory activity of IgG1 mediated by Fc galactosylation and association of FcγRIIB and dectin-11. *Nat. Med*. 2012, 18, 1401-1406.
79. Anthony, R. M. et al. Recapitulation of IVIG anti-inflammatory activity with a recombinant IgG Fc. *Science* 2008, 320, 373-376.
80. Leontyev, D. et al. Sialylation-independent mechanism involved in the amelioration of murine immune thrombocytopenia using intravenous gammaglobulin. *Transfusion* 2012, 52, 1799-1805.
81. Li, T., DiLillo, D.J., Bournazos, S., Giddens, J.P., Ravetch, J.V., Wang, L-X. Modulating IgG effector function by Fc glycan engineering. *PNAS* 2017, 114, 3485-3490.
82. Lehoux S, et al. Transcriptional regulation of the human ST6GAL2 gene in cerebral cortex and neuronal cells. *Glycoconj J*. 2010, 27, 99-114.
83. Oefner, C. M. et al. Tolerance induction with T cell-dependent protein antigens induces regulatory sialylated IgGs. *J. Allergy Clin. Immunol*. 2012, 129, 1647-1655 e1613.
84. Hess, C. et al. T cell-independent B cell activation induces immunosuppressive sialylated IgG antibodies. *J. Clin. Invest*. 2013, 123, 3788-3796.
85. Jones, M.B., Oswald, D.M., Joshi, S., Whiteheart, S.W., Orlando, R., Cobb, B.A. B cell independent sialylation of IgG. *Proc. Natl. Acad. Sci. USA* 2016, 113, 7207-7212.
86. Colley, K.J., Lee, E.U., Adler, B., Browne, J.K., Paulson, J.C. Conversion of a Golgi apparatus sialyltransferase to a secretory protein by replacement of the NH2 terminal signal anchor with a signal peptide. *J. Biol. Chem*. 1989, 264, 17619-17622.
87. Ferwerda, W., Blok, C.M., Heijlman, J. Turnover of free sialic acid, CMP sialic acid, and bound sialic acid in rat brain. *J. Neurochem*. 1981, 36, 1492-1499.

88. Reffitt DM, Ogston N, Jugdaohsingh R, Cheung HF, Evans BA, Thompson RP, Powell JJ, Hampson GN. Orthosilicic acid stimulates collagen type 1 synthesis and osteoblastic differentiation in human osteoblast-like cells in vitro. *Bone*. 2003, 32, 127-35.

## 8. CURRICULUM VITAE

### **MSc Tamara Martinović**

Date of birth: 24th June 1986

Place of birth: Rijeka, Croatia

Nationality: Croatian

Address: Radmile Matejčić 2, 51000 Rijeka, Croatia

*E-mail address: tamara.martinovic@uniri.hr*

### **EDUCATION**

- 11/2012 – 03/2018    **Department of Biotechnology, University of Rijeka, Rijeka, Croatia**  
PhD student
- 09/2007 - 06/2009    **University Utrecht, Utrecht, The Netherlands**  
*Master of Science (Biomolecular sciences)*
- 09/2004 - 05/2007    **University College Utrecht, Utrecht, Nizozemska**  
*Bachelor of Science*  
Major in Biomolecular sciences, Minor in History
- 09/2000 - 06/2004    **Prva Sušačka Hrvatska Gimnazija, Rijeka, Croatia**

## **PARTICIPATION IN SUMMER SCHOOLS AND CONFERENCES**

- 07/2016                    **10th Mass Spectrometry in Biotechnology & Medicine Summer School, Dubrovnik, Croatia**  
Poster presentation
- 05/2016                    **7th Monolith Summer School & Symposium, Portorož, Slovenia**  
Oral and poster presentation; best oral presentation award (Young researcher's award)
- 08/2011                    **5th EU Summer School in “Proteomic Basics”, Bressanone, Italy**

## **EDUCATION IN FOREIGN INSTITUTIONS**

- 11/2016                    **Chemical faculty, University of Belgrade, Belgrade, Serbia**  
Two week stay in the scope of a bilateral project
- 10/2015                    **Bruker Daltonik GmbH, Bremen, Germany**  
MALDI-TOF/TOF mass spectrometry education
- 10/2014 – 12/2014        **Department of Clinical Chemistry, University Medical Center Hamburg-Eppendorf, Hamburg, Germany**  
Two month stay, working on MALDI-TOF/TOF and Orbitrap mass spectrometers.

## **JOURNAL PUBLICATIONS**

**Martinović T**, Andjelković U, Klobučar M, Černigoj U, Vidič J, Lučić M, Pavelić K, Josić D (2017) Affinity chromatography on monolithic supports for simultaneous and high-throughput isolation of immunoglobulins from human serum. **Electrophoresis** 38:2909-2913.

Andjelković U, Gavrović-Jankulović M, **Martinović T**, Josić Dj. (2017) Omics methods as a tool for investigation of food allergies. **Trends Analyt Chem** 96:107-115.



**Martinović T**, Josić Dj. (2017) Polymethacrylate-based monoliths as stationary phases for separation of biopolymers and immobilization of enzymes. **ELECTROPHORESIS** 38:2821-2826.

Šrajter Gajdošik M, Andjelković U, Gašo-Sokač D, Pavlović H, Shevchuk O, **Martinović T**, Clifton J, Josić Dj (2017) Proteomic analysis of food borne pathogens following the mode of action of the disinfectants based on pyridoxal oxime derivatives. **Food Res Int** 99:560-570.

Andjelković U, Šrajter Gajdošik M, Gašo-Sokač D, **Martinović T** and Josić Dj (2017) Foodomics and Food Safety: Where We Are. **Food Tech Biotech** 55:290-307.

Tireli M, Starčević K, **Martinović T**, Pavelić SK, Karminski-Zamola G, Hranjec M (2017) Antioxidative and antiproliferative activities of novel pyrido[1,2-a]benzimidazoles. **Mol Divers** 21:201-210.

**Martinović T**, Andjelković U, Šrajter Gajdošik M, Rešetar D, Josić D. Foodborne pathogens and their toxins. **J. Proteom.** (2016) 147:226-35.

Stipković Babić M, Makuc D, Plavec J, **Martinović T**, Kraljević Pavelić S, Pavelić K, Snoeck R, Andrei G, Schols D, Wittine K, Mintas M. Novel halogenated 3-deazapurine, 7-deazapurine and alkylated 9-deazapurine derivatives of l-ascorbic or imino-l-ascorbic acid: Synthesis, antitumour and antiviral activity evaluations. **Europ J Med. Chem** (2015) 102:288–302.

Andjelkovic U, **Martinovic T**, Josic Dj. Foodomic investigations of food allergies. **Current Opinion in Food Science** (2015) 4:92-98.

Pavelić K, **Martinović T**, Kraljević Pavelić S. Do we understand the personalized medicine paradigm? **EMBO Rep.** (2015) 16 (2):133-6.

## **BOOK CHAPTERS**

Josić D, Peršurić Ž, Rešetar D, **Martinović T**, Saftić L, Kraljević Pavelić S: Use of Foodomics for Control of Food Processing and Assessing of Food Safety, In: **Advances in Food and Nutrition Research**, Elsevier, 81: 187-229.

Rešetar D, **Martinović T**, Kraljević Pavelić S. Andjelković U, Josić Dj (2016) Proteomics and peptidomics as tools for detection of food contamination by bacteria. In: **Proteomics in Food**, edited by Fidel Toldra.

Josić Dj, Rešetar D, Peršurić Z, **Martinović T**, Kraljević Pavelić S (2017): Detection of Microbial Toxins by -Omics Methods: A Growing Role of Proteomics, In: **Proteomics in Food Science**, edited by Michelle L. Colgrave, Academic Press, 485-506.

## **COMPUTER SKILLS**

Microsoft Office (Microsoft Word, Microsoft Excel, Microsoft Powerpoint, E-mail clients)

Adobe Photoshop

## **FOREING LANGUAGE SKILLS**

/Mother tongue Croatian/

**English:** C2 level

**Dutch:** B1 level

**Italian:** B1 level

**Spanish:** Basic

## 9. SUPPLEMENT

### 9.1 List of tables

- 1 – Comparison of two chromatographic media, monoliths and particulate material
- 2 – Animal groups and treatment
- 3 – MASCOT search results for human IgA, IgG and IgM after tryptic digestion
- 4 – Immunoglobulin concentrations in rat and human
- 5 – A list of MALDI TOF measured glycan experimental masses, glycans' exact glycoform mass, the difference between experimental and glycoform masses expressed in Daltons, and the suggested glycan structures for samples from the control group (0)
- 6 – A list of MALDI TOF measured glycan experimental masses, glycans' exact glycoform mass, the difference between experimental and glycoform mass expressed in Daltons, and the suggested glycan structure for samples from the sham group (1)
- 7 – A list of MALDI TOF measured glycan experimental masses, glycans' exact glycoform mass, the difference between experimental and glycoform mass expressed in Daltons, and the suggested glycan structure for samples from the OVX group (2)
- 8 – A list of MALDI TOF measured glycan experimental masses, glycans' exact glycoform mass, the difference between experimental and glycoform mass expressed in Daltons, and the suggested glycan structure for samples from the OVX group supplemented with zeolite A (3)
- 9 – A list of MALDI TOF measured glycan experimental masses, glycans' exact glycoform mass, the difference between experimental and glycoform mass expressed in Daltons, and the suggested glycan structure for samples from the OVX group supplemented with clinoptilolite (4)
- 10 – A list of MALDI TOF measured glycan experimental masses, glycans' exact glycoform mass, the difference between experimental and glycoform mass expressed in Daltons, and the suggested glycan structure for samples from the OVX group supplemented with PMA clinoptilolite (5)
- 11 – A list of all detected peaks and detected glycan structures for each sample.
- 12 – A table depicting all detected glycan structures in all samples (groups 0 to 5). Composite glycans are shown in blue; glycans with sialic acid residues are shown in green.
- 13 – Comparison between measured rat IgG glycan peaks and human IgG glycan peaks. Peaks highlighted in blue are detected in both species.

## **9.2 List of figures**

**1** – Bone remodelling

**2** – The molecular triad OPG/RANK/RANKL

**3** – IgG sialylation is the key checkpoint that determines the engagement of pro- or anti-inflammatory Fcγ receptors

**4** – Binding sites of protein A, G and L

**5** – Structural formula of clinoptilolite

**6** - Scanning electron microscope pictures of **(A)** synthetic zeolite A and **(B)** natural clinoptilolite

**7** – A typical affinity chromatography scheme

**8** – IgG dynamic binding capacities of CIM protein G **(A)** and protein L **(B)** columns

**9** – SDS PAGE of a comparison of elution patterns between CIM monoliths with immobilized protein G, A or L. M - Roti-Mark TRICOLOR molecular mass standard. Lanes: (1) pG flow through; (2) pG eluate; (3) pL flow through; (4) pL eluate

**10** – SDS PAGE of immunoglobulin A, G and M isolation using affinity monolith chromatography. Lanes marked with \* refer to the second chromatographic step. M - Roti-Mark TRICOLOR molecular mass standard. Lanes: (1) pG flow through; (2) pG eluate; (3) pL flow through\*; (4) pL eluate\*; (5) pL flow through; (6) pL eluate; (7) pG flow through\*; (8) pG eluate\*

**11** - A MALDI TOF fingerprint spectrum of the IgA heavy chain

**12** – A MALDI TOF fingerprint spectrum of the IgG heavy chain

**13** – A MALDI TOF fingerprint spectrum of the IgM heavy chain

**14** – A 96-well plate with mounted small monolithic columns for HTP sample preparation

**15** – CIM monolith with immobilized pL binds rat IgG. M - Roti-Mark TRICOLOR molecular mass standard. Lanes: (1) control, human IgG; (2) control, human IgM; (3) control, human IgG and IgM; (4) pL eluate

- 16** – IgG isolation from rat sera. CIM monolith with immobilized pL binds rat IgG. M - Roti-Mark TRICOLOR molecular mass standard. Lanes: (1) group 0 flowthrough (FT); (2) group 0 eluate (E); (3) group 1 FT; (4) group 1 E; (5) group 2 FT; (6) group 2 E; (7) group 3 FT; (8) group 3 E; (9) group 4 FT; (10) group 4 E; (11) group 5 FT; (12) group 5 E
- 17** – A chromatogram of IgG elution, sample: 0-1, healthy control
- 18** – A chromatogram of IgG elution, sample: 1-1, sham
- 19** – A chromatogram of IgG elution, sample: 2-1, OVX control
- 20** – A chromatogram of IgG elution, sample: 3-1, zeolite A
- 21** – A chromatogram of IgG elution, sample: 4-1, clinoptilolite
- 22** – A chromatogram of IgG elution, sample: 5-1, PMA clinoptilolite
- 23** – A MALDI TOF fingerprint spectrum of the rat IgG heavy chain
- 24** – A comparison of MALDI TOF spectra of trypsinized rat IgG peptides from all analysed groups (0-6)
- 25** – A comparison of MALDI TOF spectra of glycans released from all analysed groups (0-6)
- 26** – Glycan legend
- 27** – MALDI TOF spectrum of glycans released from rat IgG (group 0 – control)
- 28** – MALDI TOF spectrum of glycans released from rat IgG (group 1 – sham operated)
- 29** – MALDI TOF spectrum of glycans released from rat IgG (group 2 – OVX)
- 30** – MALDI TOF spectrum of glycans released from rat IgG (group 4 – OVX supplemented with zeolite A)
- 31** – MALDI TOF spectrum of glycans released from rat IgG (group 5 – OVX supplemented with clinoptilolite)
- 32** – MALDI TOF spectrum of glycans released from rat IgG (group 6 – OVX supplemented with PMA clinoptilolite)
- 33** – A MALDI TOF MS spectrum of the human IgG glycome
- 34** – The 20 most abundant released glycans of total mouse fragment crystallisable (Fc) region IgG analysed by MALDI-TOF-MS after linkage-specific sialic acid derivatization
- 35** – A graphical representation of the relative intensity of the most prominent peak in rat IgG glycome (1485 Da) detected in rat, mouse and human.

**36** – A graphical representation of the intensity of mutual glycan peaks detected in rat, mouse and human IgG, relative to the reference peak in rat IgG glycome (1485 Da) whose value is considered to be 1.

**37** – A graphical representation of the intensity of mutual glycan peaks detected in samples from groups 1, 2 and 5, relative to the reference peak in rat IgG glycome (1485 Da) whose value is considered to be 1.

**38** – Rat liver fractionation – fraction I. Lanes: (1) group 0; (2) group 1; (3) group 2; (4) group 3; (5) group 4; (6) group 5.

**39** – Rat liver fractionation – fraction II. Lanes: (1) group 0; (2) group 1; (3) group 2; (4) group 3; (5) group 4; (6) group 5.

**40** – Rat liver fractionation – fraction III. Rat liver fractionation – fraction II. Lanes: (1) group 0; (2) group 1; (3) group 2; (4) group 3; (5) group 4; (6) group 5.

**41** – Rat liver fractionation – fraction IV. Lanes: (1) group 0; (2) group 1; (3) group 2; (4) group 3; (5) group 4; (6) group 5.

**42** – Rat liver fractionation – fraction V. Lanes: (1) group 0; (2) group 1; (3) group 2; (4) group 3; (5) group 4; (6) group 5.

**43** – Presence of aluminium (A) and silicone (B) in liver slices of healthy ovariectomized (OVX) rats, OVX rats treated with synthetic zeolite A, and OVX rats treated with PMA clinoptilolite.

### 9.3 List of abbreviations

AMBICA	Ammonium bicarbonate
ACN	Acetonitrile
AFM	Affinity monolith chromatography
CIM	Convective interaction media
EDC	1-ethyl-3-(3-dimethylaminopropyl)carbodiimide hydrochloride
HILIC	Hydrophilic interactions chromatography
HOBt	Hydroxybenzotriazole monohydrate
HTP	High-throughput
HPLC	High pressure liquid chromatography
IgA	Immunoglobulin A
IgG	Immunoglobulin G
IgM	Immunoglobulin M
IVIG	Intravenous immunoglobulin G
MALDI	Matrix assisted laser desorption ionisation
MS	Mass spectrometry
NeuAc	N-Acetylneuraminic acid
NeuGc	N-Glycolylneuraminic acid
OVX	Ovariectomized
PMA	Panaceo Micro Activated
TOF	Time of flight